Study on Plasmonic Enhancement for Photocatalytic Activity of TiO$_2$-based Materials and the Underlying Mechanism

Von der Naturwissenschaftlichen Fakultät der Gottfried Wilhelm Leibniz Universität Hannover

zur Erlangung des Grades

Doktor der Naturwissenschaften (Dr. rer. nat.)

genehmigte Dissertation

von

Jinlin Nie, Lixue boshi (Doctor of Natural Science), Master of Engineering, Ocean University of China.

2023

Preface

This cumulative dissertation is submitted for the degree of Dr.rer.nat. at the Gottfried Wilhelm Leibniz University of Hannover. The research described herein was conducted under the supervision of Prof. Dr. Detlef Bahnemann in the Institute of Technical Chemistry since September 2015.

This work is to the best of my knowledge original, expect where acknowledgements and references are made to previous studies. The results of the work were published in peer-reviewed journals and presented in international congresses. The structure of the thesis is adapted in the form of "Cumulative dissertation" where experimental investigations, figure lists, as well as references were organized according to their appearance in the respective publications

Jinlin Nie

Hannover, 2023

Acknowledgement

First and foremost, I would like to express my deepest gratitude to Prof. Dr. Detlef W. Bahnemann for giving me the opportunity to work under his supervision in the group, as well as for his valuable guidance, inspiring reviews, and stimulating discussions.

I am appreciative to apl. Prof. Dr. rer. nat. Dirk Dorfs and apl. Prof. Dr.rer. nat. Sascha Beutel for their kindness of being members of the examination committee.

I also would like to express my special appreciation to Dr. Jenny Schneider for her guidance, inspiration and whatever she has done during my whole research. You opened the door for my work in the research field and enlightened me in the subsequent research.

I also would like to express my special appreciation to Prof. Shuwei Xia for being co-supervisor of this work. She encouraged me to follow my heart and to continue my academic pursuit.

I owe special thanks to Dr. Ralf Dillert, Dr. Antonio Patrocinio, Dr. Fabian Sieland and Dr. Saher Hamid for numerous scientific discussions and their help in this research area, as well as in my publications.

I am also deeply thankful to my colleagues and office mates for their assistance in lab related issues and for the very good atmosphere of work.

I would like to express my deepest gratitude to my family especially to my parents. They really did their best to give me support in both my life and study.

Every single day, I thank my wonderful wife Hongzhen Zhang for her love, supports and her presence in my life. Her understanding, consideration and persistence strongly encouraged me to continue my academic pursuit.

Kurzzusammenfassung

Der Effekt der Oberflächenplasmonresonanz (SPR) auf photokatalytische Effizienz der TiO$_2$-Photokatalysatoren unter Bestrahlung mit sichtbarem Licht wurde bereits eingehend untersucht, wobei der zugrunde liegende Mechanismus noch kontrovers diskutiert wird. Hierbei sind zwei Reaktionsmechanismen bakannt, nämlich der Resonanzenergietransfer (RET) und der direkte Elektronentransfer (DET). Diese Arbeit konzentriert sich auf die Aufklärung des SPR-Effekts auf die photokatalytische Wasserspaltung unter Verwendung von Au- und Cu-modifiziertem TiO$_2$ Photokatalysatoren. Die Forschungsarbeiten bestehen aus drei Hauptteilen.

Der erste Teil beschäftigt sich mit der photokatalytischen Aktivität von Au-modifizierten Anatas TiO$_2$. Die Au-TiO$_2$ Photokatalysatoren wurden auf photokatalytische H$_2$-Gasbildung getestet. Mittels EPR- und Laser-Flash-Photolyse-Spektroskopie wurde bestätigt, dass reines Anatas-TiO$_2$ unter Bestrahlung mit sichtbarem Licht angeregt werden kann (höchstwahrscheinlich aufgrund von bereits vorhandenen Defekten, wie Sauerstoffleerstellen) und die angeregten Elektronen migrieren zu den Au-Nanopartikel. Somit wurde die katalytische Wirkung von Au bewiesen.

Im zweiten Teil dieser Arbeit wurde der Au-SPR-Effekt auf die photokatalytische Aktivität der Rutil:Anatas TiO$_2$-Probe (P25) untersucht. Die EPR- und Laserblitz-Photolyse-Spektroskopie-Untersuchngen in Kombination mit DFT-Rechnungen zeigten, dass zwei Reaktionswege kooperativ zur SPR-induzierten photokatalytischen H$_2$ Produktionsfähigkeit des Au-TiO$_2$-Photokatalysatoren unter Bestrahlung mit sichtbarem Licht beitragen. Zum einen Elektronen weren vom Au-NPs in das Leitungsband von TiO$_2$ injiziert und zum anderen findet Elektronentranport direkt vom Valenzband des TiO$_2$ zur Au-Oberfläche. Darüber hinaus liefert die DFT-Rechnungsanalyse den Nachweis dafür, dass durch die Modifizierung von TiO$_2$ mit Au-Clustern zusätzliche Energieniveaus innerhalb der Bandlücke von TiO$_2$ erzeugt werden.

Um die Effektivität der kostengünstigen plasmonischen Metalle wie Kupfer zu untersuchen wurde Cu-TiO$_2$ (P25) -Photokatalysatoren hergestellt. Es wurde festgestellt, dass Cu während der photokatalytischen Reaktion durch die Reduktion von CuO regeneriert wurde, wodurch der negative Effekt des bei Umgebungsbedingungen gebildeten CuO minimiert wurde. Die durch sichtbares Licht induzierte Ladungsträgerbildung in den Cu-TiO$_2$-Photokatalysatoren wurde auf zwei Prozesse zurückgefürht: die direkte Anregung von TiO$_2$ und die SPR-Anregungs der Cu-Nanopartikeln.

Abstract

The Surface Plasmon Resonance (SPR) enhanced visible-light driven photocatalytic efficiency of TiO$_2$-based photocatalysts has been extensively investigated in the past. The contribution of SPR to the enhancement of photocatalytic activity as well as the underlying mechanism have not yet been fully understood and are controversially discussed. Two possible reaction mechanisms are considered as operative in SPR photocatalysis with noble metal modified metal oxides, namely, the resonance energy transfer (RET) and the direct electron transfer (DET). This work focuses on the elucidation of the SPR effect on the photocatalytic water splitting utilizing Au and Cu modified TiO$_2$ as photocatalysts. The research was comprised of three major parts.

The first part deals with the photocatalytic performance of Au modified anatase TiO$_2$ (UV100). Au-TiO$_2$ photocatalysts were tested for photocatalytic H$_2$ gas formation upon visible light illumination. By means of EPR spectroscopy and Laser Flash Photolysis, it was confirmed that bare anatase TiO$_2$ can be excited by visible light illumination at wavelength > 420 nm (most likely due to pre-existing defects, such as oxygen vacancies) and the excited electrons migrate to the surface-loaded Au nanoparticles. Here it has been shown that Au serves as a catalyst rather than as SPR sensitizer.

In the second part, the Au-SPR effect on rutile: anatase TiO$_2$ sample (P25) was studied. Analysis of the data obtained from EPR and laser flash photolysis spectroscopy in combination with DFT calculation evinced that, two pathways cooperatively contribute to the SPR-induced visible-driven photocatalytic H$_2$ production ability of Au–TiO$_2$ photocatalyst upon visible light illumination. Au NPs can inject electrons into the conduction band of rutile: anatase TiO$_2$ and that the electrons can directly be transferred from the valence band of TiO$_2$ to the surface of Au, process called Interfacial Charge Transfer. Moreover, the DFT calculation analysis clearly shows how the d orbitals of Au clusters create impurity energy levels within the band gap of TiO$_2$ and thus contribute to enhancement of photocatalytic efficiency of Au–TiO$_2$.

Low cost plasmonic metals, such as copper, should be investigated aiming at cost-effective photocatalysts. Hence, Cu-TiO$_2$ (P25) photocatalysts were prepared and the photocatalytic H$_2$ production rates were evaluated. It was found that the Cu was regenerated during the photocatalytic reaction through the reduction of CuO, thus minimizing the negative effect of CuO formed at ambient conditions. Moreover, the results evidenced that the visible light induced charge carrier formation in the Cu–TiO$_2$ photocatalysts consists of two distinct pathways: the direct excitation of TiO$_2$ and the induced excitation SPR effect of the Cu nanoparticles on the TiO$_2$ surface. Both pathways are present when the full visible range of the spectrum is used ($\geqslant$420 nm), while for illumination at longer wavelengths ($\geqslant$500 nm), the photocatalytic activity is solely promoted by the Cu-SPR effect.

Key Words: Surface Plasmon Resonance (SPR); H_2 production; visible light; EPR; Laser Flash Photolysis, DFT calculation

List of Abbreviations

SPR	Surface Plasmon Resonance
SIM	Sol Immobilization
PD	Photodeposition
DP	Deposition-Precipitation
TEM	Transmission Electron Microscopy
UV-Vis	Ultraviolet-Visible
GC/ TCD	Gas Chromatograph/ Thermal Conductivity Detector
XRD	X-ray Diffraction
XPS	X-ray Photoelectron Spectroscopy
EPR	Electron Paramagnetic Resonance
OPO	Optical Parametric Oscillator
DFT	Density Functional Theory
DET	Direct Electron Transfer
RET	Resonance Energy Transfer
IFCT	Interfacial Charge Transfer
MV^{2+}	Methyl Viologen radical
TEMPO	2, 2, 6, 6-Tetramethylpiperidine 1-oxyl
UV100	Hombikat UV100
P25	Evonik Aeroxide P25
M	mole/liter
mL	milliliter
nm	nanometer
wt%	weight percent
eV	electron volt

Table of Content

Chapter 1 Introduction

1.1 Foreword

With the advancement of science and technology and social development, the global population has increased year by year. At the same time, people's demand for energy is also growing, and the damage caused to the ecological environment is becoming more and more serious. Currently, the energy and environmental crisis has become one of the most serious global issues in the world [1, 2]. Solar energy is an abundant and clean energy source in nature [3], and it has become a research hotspot to solve these problems by fully and effectively utilizing solar energy. Photocatalysis based on semiconductor technology has attracted much attention for solving the increasing energy and environmental crises (*e.g.*, environmental purification, organic degradation and water splitting for hydrogen generation) [4-6].

Since Kato observed the photocatalytic reaction on TiO_2 in 1964 [7], Fujishima and Honda [8] made a breakthrough by discovering the photosensitizing effect of a TiO_2 electrode for the electrolytic splitting of water into hydrogen and oxygen, which caused great response in the field of photocatalysis. The investigation showed that it is possible to directly decompose water to produce hydrogen by utilizing solar energy, and the produced hydrogen is an ideal clean energy source.

1.2 Titanium dioxide (TiO_2)

Photocatalysis has quickly become a research hotspot and has been extensively studied for decades. After that, researchers discovered a number of photocatalytic materials, such as TiO_2, ZnO, WO_3, CdS, $BiVO_4$ [9-12], etc. Accordingly, all these materials belong to the semiconductor category. Among many photocatalytic materials, the excellent n-type semiconductor material TiO_2, is a low-cost, active, environmentally friendly and stable

photocatalyst [13]. Therefore, it is one of the most extensively studied photocatalys. It is widely used in many fields such as wastewater treatment, air purification, sterilization, medical technology and preparation of environmentally friendly materials.

There are mainly three TiO_2 polymorphs existing in nature, namely: anatase, rutile and brookite.

Anatase TiO_2 belongs to the tetragonal system and exhibits best photocatalytic activity among the mentioned three phases [14,15]. It is also the most widely used phase in photocatalysis due to its high electron mobility, low dielectric constant and density [14]. Thus, anatase phase titanium dioxide is also popular in solar cell applications. The rutile phase TiO_2 belongs to the tetragonal system [14,15]. However, since it is relatively stable under normal temperature and pressure, it is mainly used as a whitening agent in coatings. The brookite TiO_2 belongs to the orthorhombic system, and it can hardly exist in nature due to the unstable crystal structure. The rutile TiO_2 is the most stable phase among the above three crystal phases. The anatase phase and the brookite phase can be converted into the rutile phase with heat treatment above 600 ℃ [14], which is an irreversible exothermic reaction. In the three forms,Ti^{4+} itoms are coordinated to 6 O^{2-} atoms, forming TiO_6 octahedra structure [14,15].

Due to the wide band gap, (namely, 3.0 eV for rutile [15], 3.2 eV for anatase [15] and 3.3 eV for brookite [16]), pure TiO_2 can only be excited by UV-light (anatase : E_g = 3.2 eV, λ_{max} = 388 nm; rutile : E_g = 3.0 eV, λ_{max} = 413 nm). The applications depend not only on the properties of the employed TiO_2, but also on the interations of TiO_2 with the surrounding environment.

1.3 TiO_2 Photocatalysis

Due to the wide band gap of TiO_2, pure TiO_2 can be excited by UV-light [17, 18, 19]. The electrons in the valence band (VB) can be transfered to the conduction band (CB), forming a highly active electron (e^-) in the conduction band while leaving a hole (h^+) in the valence band.

The formed electrons and holes carrying high energies can participate in the oxidation/reduction half reaction in the photocatalytic reaction, respectively.
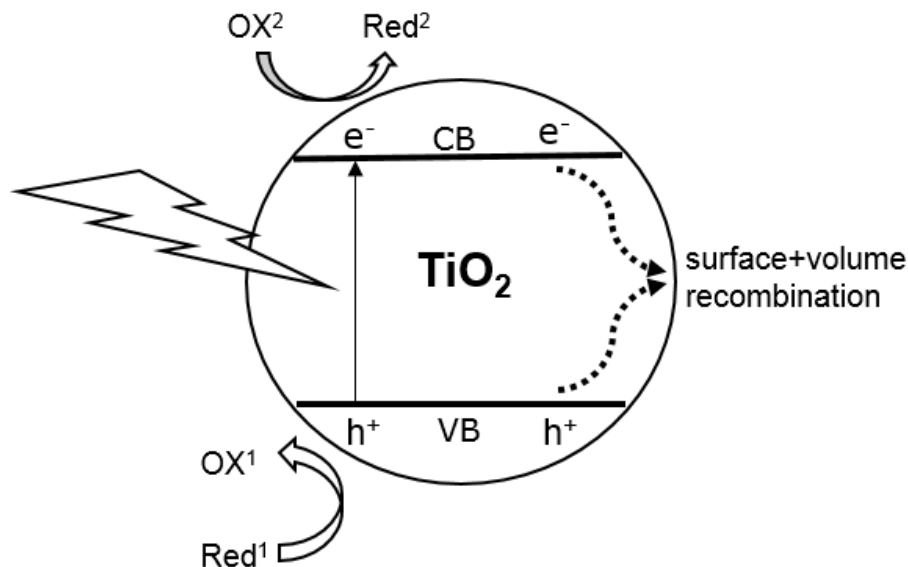
Figure 1 A schematic illustration of photocatalytic mechanism

As shown in figure 1, the photocatalytic reaction using semiconductor-based photocatalytic materials is usually composed of the following processes [20, 21]:

(1) Light absorption

(2) Migration of photogenerated charges

Photogenerated electrons and holes will have a certain lifetime once generated. With no external influence, a large part of the photo-generated electrons and holes will recombine, accompanied with an energy release. Only those electrons/holes with sufficient kinetic energy can successfully reach the photocatalyst surface and participate in the subsequent redox reactions, exhibiting photocatalytic ability. In addition, a considerable number of electrons/holes will be quenched by defects existing inside the crystal during the transfer process toward the surface.

(3) Participating in the photocatalytic reaction on the surface of catalysts

Electrons that successfully reach the surface of the photocatalyst are reductive so that they can participate in the reduction reaction on the catalyst surface. During the reaction, H^+ or CO_2

in the reaction system can be reduced to hydrogen gas or organic substance, respectively. While holes have strong oxidizing ability and can be used for degradation of organic pollutants, decomposing organic pollutants into small molecules like H_2O or CO_2, thereby contributing to the wastewater treatment.

Since the reactions mentioned in the above processes are completed in a very short time, the analysis of the specific mechanisms of the oxidation/reduction half reactions are difficult. Generally, during the reduction reaction process, the photogenerated charge carriers directly react with the species absorbed on the surface of the photocatalyst. For example, in the presence of sacrificial agents, photogenerated electrons directly react with H^+ ions in the reaction-system, forming the H_2 molecule. During the oxidation reaction process, the photogenerated holes firstly reach the surface of the catalyst and then react with small molecules, such as H_2O and O_2, forming free radicals such as $OH\bullet$ and $O_2^{\bullet-}$. The generated radicals usually have a relatively high oxidation potential, so that many organic substances can be oxidized and decomposed into small molecules. However, in the actual photocatalytic process, the two reaction mechanisms coexist.

For example, the corresponding reaction mechanism of the photocatalytic hydrogen production from methanol/water solution using TiO_2-based photocatalysts [22-24] can usually be expressed by the following formula:

$$TiO_2 + h\nu \rightarrow TiO_2\ (e^-,\ h^+) \qquad\qquad (1\text{-}1)$$

$$e^- + h^+ \rightarrow heat \qquad\qquad (1\text{-}2)$$

$$2H^+ + 2e^- \rightarrow H_2 \qquad\qquad (1\text{-}3)$$

$$2h^+ + CH_3OH \rightarrow CH_2O + 2H^+ \qquad\qquad (1\text{-}4)$$
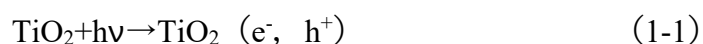
Herewith, the organic radical formed upon the one-hole oxidation of CH_3OH, such as hydroxyalkyl radical can inject an additional electron into the TiO_2 conduction band forming the respective aldehyde as stable product, i.e., CH_2O (this is the so-called current doubling effect, vide infra).

However, in recent years, by means of the isotope labeling method, researchers have found that the source of hydrogen ions reduced to hydrogen is not completely derived from water, a considerable part is the H^+ ion generated by the oxidation of the hole scavengers [25, 26]. The exact mechanism calls for further investigation.

The photocatalytic oxidation reaction of organic pollutants [27-29] can occur either *via* direct hole transfer or *via* the indirect reaction with the intermediates such as $\cdot OH$ radicals. The latter are formed either *via* oxidative pathway upon hole oxidation of surface bounded hydroxyl groups or water molecules or *via* reductive pathway upon electron reduction of adsorbed O_2. The corresponding reaction mechanism can be expressed as follows:

$$TiO_2 + h\nu \rightarrow TiO_2\ (e^-,\ h^+） \qquad (1\text{-}5)$$

$$TiO_2\ (h^+) + H_2O \rightarrow TiO_2 + \cdot OH + H^+ \qquad (1\text{-}6)$$

$$TiO_2(e^-) + O_2 \rightarrow TiO_2 + O_2^{\cdot -} \qquad (1\text{-}7)$$

$$H_2O + O_2^{\cdot -} \rightarrow HO_2\cdot + OH^- \qquad (1\text{-}8)$$

$$2HO_2\cdot \rightarrow H_2O_2 + O_2 \qquad (1\text{-}9)$$

$$H_2O_2 + O_2^{\cdot -} \rightarrow \cdot OH + OH^- + O_2 \qquad (1\text{-}10)$$

Organic pollutants $+ OH\cdot$ (or h^+) $\rightarrow$ degradation products v (1-11)
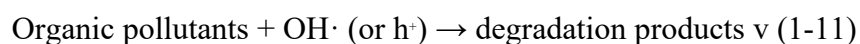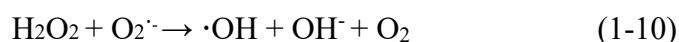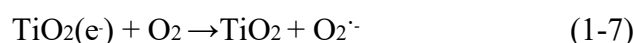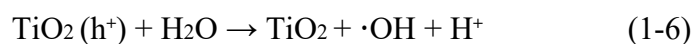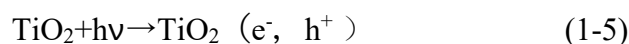
To better reveal the reaction mechanism, various techniques have been applied such as Laser flash photolysis [30] and Electron Paramagnetic Resonance (EPR) spectroscopy [31]. Besides, it has been reported that different indicators allow the detection of the intermediates and thus reveal the reaction mechanism [32, 33]. However, due to the complexity of

photocatalytic degradation of organic matter, the research of related mechanisms is poorly understood.

1.4 Catalytic Effect of Noble Metals on TiO_2 Photocatalysis

TiO_2 has been considered as one of the most promising photocatalyst materials. However, due to its wide band gap (3.2 eV), TiO_2 can only be excited by ultraviolet light with a wavelength below 387 nm. In addition, the fast recombination of the photogenerated electrons and holes also greatly limits the photocatalytic efficiency of TiO_2 [34]. In order to solve these problems and improve the efficiency of TiO_2-based photocatalytic materials to the level of industrial application, researchers have conducted extensive and in-depth researches through different ways. TiO_2-based photocatalytic materials can be modified via different approaches: metal/nonmetal ion doping, noble metal deposition, coupling with narrow band gap semiconductors, dye sensitization, et al. This work will focus on the noble metal deposition method and explore the underlying reaction mechanisms.

During the last decades, noble metal deposition method has been considered as a promising strategy to improve the photocatalytic hydrogen production efficiency of TiO_2-based photocatalysts. Due to the fast recombination of the photoexcited charge carriers, some organic compounds, such as alcohols (methanol, ethanol, etc.), organic acid (formic acid, acetic acid, etc.) and aldehydes (formaldehyde, acetaldehyde, etc.) have been used as hole scavengers [35, 36]. Among those hole scavengers, methanol is widely used in the photocatalytic hydrogen generation reactions. According to previous reports, the photocatalytic performance of TiO_2-based catalysts modified by noble metal deposition can be effectively improved [37, 38]. Presently, the commonly studied noble metals for TiO_2 modification are mainly Pt, Pd, Au, Ag, Ni, Rh and Cu. The noble metal deposited on the surface of TiO_2 can suppress the undesired-recombination reactions in TiO_2, thereby improving the photocatalytic efficiency. This can be

attributed to an electron transfer from the TiO_2 conduction band to the surface loaded metal nanoparticles. In the process, the loaded metal nanoparticles act as catalyst and a means to suppress the recombination of the photogenerated charge carriers [39, 40], as shown in figure 2.
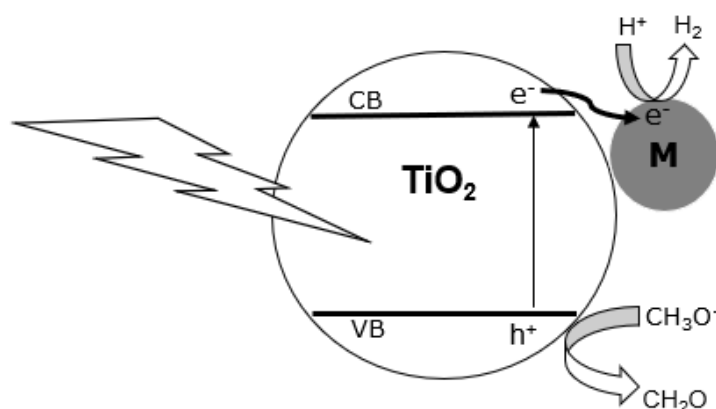
Figure 2. The electron transfer process for H_2 production using M-TiO_2 in water/methanol mixtures upon light illumination. (M=noble metal nanoparticles)

However, the modification with noble metals gained a lot of interest not only due to the catalytic role of the deposited nanoparticles, but also due to their unique optical property, known as surface plasmon resonance (SPR) effect. (The details will be elaborated later.) Some metal particles, such as Au, Ag, Cu, etc., have the SPR effect in the visible region, and thus can extend the photoresponse range of TiO_2-based photocatalyst to the visible region [3, 17, 41-47].

In addition, a large number of studies have shown that the properties of such composites are highly correlated with the composition, size, concentration, distribution, etc. of the deposited metal particles [48, 49, 50]. For example, too high concentration of metal particles on the TiO_2 surface can affect its optical properties and induce fast electron-hole recombination resulting in reduced photocatalytic efficiency [49].

1.5 Surface Plasmon Resonance (SPR) Effect on TiO$_2$ Photocatalysis

The surface plasmon resonance (SPR) is the coherent collective oscillation of free electrons in plasma metal nanoparticles in response to external oscillating electromagnetic fields (such as oscillating electromagnetic field caused by an external incident light). In particular, the electron cloud tends to be unevenly distributed near the plasmonic nanoparticles under the external oscillating electromagnetic field. Thus, a Coulomb restoring force is formed between the negatively charged electrons and the positively charged nuclei, leading to a series of electrons oscillations around the nucleus, similar to the oscillation of the tension spring. Therefore, an electric field opposite to the direction of the external electric field due to redistribution of charge density is formed [51]. Such oscillations and formed electric field are attributed to plasmon resonance phenomena [52, 53], as shown in figure 3.
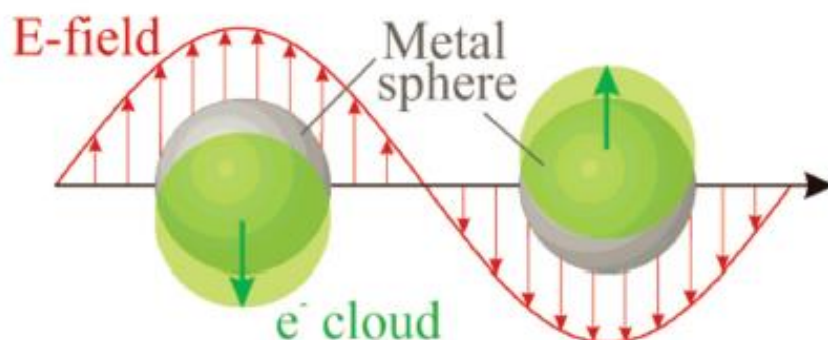
Figure 3 Schematic illustration of plasmon oscillation on a plasmonic metal sphere [53]

It has been proven, the electromagnetic field enhancement effect based on the excitation of localized surface plasmon resonance contributes not only to physical processes, such as excitation efficiency, but also to chemical processes, such as photoinduced electron transfer reactions [54].

SPR effect contributes to the enhanced photocatalytic hydrogen generation ability in visible wavelength range [17]. However, the mechanism of the SPR-driven photocatalytic H$_2$ production is still not yet fully understood, which should be interpreted clearly in further experimental and theoretical investigations [17, 55]. Taking Au-TiO$_2$ as a sample, there are two

well accepted mechanisms for explanation of the visible activity of Au-TiO$_2$ photocatalyst: direct electron transfer process (known as DET process) and resonance energy transfer process (known as RET process) [3, 17, 41-47]. The proposed mechanisms for SPR-induced H$_2$ production using Au-TiO$_2$ in water/methanol mixtures upon illumination are illustrated in figure 4:
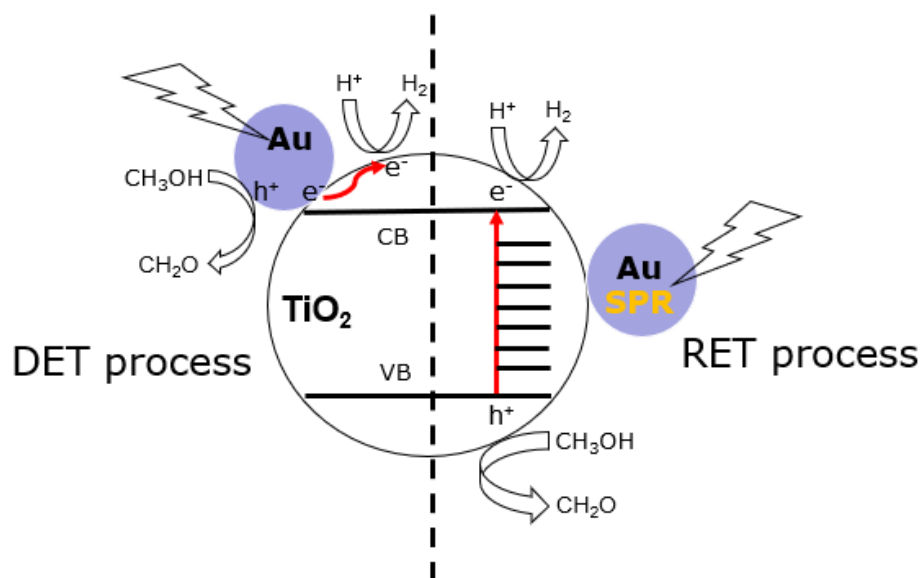
Figure 4. Two main proposed mechanisms for SPR-induced H$_2$ production using Au-TiO$_2$ in water/methanol mixtures under visible light illumination: direct electron transfer (DET) process (left); resonance energy transfer (RET) process (right)

The first mechanism known as resonance energy transfer (RET) is based on the idea that the SPR enhances the local electromagnetic field which in turn facilitates the generation of e$^-$/h$^+$ pairs near the semiconductor surface [3, 41, 42]; D. B. Ingram [41] and Z. W. She [42] proposed this mechanism according to their results based on finite-difference time-domain (FDTD) simulations and discrete-dipole approximation (DDA) simulations, respectively, yet without exhibiting any experimental evidence. In addition, K. Awazu [43] also obtained results supporting this mechanism when adding an insulating layer between the noble metal nanoparticles and the semiconductor. The second mechanism explains the visible activity of

Au-TiO$_2$ by the SPR-excited electron transfer from the Au nanoparticles to the conduction band of TiO$_2$, known as direct electron transfer (DET) [17, 44, 45, 46, 47, 56]. C. Gomes Silva [44] and coworkers proposed this mechanism based on the observation that Au-TiO$_2$ photocatalysts exhibit photocatalytic activity for H$_2$ evolution upon 532 nm laser illumination. Recently, J. B. Priebe *et al.* [17] provided experimental evidence for the DET mechanism based on results obtained employing electron paramagnetic resonance (EPR) spectroscopy.

However, both the two mechanisms have their own shortcomings. For example, the DET mechanism is based on the assumption that TiO$_2$ cannot absorb visible light ($\geq$ 400 nm) due to its wide band gap energy (E$_g$=3.2 eV). It is crucial to ensure that TiO$_2$ matrix cannot be excited by visible light ($\geq$ 400 nm), which has been long ignored in a lot of researches. In addition, there is also a big controversy existing in the RET mechanism. Since the plasmon band of Au nanoparticles is located above 500 nm, the energy of the light in this wavelength range is much lower than the band gap energy of TiO$_2$ (E$_g$=3.2 eV). Therefore, the SPR-energy is insufficient to lead to the generation of electron-hole pairs in TiO$_2$. This is inconsistent with previous reports that the SPR-powered bandgap breaking requires the energy of the surface plasmon to equal to or larger than the bandgap of the semiconductor [57, 58]. Hence, K. Ueno [54] suggested that a detailed mechanism must be elucidated to determine how the electron transfer reaction occurred or how a hole was recovered. Therefore, the relevant research mechanism calls for further investigation [59, 60].

1.6 Scope of the Thesis

Although the topic has been extensively investigated for decades, there are still some related problems remain unclear and call for further investigation. In the present work, the role of Au loading for visible light photocatalytic activity and the Au-SPR driven photocatalytic H$_2$ production of Au-TiO$_2$ were investigated. The underlying reaction mechanisms were discussed.

To reveal the role of Au loading for visible light photocatalytic activity, Au-TiO$_2$ (UV100) photocatalyst was prepared and the visible light photocatalytic H$_2$ production rates of bare TiO$_2$ and Au-TiO$_2$ were measured employing different wavelength cutoff filters (i.e., 420 nm and 500 nm filters). In some literatures, researchers observed the visible light photocatalytic H$_2$ production ability and related this visible light photocatalytic activity to the Au-SPR effect, while employing a 400 nm/420 nm cutoff filter. However, it is neglected that even pure anatase TiO$_2$ absorbs slightly around 420 nm due to pre-existing defects in its crystal structure. In the thesis, the goal of using different wavelength light illumination is to confirm the excitation wavelength of bare TiO$_2$ and Au loaded TiO$_2$, as well as clarify the origin of the photo-induced charge carriers and the corresponding transfer process.

The Au-SPR driven photocatalytic H$_2$ production ability of Au-TiO$_2$, employing commercial P25 as TiO$_2$ matrix, was investigated. As the origin of the photoinduced electrons and holes upon visible light illumination is still controversially discussed. By means of EPR and laser flash photolysis with different wavelength light illumination and laser beam excitation, the excitation process can be studied. Besides, for a better understanding of the electron transfer process in the Au-TiO$_2$ system upon visible light illumination, the DFT calculation was applied.

In addition, the most extensively investigated noble metals (e.g. Au and Ag) are too expensive. Therefore, they are not suitable for large-scale industrial applications. Thus, low cost plasmonic metals should be discovered for further utilization. Copper, as one of the most abundantly used metal due to its conductivity and low cost, has been reported to exhibit excellent surface plasmon resonance effect. Therefore, the Cu-SPR enhanced photocatalytic H$_2$ production ability has been investigated and a reasonable mechanism was provided.

As known, Cu nanoparticles are not as stable as Au nanoparticles and are easy to be oxidized. As a result, copper oxides exist in the Cu-TiO$_2$ photocatalysts, which will directly affect the photocatalytic H$_2$ production ability of Cu-TiO$_2$ upon visible light illumination.

Therefore, the impact of copper oxides and copper nanoparticles should be revealed. In addition, the underlying reaction mechanism of Cu-SPR driven photocatalytic reaction is still under debate. The work also aims to provide some insights on the mechanism of the enhanced visible light photocatalytic H_2 production ability of Cu-TiO$_2$ photocatalysts.

The photocatalytic performances of the TiO$_2$ based photocatalysts, the influencing factors and the underlying mechanisms are the research emphasis of this thesis. The aim of the work is to provide some clear experimental evidences and DFT calculation results that can contribute to the existing research controversies.

The above-mentioned tasks of the thesis can contribute to a better understanding of the SPR enhanced photocatalytic reactions of the noble metal loaded TiO$_2$ photocatalysts and provide a new horizon for further investigations on exploring more effective visible light harvesting photocatalysts for solar energy conversion.

1.7 References

[1] J. Schneider, M. Matsuoka, M. Takeuchi, J. Zhang, Y. Horiuchi, M. Anpo, D. W. Bahnemann, Understanding TiO$_2$ photocatalysis: mechanisms and materials, Chem. Rev. 2014, 114, 9919−9986. Doi: 10.1021/cr5001892.

[2] M. G. Walter , E. L. Warren , J. R. McKone , S. W. Boettcher , Q. Mi , E. A. Santori , N. S. Lewis, Solar water splitting cells. Chem. Rev. 2010, 110(11), 6446-6473. Doi: 10.1021/cr1002326

[3] S. K. Cushing, J. Li, F. Meng, T. R. Senty, S. Suri, M. Zhi, M. Li, A. D. Bristow, N. Wu, Photocatalytic activity enhanced by plasmonic resonant energy transfer from metal to semiconductor, J. Am. Chem. Soc. 2012, 134, 15033−15041. Doi: 10.1021/ja305603t

[4] Chen, X. B.; Shen, S. H.; Guo, L. J.; Mao, S. S. Semiconductor-based Photocatalytic Hydrogen Generation, Chem. Rev. 2010, 110, 6503-6570. Doi: 10.1021/cr1001645.

[5] A. Fujishima, X. Zhang, D. A. Tryk, TiO$_2$ photocatalysis and related surface phenomena, Surf. Sci. Rep. 2008, 63, 515-582. Doi: 10.1016/j.surfrep.2008.10.001.

[6] K. Maeda, K. Domen, Photocatalytic water splitting: Recent progress and future challenges. J. Phys. Chem. Lett. 2010, 1, 2655-2661. Doi:10.1021/jz1007966.

[7] S. Kato, F. Masuo, Titanium dioxide-photocatalyzed oxidation. I. Titanium dioxide-photocatalyzed liquid phase oxidation of tetralin. Kogyo Kagaku Zasshi 1964, 67, 42–50.

[8] A. Fujishima, K. Honda, Electrochemical photolysis of water at a semiconductor electrode. Nature 1972, 238, 37-38. Doi: 10.1038/238037a0

[9] J. Lee, H. S. Shim, M. Lee, J. K. Song, D. Lee, Size-controlled electron transfer and photocatalytic activity of ZnO-Au nanoparticle composites. The Journal of Physical Chemistry Letters. 2011, 2(22): 2840-2845. Doi:10.1021/jz2013352

[10] Y. Miseki, H. Kusama, H. Sugihara and K. Sayama, Cs-modified WO_3 photocatalyst showing efficient solar energy conversion for O_2 production and Fe (III) ion reduction under visible light. The Journal of Physical Chemistry Letters. 2010, 1(8): 1196-1200. Doi:10.1021/jz100233w

[11] C. C. Nascimento, G. R. S. Andrade , E. C. Neves, C. L. P. Costa, L. S. Barreto, I. F. Gimenez, Nanocomposites of CdS nanocrystals with montmorillonite functionalized with thiourea derivatives and their use in photocatalysis. The Journal of Physical Chemistry C. 2012, 116(41): 21992-22000. Doi: 10.1021/jp3019556

[12] S. Usai, S. Obregón, Becerro A. I.Becerro, and G. Colón, Monoclinic-Tetragonal heterostructured $BiVO_4$ by Yttrium doping with improved photocatalytic activity. The Journal of Physical Chemistry C. 2013, 117(46): 24479-24484. Doi: 10.1021/jp409170y

[13] M. R. Hoffmann, S. T. Martin, W. Choi and D. W. Bahnemann, Environmental applications of semiconductor photocatalysis, Chem. Rev., 1995, 95, 69–96. Doi: 10.1021/cr00033a004

[14] A. A. Ismail, and D.W. Bahnemann, Photochemical splitting of water for hydrogen production by photocatalysis: a review, Solar Energy Materials and Solar Cells. 2014, 128, 85-101. Doi:10.1016/j.solmat.2014.04.037.

[15] M. A. Henderson. A surface science perspective on TiO_2 photocatalysis. Surface Science Reports. 2011, 66(6-7), 185-297. Doi: 10.1016/j.surfrep.2011.01.001.

[16] B. Drevillon. Spectroscopic ellipsometry in the infrared range. Thin Solid Films. 1998, 313-314, 625-630. Doi: 10.1016/S0040-6090(97)00968-1.

[17] J. B. Priebe, M. Karnahl, H. Junge, M. Beller, D. Hollmann, A. Brückner, Water reduction with visible light: synergy between optical transitions and electron transfer in Au-TiO$_2$ catalysts visualized by in situ EPR spectroscopy, Angew. Chem., Int. Ed. 2013, 52, 11420-11424.Doi:10.1002/anie.201306504.

[18] X. Chen and S. S. Mao, Titanium dioxide nanomaterials:synthesis，properties，modifications，and applications, Chem. Rev.2007, 107, 2891-2959. Doi: 10.102/cr0500535.

[19] P.Zhang, T. Wang, J. Gong, Mechanistic understanding of the plasmonic enhancement for solar water splitting, Adv. Mater. 27 (2015) 5328-5342. Doi:10.1002/adma.201500888.

[20] Y. Shiraishi, T. Hirai, Selective organic transformations on titanium oxide-based photocatalysts. Journal of Photochemistry and Photobiology C: Photochemistry Reviews. 2008, 9(4): 157-170. Doi: 10.1016/j.jphotochemrev.2008.05.001

[21] Y. Ma, X. Wang, Y. Jia, X.Chen, H. Han, and C. Li, Titanium dioxide-based nanomaterials for photocatalytic fuel generations. Chemical Reviews. 2014, 114(19): 9987-10043. Doi: 10.1021/cr500008u

[22] C. G. Silva, R. Juárez, T. Marino, R. Molinari, H. García, Influence of excitation wavelength (UV or visible light) on the photocatalytic activity of titania containing gold nanoparticles for the generation of hydrogen or oxygen from water, J. Am. Chem. Soc. 2011, 133, 595 – 602. Doi:10.1021/ja1086358

[23] J. J. Chen, J. C. S. Wu, P. C. Wu, D. P. Tsai, Plasmonic photocatalyst for H$_2$ evolution in photocatalytic water splitting. J. Phys. Chem. C 2011, 115, 210 – 216. Doi: 10.1021/jp1074048

[24] J. Sá, M. Fernández-García, J. A. Anderson, Photoformed electron transfer from TiO$_2$ to metal clusters. Catal. Commun. 2008, 9, 1991 – 1995. Doi:10.1016/j.catcom.2008.03.041

[25] T. A. Kandiel, I. Ivanova, and D. W. Bahnemann, Long-term investigation of the photocatalytic hydrogen production on platinized TiO$_2$: an isotopic study. Energy Environ. Sci., 2014, 7, 1420–1425. Doi:10.1039/C3EE41511B

[26] S. Hamid, I. Ivanova, T. H. Jeon, R. Dillert, W. Choi and D. W. Bahnemann, Photocatalytic conversion of acetate into molecular hydrogen and hydrocarbons over Pt/TiO$_2$: pH dependent formation of Kolbe and Hofer-Moest products. Journal of Catalysis. 2017, 349, 128–135. Doi: 10.1016/j.jcat.2017.02.033

[27] I. K. Konstantinou, T. A. Albanis, TiO$_2$-assisted photocatalytic degradation of azo dyes in aqueous solution: kinetic and mechanistic investigations. Applied Catalysis B: Environmental. 2004, 49(1): 1-14. Doi:10.1016/j.apcatb.2003.11.010

[28] A. L. Linsebigler, G. Lu, J. T. Yates, Photocatalysis on TiO$_2$ surfaces: principles, mechanisms, and selected results. Chemical Reviews. 1995, 95(3): 735-758. Doi:10.1021/cr00035a013

[29] A. Mills, R. H. Davies, D. Worsley, Water purification by semiconductor photocatalysis. Chemical Society Reviews. 1993, 22(6): 417-425. Doi:10.1039/CS9932200417

[30] A. Furube, T. Asahi, H. Masuhara, H. Yamashita, and M. Anpo, Charge carrier dynamics of standard TiO$_2$ catalysts revealed by femtosecond diffuse reflectance spectroscopy. J. Phys. Chem. B, 1999, 103 (16), pp 3120–3127. Doi: 10.1021/jp984162h

[31] Z. Wang, W. Ma, C. Chen, H. Ji, J.Zhao, Probing paramagnetic species in titania-based heterogeneous photocatalysis by electron spin resonance (ESR) spectroscopy—A mini review. Chemical Engineering Journal. 2011, 170(2-3): 353-362. Doi: 10.1016/j.cej.2010.12.002

[32] H. Czili, A. Horváth, Applicability of coumarin for detecting and measuring hydroxyl radicals generated by photoexcitation of TiO$_2$ nanoparticles. Applied Catalysis B: Environmental. 2008, 81(3-4): 295-302. Doi: 10.1016/j.apcatb.2008.01.001

[33] A. Y. Ahmed, T. A. Kandiel, T. Oekermann, D. W. Bahnemann, Photocatalytic activities of different welldefined single crystal TiO$_2$ surfaces: anatase versus rutile, The Journal of Physical Chemistry Letters. 2011, 2(19): 2461-2465. Doi: 10.1021/jz201156b

[34] S. G. Kumar, L. G. Devi, Review on modified TiO$_2$ photocatalysis under UV/visible light: selected results and related mechanisms on interfacial charge carrier transfer dynamics. J. Phys. Chem. A, 2011, 115 (46), 13211–13241. Doi: 10.1021/jp204364a

[35] X. Chen, S. Shen, L. Guo, S. S. Mao, Semiconductor-based photocatalytic hydrogen generation. Chem. Rev. 2010, 110 (11), 6503-6570. Doi: 10.1021/cr1001645

[36] T. A. Kandiel, I. Ivanova, and D. W. Bahnemann, Long-term investigation of the photocatalytic hydrogen production on platinized TiO$_2$: an isotopic study. Energy Environ. Sci. 2014, 7, 1420–1425. Doi:10.1039/c3ee41511b

[37] H. Kisch, L. Zang, C. Lange, W. F. Maier, C. Antonius, D. Meissner, Modified, amorphous titania-a hybrid semiconductor for detoxification and current generation by visible light. Angew. Chem. Int. Ed. 1998, 37, 3034-3036. Doi:10.1002/(SICI)1521-3773(19981116)37:21<3034::AID-ANIE3034>3.0.CO;2-2

[38] N. N. Binitha, Z. Yaakob, M. R. Reshmi, S. Sugunan, V. K. Ambili, A. A. Zetty, Preparation and characterization of nano silver-doped mesoporous titania photocatalysts for dye degradation. Catalysis Today 2009, 147, S76-S80. Doi: 10.1016/j.cattod.2009.07.014

[39] A. Kudo, and Y. Miseki, Heterogeneous photocatalyst materials for water splitting. Chem. Soc. Rev. 2009, 38, 253−278. Doi:10.1039/B800489G

[40] J. Sáa, M. Fernández-García, J. A. Andersona, Photoformed electron transfer from TiO_2 to metal clusters. Catalysis Communications. 2008, 9, 1991-1995. Doi:10.1016/j.catcom.2008.03.041

[41] a) D. B. Ingram, S. Linic, Water splitting on composite plasmonic-metal/semiconductor photoelectrodes: evidence for selective plasmon-induced formation of charge carriers near the semiconductor surface. J. Am. Chem. Soc. 2011, 133, 5202−5205. Doi:10.1021/ja200086g; b) S. Linic, P. Christopher, D. B. Ingram, Plasmonic-metal nanostructures for efficient conversion of solar to chemical energy. Nature Materials. 2011, 10, 911-921. Doi: 10.1038/NMAT3151

[42] Z. W. Seh, S. Liu, M. Low, S. Y. Zhang, Y. Liu, Z. Liu, A. Mlayah, M-Y. Han, Janus Au-TiO_2 photocatalysts with strong localization of plasmonic near-fields for efficient visible-light hydrogen generation. Adv. Mater. 2012, 24, 2310–2314. Doi: 10.1002/adma.201104241

[43] K. Awazu, M. Fujimaki, C. Rockstuhl, J. Tominaga, H. Murakami, Y. Ohki, N. Yoshida, T. Watanabe, A plasmonic photocatalyst consisting of silver nanoparticles embedded in titanium dioxide. J. Am. Chem. Soc. 2008, 130, 1676-1680. Doi: 10.1021/ja076503n

[44] C. G. Silva, R. Juárez, T. Marino, R. Molinari, H. García, Influence of excitation wavelength (UV or visible light) on the photocatalytic activity of titania containing gold nanoparticles for the generation of hydrogen or oxygen from water J. Am. Chem. Soc. 2011, 133, 595– 602. Doi:10.1021/ja1086358

[45] K. Qian, B. C. Sweeny, A. C. Johnston-Peck, W. Niu, J. O. Graham, J. S. DuChene, J. Qiu, Y.-C. Wang, M. H. Engelhard, D. Su, E. A. Stach, W. D. Wei, Surface plasmon-driven water reduction: gold nanoparticle size matters. J. Am. Chem. Soc. 2014, 136, 9842−9845. Doi:10.1021/ja504097v

[46] Z. Bian, T. Tachikawa, P. Zhang. M. Fujitsuka, T. Majima, Au/TiO$_2$ Superstructure-based plasmonic photocatalysts exhibiting efficient charge separation and unprecedented activity. J. Am. Chem. Soc. 2014,136, 458-465. Doi: 10.1021/ja410994f

[47] Z. Liu, W. Hou, P. Pavaskar, M. Aykol, S. B. Cronin, Plasmon resonant enhancement of photocatalytic water splitting under visible illumination. Nano Lett. 2011, 11 (3), 1111–1116. Doi; 10.1021/nl104005n

[48] M. Turner, V. B. Golovko, O. P. H. Vaughan, P. Abdulkin, A. Berenguer-Murcia, M. S. Tikhov, B. F. G. Johnson, R. M. Lambert, Selective oxidation with dioxygen by gold nanoparticle catalysts derived from 55-atom clusters. Nature 2008, 454 (7207), 981-983. Doi:10.1038/nature07194

[49] S. Sakthivel, M. V. Shankar, M. Palanichamy, B. Arabindoo, D. W. Bahnemann, V. Murugesan, Enhancement of photocatalytic activity by metal deposition: characterisation and photonic efficiency of Pt, Au and Pd deposited on TiO$_2$ catalyst. Water Research 2004, 38 (13), 3001-3008. Doi:10.1016/j.watres.2004.04.046

[50] Y. Gao, W. Nie, Q. Zhu, X. Wang, S. Wang, F. Fan, C. Li, The polarization effect in surface-plasmon-induced photocatalysis on Au/TiO$_2$ nanoparticles. Angew. Chem., Int. Ed., 2020, *59* (41), 18218-18223. Doi: 10.1002/ange.202007706

[51] K. L. Kelly, E. Coronado, L. L. Zhao, G. C. Schatz, The optical properties of metal nanoparticles: the influence of size, shape, and dielectric environment, J. Phys. Chem. B, 2003, 107 (3), 668–677. Doi: 10.1021/jp026731y

[52] S. C. Warren, E. Thimsen , Plasmonic solar water splitting, Energ. Environ. Sci. 2012, 5, 5133-5146. Doi: 10.1039/c1ee02875h.

[53] P. Zhang , T. Wang , J. Gong, Mechanistic understanding of the plasmonic enhancement for solar water splitting, Adv. Mater. 2015, 27, 5328–5342. Doi: 10.1002/adma.201500888.

[54] K. Ueno, H. Misawa, Surface plasmon-enhanced photochemical reactions, Journal of Photochemistry and Photobiology C: Photochemistry Reviews. 2013, 15, 31–52. Doi: 10.1016/j.jphotochemrev.2013.04.001

[55] Z. Zhang, P. Xu, X. Yang , W. Liang , M. Sun, Surface plasmon-driven photocatalysis in ambient, aqueous and high-vacuum monitored by SERS and TERS, Journal of Photochemistry and Photobiology C: Photochemistry Reviews. 2016, 27, 100–112. Doi:10.1016/j.jphotochemrev.2016.04.001

[56] M. Radzig, O. Koksharova, I. Khmel, V. Ivanov, K. Yorov, J. Kiwi, S. Rtimi, E. Tastekova, A. Aybush, V. Nadtochenko, Femtosecond spectroscopy of Au hot-electron injection into TiO_2: evidence for Au/TiO_2 plasmon photocatalysis by bactericidal Au Ions and related phenomena, Nanomaterials. 2019, 9(2), 217, Doi: 10.3390/nano9020217

[57] X. Zhang, Y. L. Chen, R. Liu, D. P. Tsai, Plasmonic photocatalysis, Rep. Prog. Phys. 2013, 76, 046401-046441. Doi:10.1088/0034-4885/76/4/046401

[58] T. Torimoto, H. Horibe, T. Kameyama, K. Okazaki, S. Ikeda, M. .Matsumura, A. Ishikawa, H. Ishihara, Plasmon-enhanced photocatalytic activity of cadmium sulfide nanoparticle immobilized on silica-coated gold particles, J. Phys. Chem. Lett. 2011, 2 (16), 2057–2062. Doi: 10.1021/jz2009049

[59] C. W. Moon, M. Choi, J. K. Hyun, H. W. Jang, Enhancing photoelectrochemical water splitting with plasmonic Au nanoparticles. Nanoscale Adv. 2021, 3, 5981–6006. Doi: 10.1039/d1na00500f

[60] A. P. Manuel, K. Shankar, Hot electrons in TiO_2–noble metal nano-heterojunctions: fundamental science and applications in photocatalysis. Nanomaterials. 2021, 11 (5) , 1249. Doi: 10.3390/nano11051249

Chapter 2

The role of Au loading for visible-light photocatalytic activity of Au-TiO₂ (anatase)

Jinlin Nie, Jenny Schneider, Fabian Sieland, Shuwei Xia, and Detlef W. Bahnemann

Chapter 2. The role of Au loading for visible-light photocatalytic activity of Au-TiO₂ (anatase)

2.1 Abstract:

Plasmonic photocatalysis has recently accelerated the rapid progress in enhancing photocatalytic efficiency upon visible light illumination, increasing the prospect of utilizing sunlight for environmental and energy applications. It has been reported that $Au-TiO_2$ photocatalysts exhibit photocatalytic activity for H_2 evolution under visible light illumination above 420 nm. This visible-light photocatalytic activity was attributed to the surface plasmon resonance (SPR) effect of the Au nanoparticles and the underlying mechanism has been discussed between the direct electron transfer (DET) process and resonance energy transfer (RET) process. However, most of the experiments have been reported to employ a 420 nm cutoff filter which indeed covers the absorbance tail of TiO_2. In this contribution, it was confirmed that photocatalytic H_2 gas formation over $Au-TiO_2$ (anatase) can be obtained upon visible light illumination near the absorption edge of TiO_2 (using a 420 nm filter). By means of EPR spectroscopy and Laser flash photolysis, we obtained direct experimental evidence that bare anatase TiO_2 can be excited by visible light illumination at 420 nm and excited-state electrons migrate to the surface-loaded Au nanoparticles. In the presence of a 500 nm cutoff filter, however, no SPR-induced H_2 formation was detected, although the plasmon band maximum of Au was completely illuminated. The obtained results revealed the catalytic role of Au on $Au-TiO_2$ for H_2 evolution upon visible light illumination ($\geq$ 420 nm), employing pure anatase as TiO_2 source.

2.2. Introduction

Energy and environmental crises are presently some of the most serious global issues [1,2]. Solar energy, as a clean and abundant energy source [3], can only be fully exploited when it can be stored and released on demand [4-6]. Since 1969 [7], TiO_2 has been recognized as one of the most widely used photocatalysts which shows relatively good photoelectrochemical solar-

energy conversion properties [8], as it is environmentally friendly, affordable, stable, and active [9]. However, due to a critical factor, that is the fast recombination of the photo-excited electrons and holes, the photocatalytic efficiency of TiO_2 is limited. Besides this drawback, due to its wide band gap, pure TiO_2 absorbs only UV light which accounts for less than 5 % of the total solar radiation reaching the earth's surface.[3] For practical applications catalysts are required, however, to work efficiently under visible light illumination composing nearly half of the solar spectrum [10].

Hence, it is important to discover new approaches to design more efficient catalysts which can resolve the above-mentioned obstacles. One of the most promising approaches is the deposition of noble metal nanoparticles (*e.g.*, Au, Ag, Pd) on the TiO_2 surface. The unique optical properties of these noble metal nanoparticles, namely the surface plasmon resonance (SPR), enables TiO_2-based photocatalysts to respond to visible light, as well as to improve the charge carrier separation [10a]. The SPR effect refers to the coherent collective oscillation of free electrons in the vicinity of noble metal nanoparticles in response to an external oscillating electric field, such as that provided by the incident light illumination [6,11].

SPR of noble metals loaded on the TiO_2 photocatalyst has been reported to enhance the photocatalytic activity for environmental and energy applications such as waste water treatment, water splitting and air purification upon visible light illumination [12-15]. For example, there are some reports demonstrating hydrogen production from methanol/water mixtures employing Au-TiO_2 as a photocatalyst [9,10,15]. However, a lot of literatures [10,16,17,18,19] relate this visible light photocatalytic activity to the SPR effect of Au, while employing a 400 nm/420 nm cutoff filter. It is neglected that even pure anatase TiO_2 absorbs slightly around 420 nm due to pre-existing defects in its crystal structure. Anatase/rutile mixtures or pure rutile TiO_2 show even stronger absorbance at around 420 nm. Obviously, for a better design of more efficient visible light harvesting photocatalysts, the exact role of Au and its influence on the formation

of charge carriers in TiO_2 upon visible light illumination ($\geq$ 420 nm) should be derived by more detailed investigations.

Hence, in the present work, EPR spectroscopy was applied to monitor the species formed following the trapping process of the photoinduced electrons and holes. Moreover, as a time-resolved analysis method, Laser flash photolysis was performed simultaneously to investigate the transient absorption of the species induced by the electrons generated in bare TiO_2 and in Au modified TiO_2 photocatalysts at different excitation wavelength. In this contribution, the typical commercial photocatalyst, that is Huntsman Hombikat UV100 consisting of 100% anatase, which is known to exhibit pronounced photocatalytic activity, has been selected as the TiO_2 source. Besides, in contrast to the most previous studies (only using a 420 nm cutoff filter), a 500 nm cutoff filter was utilized to totally eliminate the influence of the electrons generated inside TiO_2, since anatase TiO_2 absorbs slightly above 400 nm due to pre-existing defects. Hence, a combination of different spectroscopic methods applied in the present study enables the elucidation of the reaction mechanism initiated upon illumination at $\lambda \geq$ 420 nm.

2.3 Materials and Methods

2.3.1 Photocatalyst Preparation

Au nanoparticles were synthesized by the sodium citrate reduction method [20] in which $HAuCl_4 \cdot 3H_2O$ (1 mL 0.05 M) solution was added to 99 mL distilled water and heated to boiling with vigorous stirring. After 30 min of boiling sodium citrate solution (10mL, 1wt%, Aldrich, >99%) was added quickly. A stable deeply red colored colloidal gold suspension (5 x 10^{-4} M) was produced.

Au-SiO$_2$ was prepared by depositing the prepared Au nanoparticles on the surface of fumed SiO$_2$. Herewith, 1.0 g SiO$_2$ (Aldrich, >99.8%) were added to the above described colloidal gold solution (100 mL, 5×10^{-4} M) and stirred for 2 h, followed by rotary evaporation.

Au-TiO$_2$ photocatalysts consisting of 1 wt% gold on TiO$_2$ (Hombikat UV100, 100% anatase, Sachtleben Chemie) were prepared by the typical sol immobilization (labeled as SIM) method [10], which was conducted by adding an aqueous solution of poly vinyl alcohol (PVA) (1.2 mL, 1wt % sol., Aldrich, >99%) to 1 mL HAuCl$_4$.3H$_2$O (0.05 M). A freshly prepared NaBH$_4$ solution (2.5 mL, 0.1 M, Aldrich, >96%) was added dropwise to the above solution, with the color turning dark. After 30 min, the TiO$_2$ support (1.0 g) was added and the suspension was further stirred for 12 h at 25 °C.

All samples were centrifuged, washed three times with distilled water and dried for 12 h at 70 °C. The as-prepared samples were used for catalytic and spectroscopic experiments without any other treatment.

2.3.2 Material Characterization

The UV-Vis absorption spectra were recorded employing a UV-Visible spectrophotometer (Varian Cary 100 Bio). TEM images were characterized by Transmission Electron Microscopy (TEM) (FEI Tecnai G2 F20 TMP) using a 200 kV field emission gun (FEG).

2.3.3 Photocatalytic H$_2$ Evolution Test

The photocatalytic hydrogen production experiments were conducted under argon atmosphere in a double-wall quartz glass reactor, with a cooling system (Julabo) maintaining the temperature at 20 °C. The 1 g/L photocatalyst suspensions were prepared by suspending Au (1 wt%)/TiO$_2$ in CH$_3$OH/water mixtures (volume ratio 1:5). The suspension was transferred into the reactor and flushed with argon for 1 h to remove gases dissolved in the suspension and to make sure that Ar remained in the headspace of the reactor. After this treatment no signals

for other gases were detected by GC/TCD analysis. Afterwards, the photocatalytic experiments were carried out under UV-Vis or visible light illumination, respectively, using a 450 W Xe-lamp (Muller) and solar light (Hoenle SOL 1200) in the absence and in the presence of 420 nm and 500 nm cutoff filters, respectively. During the illumination process, the gas samples were taken continuously to determine the evolved gases with a Gas Chromatograph (GC) (Shimadzu GC-8A)/Thermal Conductivity Detector (TCD).

2.3.4 Electron Paramagnetic Resonance (EPR) Spectroscopy

EPR measurements were carried out with a MiniScope MS400 spectrometer (Magnettech GmbH, Germany). A 450 W Xe-Lamp (Muller) equipped with an optical cutoff filter (GC420/GC500) enables the illumination in the UV-Vis and Visible light region. For low temperature measurements (90 K), the samples were placed in X-Band standard EPR tubes (Wilmad, 2 mm, O.D.) and cooled with a commercial EPR cold finger quartz Dewar by applying liquid nitrogen. The g values were calculated with the formula $h\nu = g\beta B_0$ (B_0 – external magnetic field, β – Bohr magneton, g_e – Landé g-factor) as described in the literature [10a]. The frequency was at around 9.42 GHz, and the B_0 was varied between 305 mT-365 mT.

2.3.5 Laser Flash Photolysis

During the laser flash photolysis measurements the samples were excited with an Nd-YAG laser (Brilliant B, Quantel) and the spectra were monitored by a laser flash photolysis spectrometer (LKS 80, Applied Photophysics). The excitation wavelength was tuned in the visible wavelength (420 and 530 nm) by employing an Optical Parametric Oscillator (OPO) (MagicPRISM, OPOTEK Inc.). Together with the OPO the 3rd harmonic (355 nm) of the Brilliant B laser was used to generate the visible light pulses with 6 mm diameter and 6 ns pulse length. All experiments were performed in diffuse reflectance mode, where the analyzing light (supplied by a 150 W xenon arc lamp) was focused onto the sample and the reflected light was guided through the monochromator into the detector (Hamamatsu R928 photomultiplier). The

light level detected by the oscilloscope was kept at 100 mV for all measurements to compensate the wavelength dependent sensitivity. Furthermore, all examinations were conducted under N_2 atmosphere and 12 shots were averaged for every transient. The energy density of the laser beam was 5 mJ/cm² per shot. The transient absorption change in reflectance ΔJ was calculated from the absorbance values according to the literature [21], which also provides more detailed information about the set-up.

2.4. Results

2.4.1 Material Characterization

Figure 1a and Figure 1b show the transmission electron microscopy (TEM) images of Au-TiO_2. As can be seen, the dark particles in the TEM images are the Au nanoparticles. The TEM images of Au-TiO_2 reveal that the Au nanoparticles are well dispersed in the TiO_2 matrix exhibiting particle sizes between 5 nm and 8 nm. The particle size of TiO_2 is relatively ambiguous, but comparable with that of Au nanoparticles, that is between 7 nm and 10 nm.
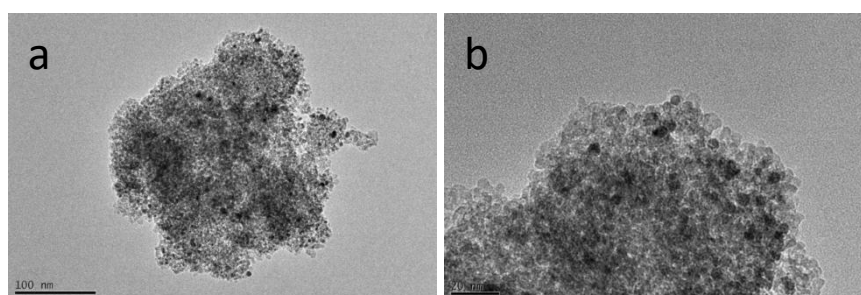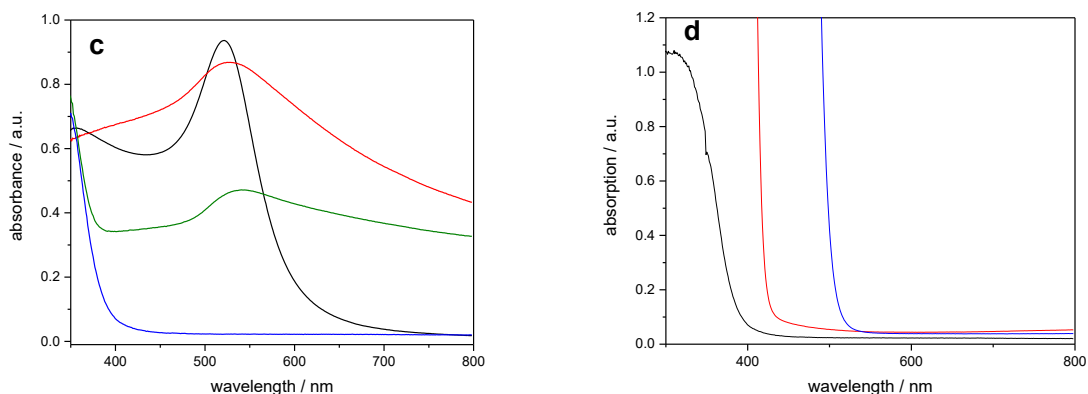
Figure 1. a, b) TEM images of Au(1 wt%)-TiO$_2$; c) Diffuse-Reflectance UV-Vis spectra of Au NPs (black), Au-TiO$_2$ (green), Au-SiO$_2$ (red), and of bare anatase TiO$_2$ (blue); d) The UV-Vis spectra of bare anatase TiO$_2$ and of the employed 420 nm (red) and 500 nm cutoff filters (blue).

In this study, the optical properties of Au nanoparticles, bare anatase TiO$_2$, Au-TiO$_2$, and Au-SiO$_2$ were characterized by UV-Vis spectroscopy. As Figure 1c shows all Au-related samples exhibit plasmon band maxima located above 500 nm, namely Au nanoparticles with λ_{max} at 522 nm, Au-TiO$_2$ with λ_{max} at 545 nm, and Au-SiO$_2$ with λ_{max} at 525 nm, respectively. The absorption edge of bare anatase TiO$_2$ is located around 400 nm, which is in good agreement with previous studies [10b]. Owing to the large band gap of SiO$_2$ (> 8 eV), it exhibits no photocatalytic activity upon excitation with UV-Vis light in the wavelength range above 200 nm, therefore, it has been selected as a photocatalytically inert support. Au-SiO$_2$ was prepared to evaluate the photocatalytic activity of Au nanoparticles, since it is claimed that due to the charge carrier separation in Au, the formed holes can oxidize methanol, while the electrons are transferred to TiO$_2$ [10]. The electron transfer to SiO$_2$ is thermodynamically not feasible thus proton reduction to form molecular hydrogen by the hot electrons is the expected reaction. Figure 1d presents the spectra of bare anatase TiO$_2$ and of the employed filters which clearly shows that bare anatase TiO$_2$ exhibits an absorption tail at around 420nm, and no absorption above 500 nm.

2.4.2 Photocatalytic H_2 Evolution Test

Table 1: Photocatalytic H_2 evolution rates from CH_3OH/H_2O mixtures (1:5, v:v) measured under UV-Vis and visible-light illumination employing different photocatalysts.

Catalyst	H_2 evolution rate / $mmolg^{-1}h^{-1}$		
--	UV-Vis	Vis ($\geq$ 420 nm)	Vis ($\geq$ 500 nm)
TiO_2	0.41	0	0
Au NPs	0	0	0
Au-TiO_2	31.22	0.40	0
Au-SiO_2	0	0	0

Table 1 presents the photocatalytic H_2 evolution rates from CH_3OH/H_2O mixtures obtained employing Au nanoparticles, bare and Au-loaded TiO_2, as well as Au-SiO_2 under UV-Vis and visible-light illumination. As shown, pure anatase TiO_2 can generate H_2 only upon UV-Vis illumination. For pure Au nanoparticles and Au loaded on SiO_2 no signal indicating H_2 formation was observed within the UV to visible wavelength range. Upon illumination above 420 nm, H_2 formation has only been detected employing Au-TiO_2 as the photocatalyst.

Furthermore, according to the UV-Vis spectrum shown in Figure 1c, bare anatase TiO_2 absorbs slightly around 420 nm due to pre-existing defects in its crystal structure. Avoiding the contribution of bare TiO_2, a 500 nm cutoff filter was utilized. It should be noted here, that in the respective literature [3,8,10,17,18,19], such a 500 nm cutoff filter has rarely been applied. When the 420 nm cutoff filter was replaced by the 500 nm cutoff filter, no formation of H_2 was detected for the Au-TiO_2 photocatalyst within the detection limit, even when the illumination time was extended to 24 h.
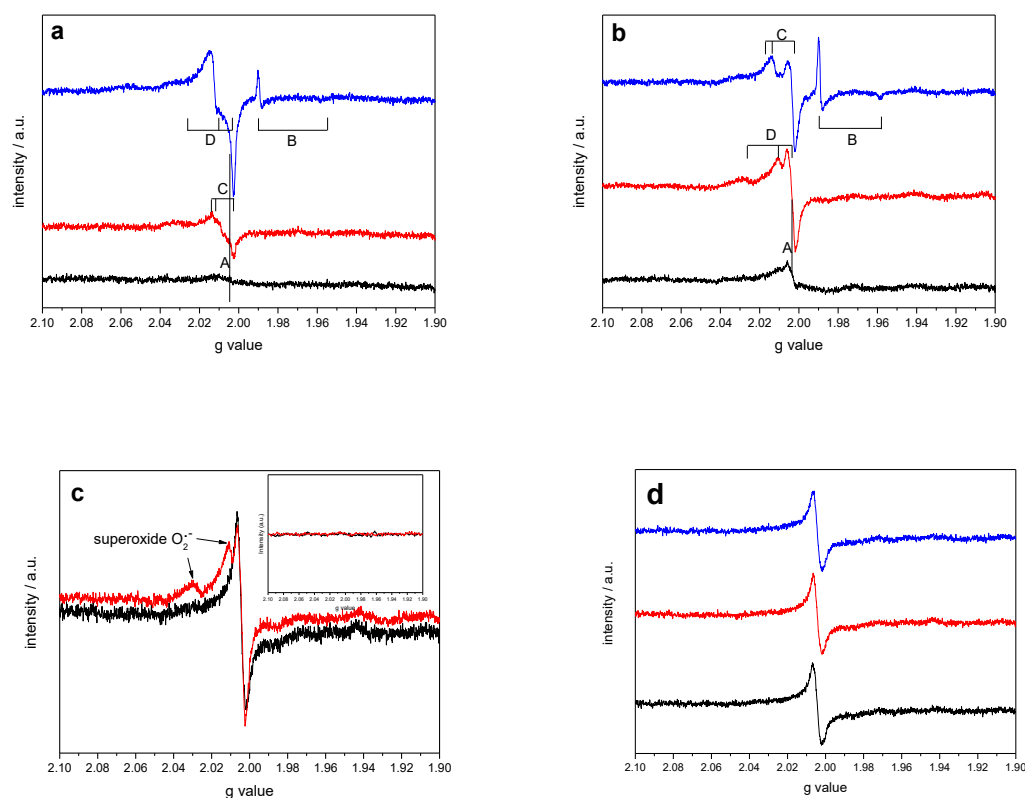
2.4.3 EPR Analysis

Figure 2. a) EPR spectra of bare anatase TiO_2 obtained in the dark (black), under visible light illumination above 420 nm (red) and under UV-Vis illumination (blue) in air at 90 K; b) EPR spectra of $Au-TiO_2$ obtained in the dark (black), under visible light illumination above 420 nm (red) and under UV-Vis illumination (blue) in air at 90 K; c) EPR spectra of $Au-TiO_2$ and $Au-SiO_2$ (inset) under visible light illumination ($\geq$ 420 nm) obtained under Ar (black) and in O_2 (red) at 90 K; d) EPR spectra of $Au-TiO_2$ measured at different conditions: in the dark in Ar (black), under visible light illumination ($\geq$ 500 nm) obtained in Ar (red) and in O_2 (blue) at 90 K.

The photoinduced EPR signals of trapped electrons and holes for bare anatase TiO_2 and $Au-TiO_2$ were recorded in air at 90 K. As shown in Figure 2a and Figure 2b, upon both, UV-Vis and pure visible light illumination electrons trapped at O vacancies (signal A) [10a] and at oxygen molecules (signal D) [22,23] were detected, as well as holes trapped at O^{2-} forming paramagnetic $O^{\bullet-}$ species (signal C) [23]. However, a signal for anatase Ti^{3+} species (signal B) was only monitored upon UV-Vis light illumination, which is in accordance with the respective

literature [22,24]. The detected signals and their respective assignments are summarized in Table 2.

Table 2: EPR parameters of detected signals shown in Figure 2 and their assignments based on the literature data.

Signal	assignment	g value		
--	--	g_1	g_2	g_3
A	e^- trapped at O vacancies	2.005	2.005	2.005 [10]
B	anatase Ti^{3+}	1.990	1.990	1.957 [22]
C	$Ti^{4+}\text{-}O^{\bullet-}\text{-}Ti^{4+}\text{-}OH^-$	2.016	2.012	2.002 [23]
D	$Ti^{4+}\text{-}O_2^{\bullet-}$ on anatase	2.026	2.010	2.003 [10]

Figure 2a clearly shows the signals of the trapped electrons and holes for bare anatase TiO_2 when comparing its EPR spectra obtained in the dark and under illumination above 420 nm, indicating that bare anatase TiO_2 can be excited upon illumination above 420 nm. In comparison to the EPR spectrum of Au-TiO_2 recorded in Ar, the EPR spectrum (see Figure 2b) obtained in O_2 exhibits a significant increase for signal D (assigned to superoxide $O_2^{\bullet-}$) at $g = 2.026$ and $g = 2.010$ (≥ 420 nm), indicating an electron transfer from Au-TiO_2 to an O_2 molecule upon visible light illumination.

On the other hand, when the 500 nm cutoff filter was used, only the signal of electrons trapped at pre-existing defects inside of TiO_2 such as O vacancies (signal A) was observed (see Figure 2d). The visible light illumination (≥ 500 nm) and the presence of O_2 showed no effect on the EPR signals of the Au-TiO_2 system (Figure 2d). This implies that upon illumination with light above 500 nm no electrons and/or holes were generated in Au-TiO_2.
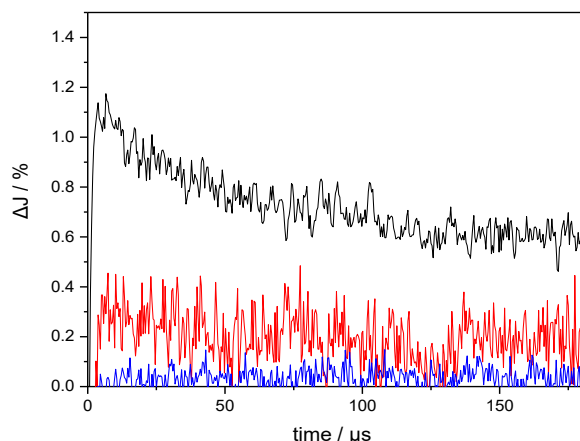
2.4.4 Laser Flash Photolysis

Figure 3. Transient absorption signals observed at 680 nm in a N_2 atmosphere: bare anatase TiO_2 excited at 420 nm (black), Au-TiO$_2$ excited at 420 nm (red) and at 530 nm (blue).

Figure 3 shows the transient absorption signals measured at 680 nm for pure anatase TiO_2 and for Au-TiO$_2$ in the absence of any electron acceptor or donor. From the literature [25], it is known that Ti^{3+} species absorb in the wavelength range around 680 nm. Hence, upon 420 nm laser excitation, in bare anatase TiO_2, a sufficient concentration of Ti^{3+} ions could be created, which are formed via the trapping of the photogenerated electrons. The obtained decay of the absorption can be related to the recombination of the electrons and holes [21,25]. In comparison to bare anatase TiO_2, the Au loaded TiO_2 presents an inconspicuous transient absorption for Ti^{3+}, indicating the transfer of the electrons photogenerated in TiO_2 to the Au nanoparticles:

$$e^-_{CB} / Ti^{3+} + Au \rightarrow Ti^{4+} + Au\ (e^-) \quad (1)$$
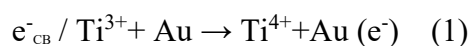
However, upon laser excitation at 530 nm, which is the plasmon band of Au-TiO$_2$, no signal for Ti^{3+} was monitored (see Figure 3), indicating no electron generation in Au-TiO$_2$ by the Au-SPR effect.

2.5. Discussion

Obviously, Au-TiO$_2$ can produce H$_2$ upon visible light illumination (that is employing a 420 nm cutoff filter). However, the origin of the electrons remains ambiguous. Recently, J. B. Priebe [10a] favored the DET mechanism based on the observation of the EPR signals of both the trapped electrons and the trapped holes upon visible light illumination ($\geq$ 420 nm). As shown in Figure 2a, the signals of both species were also recorded in this work upon visible light illumination (*i.e.*, in the presence of a 420 nm cutoff filter). However, it should be emphasized here that it is unpersuasive to assign the origin of the trapped electrons and holes to the optical excitation of the Au nanoparticles just based on the absorption edge of pure anatase TiO$_2$ (λ_{ox} = 388 nm), which is currently treated as a crucial supporting proof towards the DET mechanism [10a,16,17]. According to the RET mechanism [3,17,18], the Au-SPR effect can also initiate the generation of electron-hole pairs within TiO$_2$ upon visible light illumination. On the other hand, based upon its UV-Vis spectrum (see Figure 1c) and the EPR spectrum (see Figure 2a), even anatase TiO$_2$ absorbs slightly around 420 nm (most likely due to pre-existing defects) and upon visible light illumination (420 nm cutoff filter), signals for the trapped electrons and holes are indeed observed which are not detected in the dark, indicating that electrons can be excited inside bare anatase TiO$_2$ upon illumination above 420 nm. In case of pure anatase TiO$_2$ (E_g = 3.2 eV, λ_{ox} = 388 nm) can be excited employing a 420 nm cutoff filter which by definition absorbs 50% of the incoming photons at this wavelength (O.D.$_{420\ nm}$ = 0.3), the mixture of anatase and rutile TiO$_2$ present, for example, in Evonik Aeroxide TiO$_2$ P25 can also be excited by this type of visible light illumination considering that the bandgap energy of rutile is E_g = 3.0 eV (λ_{os} = 413 nm). As a matter of fact, this effect has been observed by Brückner and co-workers [10a] when comparing the EPR signals for bare TiO$_2$ obtained in the dark with those observed upon visible light illumination (420 nm cutoff filter).

Moreover, the Laser Flash Photolysis results presented here (see Figure 3), show a remarkable transient absorbance identified as Ti^{3+} for bare anatase TiO_2 upon 420 nm illumination, clearly evincing that bare anatase TiO_2 can be excited by 420 nm laser light. These results can be explained by an excitation of electrons from pre-existing defects (rather than from the valence band) into the TiO_2 conduction band from where they are subsequently trapped as Ti^{3+}. Hence, the strict notion that photons with an energy smaller than E_g cannot be absorbed and/or generate trapped charge carriers in the TiO_2 matrix [10a,16,26] does not seem to be correct. Figure 3 also presents direct evidence that the electrons generated in TiO_2 immediately migrate to the Au nanoparticles. This also explains the phenomenon that H_2 evolution is detected for Au-TiO_2 but not for bare TiO_2 upon visible light illumination ($\geq$ 420 nm). Besides, upon 530 nm laser excitation, no signal for Ti^{3+} has been obtained. However, upon 420 nm laser excitation, pure anatase TiO_2 rather than Au can be excited. The decrease on the intensity of the transient signal of Ti^{3+} indicates the electrons migrate from TiO_2 to Au rather than trapped in TiO_2 forming Ti^{3+}. Here, the Au islands simply act as electron transfer catalysts enabling the sequential reduction of protons on their surface by the electrons formed upon (visible light) illumination of their TiO_2 "carrier". Moreover, the presence of these Au co-catalysts also helps to minimize the undesired electron-hole recombination.

Moreover, Table 1 and Figure 2b present clear evidence that in the absence of any charge carriers provided by TiO_2, no H_2 and no EPR signals indicating the presence of species formed by visible light generated electrons can be monitored, indicating that no electrons can be transferred from the Au nanoparticles upon visible light illumination ($\geq$ 420 nm), thus contradicting the DET mechanism.

Hence, the H_2 evolution measurements, the EPR analysis, and the Laser Flash Photolysis results present clear evidence that the electrons which reduce H^+ to H_2 are solely generated in

the TiO_2 rather than in the Au nanoparticles. Therefore, there appears to be strong evidence for the fact that the DET process is indeed not operating upon visible light illumination (≥ 420 nm).

Additionally, our data also present no evidence favoring the RET mechanism. As the plasmon band of Au is centered above 500 nm (see Figure 1c), according to the RET mechanism, the Au-TiO_2 photocatalyst should be excited by the SPR-transferred resonance energy in the presence of a 500 nm cutoff filter (*i.e.*, a filter transmitting 50% of all photons at 500 nm). On the contrary, no evidence for any excitation of the Au-TiO_2 photocatalyst by these low energy photons was observed (see Table 1, Figure 2c, and Figure 3). This phenomenon has also been reported previously supporting the RET mechanism [17a]. In this contribution, based on the comparison of the water splitting and the photocurrent performance of N-TiO_2, Au/N-TiO_2, and Ag/N-TiO_2 upon visible light (400-900 nm) illumination, D.B. Ingram and co-workers proposed that the role of the noble metal islands is not only to suppress the recombination of the photogenerated electrons and holes, but also to transfer energy to their TiO_2 support through an electromagnetic field [17a]. However, the energy of the Au-SPR appeared to be insufficient to lead to the separation of the electron-hole pairs within N-TiO_2 [17a]. Besides, it should be noted here that the energy of the visible light ($\geqslant 500$ nm, i.e., $\leqslant 2.5$ eV) is not sufficient to overcome the band gap energy of TiO_2 (E_g=3.2 eV). Our present results also indicate that the Au-SPR has no influence on the photocatalytic activity of Au-TiO_2 (employing bare anatase as the TiO_2 source), at least any electromagnetic field induced by the light absorption of the Au-SPR does not appear to be powerful enough to promote the electron-hole pair generation within bare anatase TiO_2. Otherwise, species such as trapped electrons and holes should have been observed in the measurements performed here.

However, some research groups have also reported different results. For example, C. Gomes Silva and co-workers [16], showed that H_2 can be evolved upon 532 nm laser illumination. Moreover, the transient absorption signal indicating the presence of Ti^{3+} species

was also observed with 530 nm and 532 nm laser excitation, respectively [27,28], which was considered as proof supporting the DET mechanism. Nevertheless, even though these signals were observed, this is not clear evidence that the trapped electrons actually originate from the Au nanoparticles. As mentioned above, this phenomenon can also be explained by the RET mechanism, since an energy transfer can also initiate electron-hole pair generation close to the TiO_2 surface. Besides, it should be noted that, in the above mentioned publications [16,27,28], either commercial P25 or self-made TiO_2 annealed at high temperature, rather than 100% anatase TiO_2, were selected as the TiO_2 source. This implies that the TiO_2 type also plays a crucial role in the distinct photocatalytic abilities. Based upon the experimental evidence given here, we have clearly shown that the trapped electrons originate from the TiO_2 rather than from the Au nanoparticles.

It is well known that the intensity of the Au-SPR strongly depends on the particle size of the Au nanoparticles [10b,16,29,30]. This might be one reason that no signal for the trapped electrons was observed for Au-TiO_2 upon visible light illumination (≥ 500 nm). Though, visible activity of Au-TiO_2 with Au nanoparticle sizes ranging from 3 nm to 80 nm has been obtained upon 530/532 nm laser excitation [16,27,28]. According to K. Qian and co-workers [30], larger (from 4.4 nm to 67 nm) Au nanoparticles show more intense SPR that greatly facilitates SPR-excited electrons to raise the Fermi level of Au and overcome the overpotential required for H_2O reduction. Therefore, it is also recommended to perform further investigations on SPR-driven photocatalytic H_2 production under consideration of the size-dependence SPR intensity and the properties of different TiO_2 support material.

Though, there are studies involving anatase-only Au-TiO_2 composites that demonstrate SPR-driven photocataytic H_2 generation at wavelengths of 500 nm and higher [31,32]. In the two articles, Au and Pt were deposited on entirely anatase TiO_2, however, the bimetallic deposition was employed. The Au/TiO_2/Pt system is slightly different from the Au-TiO_2 system. Actually,

when we work with Pt-TiO$_2$ system, we also observed that its absorption above 500 is not 0, which might be a possible reason why they observed some activity at TiO$_2$/Pt aerogels (without SPR-active Au) at 435 nm illumination.

Direct evidence has been presented here that due to pre-existing defects, electrons can be excited in bare anatase TiO$_2$ upon visible light illumination ($\geq$ 420 nm), which has long been neglected in the previous studies [10a,17,18,19,26]. These electrons will then migrate to the Au nanoparticles (see Figure 4). In this case, the Au nanoparticles simply act as co-catalysts. Upon visible light illumination ($\geq$ 500 nm), with Au particle sizes between 5 nm and 8 nm, no SPR effect was observed for the Au-TiO$_2$ photocatalyst employing anatase nanoparticles exhibiting particle size of 12 nm as the TiO$_2$ source.
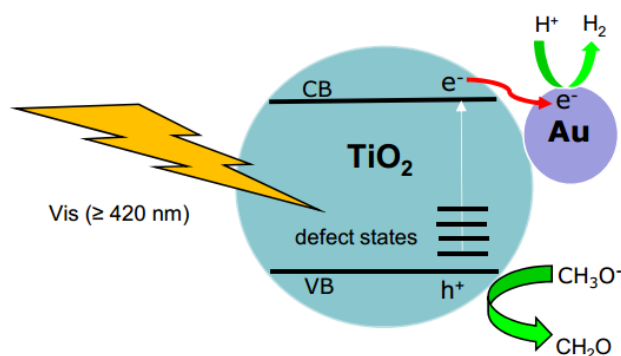

Figure 4. The role of Au nanoparticles for H$_2$ production using Au-TiO$_2$ (employing UV100 as TiO$_2$ source) in water/methanol mixtures upon visible light illumination.

2.6. Conclusions

It was confirmed by EPR and laser flash photolysis that bare anatase TiO$_2$ can be excited upon illumination above 420 nm. Simultaneously, these electrons generated in TiO$_2$ are immediately transferred to the Au nanoparticles, in which case, the Au nanoparticles simply act as co-catalysts to promote the separation of the photoinduced electrons and holes. It is unconvincing to attribute the visible light photocatalytic activity of Au-TiO$_2$ to the Au-SPR effect while using a 420 nm cutoff filter. However, due to the fact that Au nanoparticle size

strongly affects the SPR intensity and the TiO_2 type also plays a crucial role in the photocatalysis, no Au-SPR induced electrons and/or holes were observed employing anatase as TiO_2 source in the presence of a 500 nm cutoff filter or applying 530 nm laser. We are optimistic that the present work may contribute to the discussion about the origin of the visible light induced electron formation within Au-TiO_2 thus providing a new horizon concerning the influence of the TiO_2 support. Further investigations exploring a more effective visible light harvesting by photocatalysts for solar energy conversion should take both the SPR effect and the respective properties of the support materials into consideration.

2.7 Acknowledgement.

2.8 References

[1] J. Schneider, M. Matsuoka, M. Takeuchi, J. Zhang, Y. Horiuchi, M. Anpo, D. W. Bahnemann, Understanding TiO_2 Photocatalysis: Mechanisms and Materials, Chem. Rev. 114 (2014) 9919−9986.

[2] A. Kudo, Y. Miseki, Heterogeneous photocatalyst materials for water splitting, Chem. Soc. Rev. 38 (2009) 253-278.

[3] S. K. Cushing, J. Li, F. Meng, T. R. Senty, S. Suri, M. Zhi, M. Li, A. D. Bristow, N. Wu, Photocatalytic activity enhanced by plasmonic resonant energy transfer from metal to semiconductor, J. Am. Chem. Soc. 134 (2012) 15033−15041.

[4] J. A. Turner, A realizable renewable energy future, Science. 285 (1999) 687–689.

[5] L. Liu, T. D. Dao, R. Kodiyath, Q. Kang, H. Abe, T. Nagao, J. Ye, Plasmonic Janus-composite photocatalyst comprising Au and C-TiO$_2$ for enhanced aerobic oxidation over a broad visible-light range, Adv. Funct. Mater. 24 (2014) 7754–7762.

[6] S. C. Warren, E. Thimsen, Plasmonic solar water splitting, E. Energy Environ. Sci. 5 (2012) 5133–5146.

[7] A. Fujishima, K. Honda, S. Kikuchi, Photosensitized electrolytic oxidation on semiconducting n-type TiO$_2$ electrode, Kogyo Kagaku Zasshi. 72 (1969) 108-113.

[8] a) K. Awazu, M. Fujimaki, C. Rockstuhl, J. Tominaga, H. Murakami, Y. Ohki, N. Yoshida, T. Watanabe, A plasmonic photocatalyst consisting of silver nanoparticles embedded in titanium dioxide. J. Am. Chem. Soc. 130 (2008) 1676-1680; b) J. W. Hong, D. H. Wi, S-U, Lee, and S. W. Han, J. Am. Chem. Soc. 138 (2016) 15766-15773.

[9] J. Chen, J. C. S. Wu, P. C. Wu, D. P. Tsai, Improved photocatalytic activity of shell-isolated plasmonic photocatalyst Au@SiO$_2$/TiO$_2$ by promoted LSPR, J. Phys. Chem. C. 116 (2012) 26535-26542.

[10] a) J. B. Priebe, M. Karnahl, H. Junge, M. Beller, D. Hollmann, A. Brückner, Water reduction with visible light: synergy between optical transitions and electron transfer in Au-TiO$_2$ catalysts visualized by in situ EPR spectroscopy, Angew. Chem., Int. Ed. 52 (2013) 11420-11424; b) J. B. Priebe, J.Radnik, A. J. J. Lennox, M. Pohl, M. Karnahl, D. Hollmann, K. Grabow, U. Bentrup, H. Junge, M. Beller, A. Brückner, Solar hydrogen production by plasmonic Au-TiO$_2$ catalysts: impact of synthesis protocol and TiO$_2$ phase on charge transfer efficiency and H$_2$ evolution rates, ACS Catalysis. 5 (2015) 2137-2148.

[11] P.Zhang, T. Wang, J. Gong, Mechanistic understanding of the plasmonic enhancement for solar water splitting, Adv. Mater. 27 (2015) 5328-5342.

[12] M. R. Hoffmann, S.T. Martin, W. Choi, D. W. Bahnemann, Environmental applications of semiconductor photocatalysis, Chem. Rev. 95 (1995) 69-96.

[13] X. Zhang, Y. L. Chen, R. Liu, D. P. Tsai, Plasmonic photocatalysis, Rep. Prog. Phy. 76 (2013) 046401-0464042.

[14] Z. Liu, W. Hou, P. Pavaskar, M. Aykol, S. B. Cronin, Plasmon resonant enhancement of photocatalytic water splitting under visible illumination, Nano Lett. 11(2011) 1111-1116.

[15] a) T. A. Kandiel, R. Dillert, L. Robben, D. W. Bahnemann, Photonic efficiency and mechanism of photocatalytic molecular hydrogenproduction over platinized titanium dioxide from aqueous methanol solutions, Catal. Today. 161 (2011) 196-201; b) D. Friedmann, C. Mendive, D. Bahnemann, TiO_2 for water treatment: Parameters affecting the kinetics and mechanisms of photocatalysis, Appl. Catal. B: Environ. 99 (2011) 398–406.

[16] C. Gomes Silva, R. Juárez, T. Marino, R. Molinari, H. García, Influence of excitation wavelength (UV or visible light) on the photocatalytic activity of titania containing gold nanoparticles for the generation of hydrogen or oxygen from water, J. Am. Chem. Soc. 133 (2011) 595– 602.

[17] a) D. B. Ingram, S. Linic, Water splitting on composite plasmonic-metal/semiconductor photoelectrodes: evidence for selective plasmon-induced formation of charge carriers near the semiconductor surface, J. Am. Chem. Soc. 133 (2011) 5202−5205; b) S. Linic, P. Christopher, D. B. Ingram, Plasmonic-metal nanostructures for efficient conversion of solar to chemical energy, Nature Materials. 10 (2011) 911-921.

[18] Z. W. Seh, S. Liu, M. Low, S. Y. Zhang, Y. Liu, Z. Liu, A. Mlayah, M-Y Han, Janus Au-TiO_2 photocatalysts with strong localization of plasmonic near-fields for efficient visible-light hydrogen generation. Adv. Mater. 24 (2012) 2310–2314.

[19] S. Zhu, S. Liang, Q. Gu, L. Xie, J. Wang, Z. Ding, P. Liu, Effect of Au supported TiO_2 with dominant exposed {0 0 1} facets on the visible-light photocatalytic activity, Applied Catalysis B: Environmental.119–120 (2012) 146–155.

[20] B. V. Enüstün, J. Turkevich, Coagulation of colloidal gold, J. Am. Chem. Soc. 85 (1963) 3317-3328.

[21] J. Schneider, K. Nikitin, M. Wark, D. W. Bahnemann, R. Marschall, Improved charge carrier separation bariumtantalate composites investigated by laser flash photolysis, Phys. Chem. Chem. Phys, 18 (2016) 10719—10726.

[22] D. C. Hurum, A. G. Agrios, K. A. Gray, T. Rajh, M. C. Thurnauer, Explaining the enhanced photocatalytic activity of Degussa P25 mixed-phase TiO_2 using EPR, J. Phys. Chem. B. 107 (2003) 4545-4549.

[23] a) T. Hirakawa, H. Kominami, B. Ohtani, Y. Nosaka, Mechanism of photocatalytic production of active oxygens on highly crystalline TiO_2 particles by means of chemiluminescent probing and ESR spectroscopy, J. Phys. Chem. B. 105 (2001) 6993-6999; b) C. P. Kumar, N. O. Gopal, T. C. Wang, M.-S. Wong, S. C. Ke, EPR

Investigation of TiO$_2$ nanoparticles with temperature-dependent properties, J. Phys. Chem. B. 110 (2006) 5223-5229.

[24] V. Jovic, K.E. Smith, H. Idriss, G. I. N. Waterhouse, Heterojunction synergies in titania-supported gold photocatalysts: implications for solar hydrogen production, ChemSusChem. 8 (2015) 2551-2559.

[25] D. W. Bahnemann, M. Hilgendorff, R. Memming, Charge carrier dynamics at TiO$_2$ particles: reactivity of free and trapped holes, J. Phys. Chem. B. 101 (1997) 4265-4275.

[26] a) M. Serra, J. Albero, H. Garcia, Photocatalytic activity of Au/TiO$_2$ photocatalysts for H$_2$ evolution: role of the Au nanoparticles as a function of the irradiation wavelength, ChemPhysChem. 16 (2015) 1842-1845; b) H. G. Baldoví, Ş. Neaţu, A. Khan, A. M. Asiri, S. A. Kosa, H. Garcia, Understanding the origin of the photocatalytic CO$_2$ reduction by Au- and Cu-loaded TiO$_2$: a microsecond transient absorption spectroscopy study, J. Phys. Chem. C. 119 (2015), 6819-6827.

[27] Z. Bian, T. Tachikawa, P. Zhang. M. Fujitsuka, T. Majima, Au/TiO$_2$ superstructure-based plasmonic photocatalysts exhibiting efficient charge separation and unprecedented activity, J. Am. Chem. Soc. 136 (2014) 458-465.

[28] H.G. Baldovi, F. Albarracin, P. Atirnzar, B. Ferrer, M. Alvaro, H. Garcia, Visible-light photoresponse of gold nanoparticles supported on TiO$_2$: a combined photocatalytic, photoelectrochemical, and transient spectroscopy study, ChemPhysChem. 16 (2015) 335-341.

[29] V. Subramanian, E. E. Wolf, P. V. Kamat, Catalysis with TiO$_2$/gold nanocomposites. Effect of metal particle size on the fermi level equilibration, J. Am. Chem. Soc. 126 (2004) 4943−4950.

[30] K. Qian, B. C. Sweeny, A. C. Johnston-Peck, W. Niu, J. O. Graham, J. S. DuChene, J. Qiu, Y.-C. Wang, M. H. Engelhard, D. Su, E. A. Stach, W. D Wei, Surface plasmon-driven water reduction: gold nanoparticle size matters, J. Am. Chem. Soc. 136 (2014) 9842−9845.

[31] A. Tanaka, S. Sakaguchi, K. Hashimoti, H. Kominami, Preparation of Au/TiO$_2$ with Metal Cocatalysts Exhibiting Strong Surface Plasmon Resonance Effective for Photoinduced Hydrogen Formation under Irradiation of Visible Light. ACS Catalysis. 3 (2013) 79-85.

[32] P. A. DeSario, J. J. Pietron, A. Dunkelberger, T. H. Brintlinger, O. Baturina, R. M. Stroud, J. C. Owrutsky, D. R. Rolison, Plasmonic Aerogels as a Three-Dimensional Nanoscale Platform for Solar Fuel Photocatalysis. Langmuir. 33 (2017) 9444-9454.
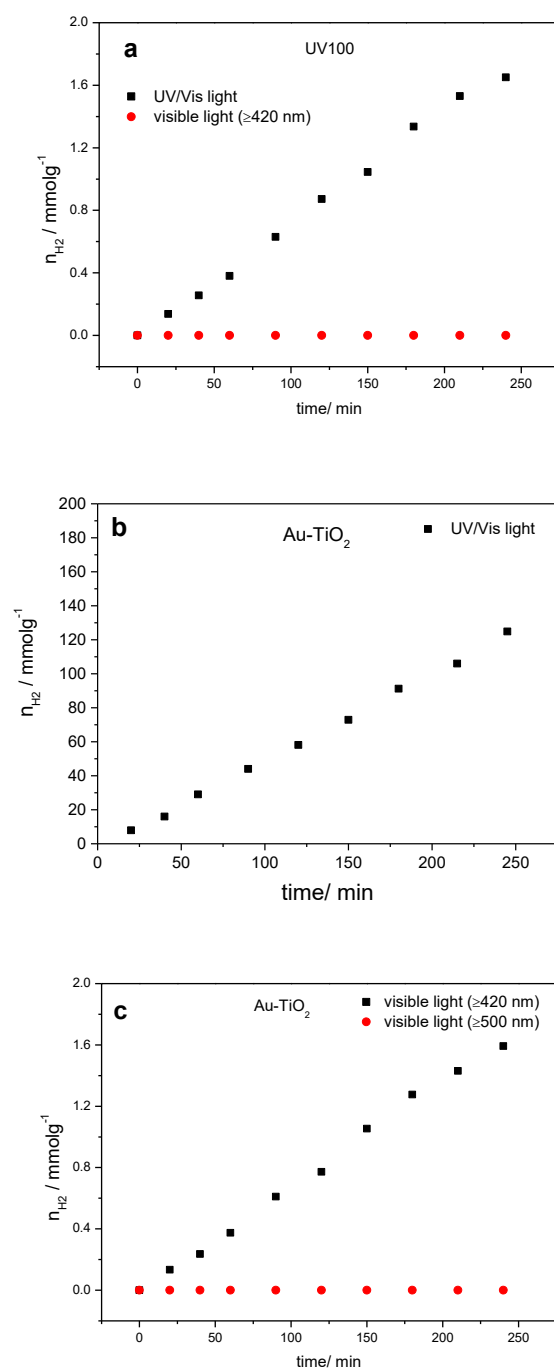
2.9 Suppleymentary Information

Figure S1 Photocatalytic H_2 evolution rates from CH_3OH/H_2O mixtures measured under UV-Vis and visible-light illumination employing different photocatalysts.
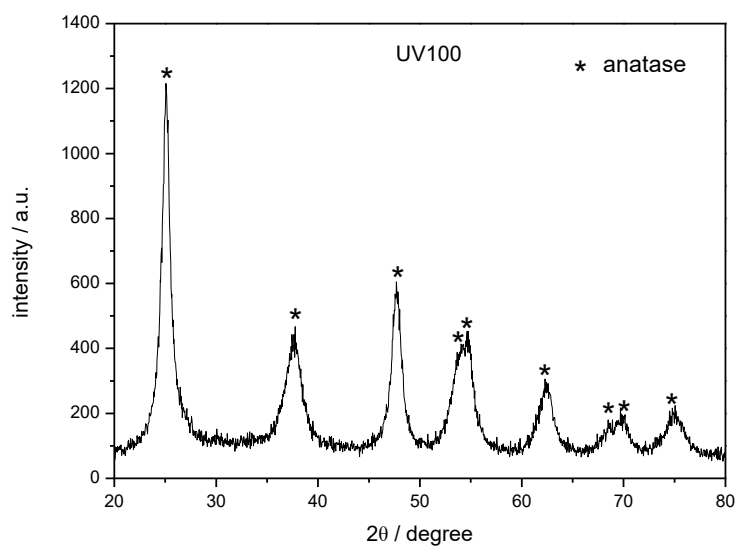
Figure S2 XRD pattern of UV100

As mentioned in chapter 2, some reports have shown that Au-SPR induced H_2 can be evolved upon illumination above 500 nm, employing Au-TiO_2 as photocatalyst, which is not observed in our experiments. However, in the above mentioned experiments, either commercial P25 or self-made TiO_2 annealed at high temperature, was selected as the TiO_2 source, instead of 100% anatase TiO_2 (such as UV100). This implies that the TiO_2 crystallographic phase also plays a crucial role in the distinct photocatalytic abilities. Therefore, another typical commercial photocatalyst, that is Evonik Aeroxide P25, consisting of 80 wt% anatase and 20 wt% rutile, has been selected as the TiO_2 source in the new experiments. Besides, we directly focus on the Au plasmon band, that is employing a 500 nm cutoff filter ($\geq$ 500 nm) or using the 532 nm laser beam to avoid a direct excitation of TiO_2. The details are presented in chapter 3.

Chapter 3

New Insights into the Surface Plasmon Resonance (SPR) Driven Photocatalytic H_2 Production of Au-TiO$_2$

Jinlin Nie, Jenny Schneider, Fabian Sieland, Long Zhou, Shuwei Xia and Detlef W. Bahnemann

Chapter 3. New Insights into the Surface Plasmon Resonance (SPR) Driven Photocatalytic H_2 Production of Au-TiO$_2$

3.1 Abstract

The Surface Plasmon Resonance (SPR) driven photocatalytic H_2 production upon visible light illumination ($\geq$ 500 nm) was investigated on gold-loaded TiO$_2$ (Au-TiO$_2$). It has been clearly shown that the Au-SPR can directly lead to photocatalytic H_2 evolution under illumination ($\geq$ 500 nm). However, there are still some open issues about the underlying mechanism for the SPR-driven photocatalytic H_2 production, especially the explanation between the resonance energy transfer (RET) theory and the direct electron transfer (DET) theory. In this contribution, by means of the EPR and Laser flash photolysis, we clearly showed the signals for different species formed by trapped electrons and holes in TiO$_2$ upon visible light illumination ($\geq$ 500 nm). However, the energy of the Au-SPR is insufficient to overcome the bandgap of TiO$_2$. The signals of the trapped electrons and holes are originated from two distinct processes, rather than the simple electron-hole pair excitation. Results obtained by the Laser flash photolysis evinced that, due to the Au-SPR effect, Au NPs can inject electrons to the conduction band of TiO$_2$ and the Au-SPR can also initiate e^-/h^+ pair generation (Interfacial Charge Transfer process) upon visible light illumination ($\geq$ 500 nm). Moreover, the Density Functional Theory (DFT) calculation provided direct evidence that, due to the Au-SPR, new impurity energy levels occurred, thus further theoretically elaborated the proposed mechanisms.

3.2 Introduction

Photocatalytic H_2 evolution from water utilizing sun light is gaining importance for providing clean and sustainable energy. [1-3] However, for practical applications, photocatalysts are desired to work efficiently under visible light which accounts for nearly half of the solar

light.[4] Recently, the rapid advances in plasmonic photocatalysis have accelerated the progress in visible-light harvesting ability of TiO_2-based photocatalysts. For instance, it has been reported that the surface-loading of Au nanoparticles can greatly increase the photocatalytic H_2 production ability of Au-TiO_2 upon visible light illumination.[4-9]

However, the underlying mechanism remains unclear in the respective literatures.[4a, 10-14] Generally, two main mechanisms have been proposed to explain the visible light activity of Au-TiO_2 photocatalysts (summarized in Figure 1). The first mechanism known as resonance energy transfer (RET) is based on the idea that the SPR enhances the local electromagnetic field which in turn facilitates the generation of e^-/h^+ pairs near the semiconductor surface;[3, 11, 12] D. B. Ingram[11] and Z. W. Seh[12] proposed this mechanism according to their results based on finite-difference time-domain (FDTD) simulations and discrete-dipole approximation (DDA) simulations, respectively, yet without exhibiting any experimental evidence. In addition, K. Awazu[15] also obtained results supporting this mechanism when adding an insulating layer between the noble metal nanoparticles and the semiconductor. In this study, the plasmonic metal nanoparticles were homogeneously covered with a SiO_2 shell thus preventing the direct electron transfer process. However, due to the energy transfer the enhanced photocatalytic activity was still achieved. The second mechanism explains the visible activity of Au-TiO_2 by the SPR-excited electron transfer from the Au nanoparticles to the conduction band of TiO_2, known as direct electron transfer (DET).[4a, 10, 13, 16] C. Gomes Silva[10] and coworkers proposed this mechanism based on the observation that Au-TiO_2 photocatalysts exhibit photocatalytic activity for H_2 evolution upon 532 nm laser illumination. Recently, J. B. Priebe *et al.*[4a] provided experimental evidence for the DET mechanism based on results obtained employing electron paramagnetic resonance (EPR) spectroscopy. In the EPR measurements, the authors detected the signals for electrons trapped at oxygen vacancies and for Ti^{3+} ions, which was considered as evidence for the electron transfer process from Au to TiO_2. Herein, it was emphasized that

the absorption of TiO_2 is situated absolutely below 420 nm, therefore, the signals occurred due to the action of the Au nanoparticles rather than of TiO_2. Moreover, it was excluded that the signals originated from electrons located in the Au nanoparticles themselves, as much higher g values and line widths are the requisites for these electrons to yield such signals.[4] In conclusion, J. B. Priebe and co-worker argued that the obtained EPR-signals provide evidence for trapped electrons in TiO_2 thus indicating a hot electron injection from the Au nanoparticles to TiO_2. However, it should be mentioned here that the results obtained by these EPR measurements can also be explained by means of the RET mechanism, since according to this mechanism the SPR-enhanced electromagnetic field can initiate electron-hole pair excitation close to the TiO_2 surface and thus the formation of the trapped electrons at this surface. Besides, due to pre-existing defects in TiO_2,[11b, 16] such as oxygen vacancies, TiO_2 exhibits also a small absorption shoulder above 400 nm indicative for surface defects. Actually, by means of EPR and laser flash photolysis, the obtained results clearly showed that bare TiO_2 can be activated by the visible light illumination ($\geq$ 420 nm) or using the 420 nm laser beam, which has long been neglected in the previous studies.[4a, 11, 12, 17]

Therefore, the origin of the photoinduced electrons and the underlying mechanism upon visible light illumination remains unclear. Herein, we directly focus on the Au plasmon band, that is employing a 500 nm cutoff filter ($\geq$ 500 nm) or using the 532 nm laser beam to totally get rid of the confusion caused by the direct excitation of TiO_2.
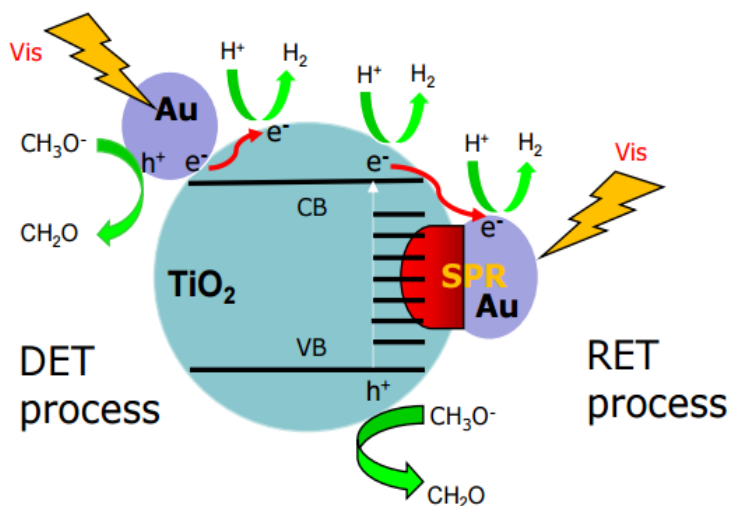
Figure 1. Two main proposed mechanisms for H_2 production using Au-TiO_2 in water/methanol mixtures under visible light illumination: direct electron transfer (DET) process (left); resonance energy transfer (RET) process (right).

3.3. Experimental Section

3.3.1 Photocatalyst Preparation

Au-TiO_2 photocatalysts consisting of 1 wt% gold on TiO_2 (Evonik Aeroxide P25) were prepared by the typical sol immobilization (labeled as SIM) method,[4] which was conducted by adding an aqueous solution of poly vinyl alcohol (PVA) (1.2 mL, 1wt % sol., Aldrich, >99%) to 1 mL $HAuCl_4.3H_2O$ (0.05 M). A freshly prepared $NaBH_4$ solution (2.5 mL, 0.1 M, Aldrich, >96%) was added dropwise to the above solution, with the color turning dark. After 30 min, the TiO_2 support (1.0 g) was added and the suspension was further stirred for 12 h at 25 °C. Then, the suspension was centrifuged, washed three times with distilled water and dried for 12 h at 70 °C. The as-prepared samples were used for catalytic and spectroscopic experiments without any other treatment.

3.3.2 Material Characterization

The UV-Vis absorption spectra were recorded employing a UV-Visible spectrophotometer (Varian Cary 100 Bio). TEM images were characterized by Transmission Electron Microscopy

(TEM) (FEI Tecnai G2 F20 TMP) using a 200 kV field emission gun (FEG). XRD patterns were monitored using a Bruker D8 Advance X-ray Diffraction system.

3.3.3 Photocatalytic H_2 Evolution Test

The photocatalytic hydrogen production experiments were conducted under argon atmosphere in a double-wall quartz glass reactor, with a cooling system (Julabo) maintaining the temperature at 20 °C. The 1 g/L photocatalyst suspensions were prepared by suspending Au (1 wt%)-TiO_2 in methanol/water mixtures (volume ratio 1:5). The suspension was sonicated for 30 min before being transferred into the reactor and flushed with argon for 15 min to remove gases dissolved in the suspension and to make sure that Ar remained in the headspace of the reactor. The argon gas rate was kept constant at 10 cm^3 min^{-1} during the photocatalytic measurement and the inlet gas flow rate for QMS was 1 cm^3 min^{-1}. Before illumination, the system was stabilized in the dark for 1 h to get a stable baseline. Afterwards, the suspension was illuminated employing an Osram XBO 1000 W Xe-Lamp (Müller) equipped with a 420 nm/500 nm cutoff filter.

3.3.4 Electron Paramagnetic Resonance (EPR) Spectroscopy

EPR measurements were carried out with a MiniScope MS400 spectrometer (Magnettech GmbH, Germany). A 500 W Mercury-Lamp (Muller) equipped with an optical cutoff filter (GC420/GC500) enables the illumination in the UV-Vis and visible light region. For low temperature measurements (90 K), the samples were placed in X-Band standard EPR tubes (Wilmad, 2 mm, O.D.) and cooled with a commercial EPR cold finger quartz Dewar by applying liquid nitrogen. The *g* values were calculated with the formula $h\nu = g\beta B_0$ (B_0 – external magnetic field, β – Bohr magneton, g_e – Landé g-factor) as described in the literature.[4a] The frequency was at around 9.42 GHz, and the B_0 was varied between 305 mT-365 mT.

3.3.5 Laser Flash Photolysis

During the laser flash photolysis measurements the samples were excited with an Nd-YAG laser (Brilliant B, Quantel) and the spectra were monitored by a laser flash photolysis spectrometer (LKS 80, Applied Photophysics). The excitation wavelength was tuned to 420 nm by employing an Optical Parametric Oscillator (OPO) (MagicPRISM, OPOTEK Inc.). Together with the OPO the 3rd harmonic (355 nm) of the Brilliant B laser was used to generate the visible light pulses with 6 mm diameter and 6 ns pulse length. The 532 nm laser was supplied by the 2rd harmonic (532 nm) of the Brilliant B laser. All experiments were performed in diffuse reflectance mode, where the analyzing light (supplied by a 150 W xenon arc lamp) was focused onto the sample and the reflected light was guided through the monochromator into the detector (Hamamatsu R928 photomultiplier). The light level detected by the oscilloscope was kept at 100 mV for all measurements to compensate the wavelength dependent sensitivity. Furthermore, all examinations were conducted under N_2 atmosphere and 12 shots were averaged for every transient. The energy density of the 420 nm and 532 nm laser beam was around 5 mJ/cm² per shot, respectively. The transient absorption change in reflectance ΔJ was calculated from the absorbance values according to the literature,[18] which also provides more detailed information about the set-up.

3.3.6 Theoretical Calculation Details

All spin-polarized calculations of optimization and energy bands were performed by Cambridge Sequential Total Energy Package (CASTEP). Projected augmented wave (PAW) pseudopotential was used to describe core electrons and plane wave basis set with 380 eV to represent valance electrons. Exchange-correlation energy was approximated by Perdew-Burke-Ernzerhof (PBE) functional of the generalized gradient approximation (GGA). Since the majority of P25 is anatase, we chose it for calculation. The model for anatase TiO_2 dominant (101) surface was represented with a 12 monolayer unit cell with a 15 Å vacuum slab. Au-TiO_2

model was constructed with a two gold atom cluster, to get rid of multi isomers of Au clusters[19-21], and TiO$_2$ (101) surface, with bottom six atomic layers fixed and upper six layers relax (supporting information Figure S4). A 4 × 4 × 2 k-points girds was used to optimize anatase cell, 2 × 2 × 1 k-points girds was used for TiO$_2$ (101) surface and Au-TiO$_2$ optimization and energy bands calculation both. The optimized lattice values of anatase were 3.78 and 9.49 Å, close to experimental values (3.78 and 9.5 Å). To overcome the self-interaction error of GGA method, a Hubbard correction (DFT+U) of 8.3 eV was imposed on Ti d-states; a good qualitative description of the electronic was obtained (Figure S5) with 3.23 eV band gap for bulk and 3.43 eV for (101) surface. No correction was applied to gold.

3.4. Results
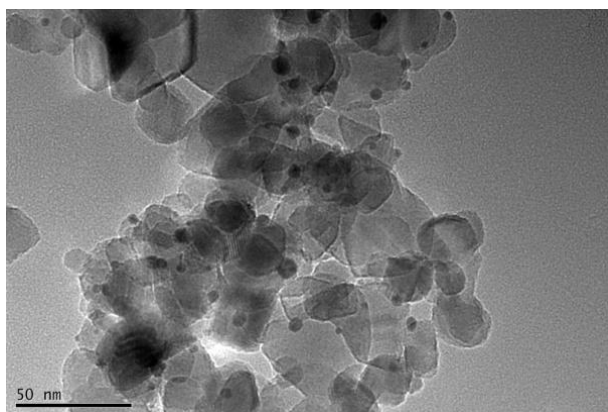
3.4.1 Material Characterization

Figure 2. TEM image of Au (1 wt%)-TiO$_2$.

Figure 2 shows the transmission electron microscopy (TEM) image of Au-TiO$_2$. As can be seen, the lighter particles are the TiO$_2$ matrix and the darker particles are the Au nanoparticles. The TEM images of Au-TiO$_2$ reveal that the Au nanoparticles are well deposited on the surface of TiO$_2$ matrix exhibiting particle sizes between 5 nm and 10 nm. Besides, the contents of Au-TiO$_2$ photocatalyst were analyzed by means of X-ray Diffraction (XRD). Accordingly, in addition to the peaks of anatase TiO$_2$ (JCPDS # 01-070-7347) and rutile TiO$_2$ (JCPDS # 03-

065-5714), the XRD pattern exhibited peaks for Au (JCPDS # 03-065-2870), as shown in Figure S1. Due to the low concentration, the peaks of Au are weak. However, no peaks for other impurities (*e.g.* Carbon or PVA) were detected within the detection limit.
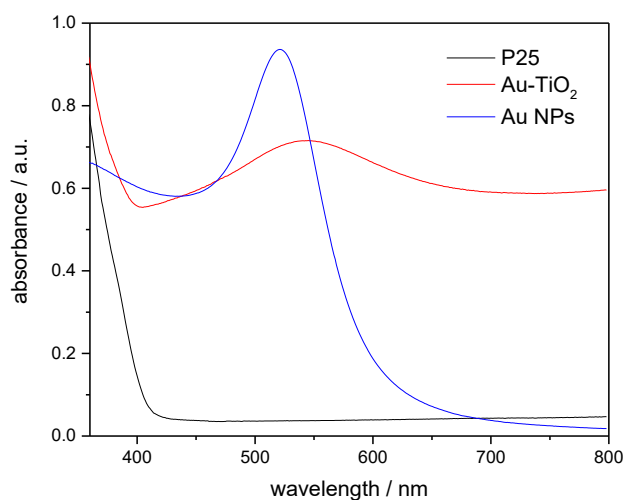

Figure 3. Diffuse-Reflectance UV-Vis spectra of bare TiO_2 (black), Au NPs (blue) and Au-TiO_2 (red).

In this study, the optical properties of Au nanoparticles, bare TiO_2 and Au-TiO_2 were characterized by UV-Vis spectroscopy. As Figure 3 shows Au-related samples exhibit plasmon band maxima located above 500 nm, namely Au nanoparticles with λ_{max} at 520 nm, Au-TiO_2 with λ_{max} at 543 nm, respectively. The absorption edge of bare TiO_2 is located around 400 nm, which is in good agreement with previous studies.[4b] Spectra of bare TiO_2 and the employed filters are presented in the supporting information Figure S2.
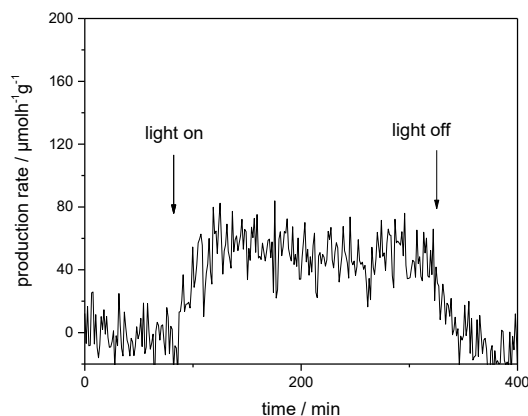
3.4.2 Photocatalytic H$_2$ Evolution Test

Figure 4. Photocatalytic H$_2$ evolution rate of Au-TiO$_2$ obtained from CH$_3$OH/H$_2$O mixtures upon visible light illumination in the presence of a 500 nm cutoff filter.

Figure 4 presents the photocatalytic H$_2$ evolution rates from CH$_3$OH/H$_2$O mixtures obtained employing Au-loaded TiO$_2$ under visible-light illumination in the presence of a 500 nm cutoff filter. However, no formation of H$_2$ was detected for bare TiO$_2$ photocatalyst within the detection limit under the same reaction condition. In comparison to bare TiO$_2$, Au-TiO$_2$ exhibited H$_2$ production ability upon visible light illumination in the presence of a 500 nm cutoff filter, indicating that Au-SPR can directly lead to photocatalytic H$_2$ production.
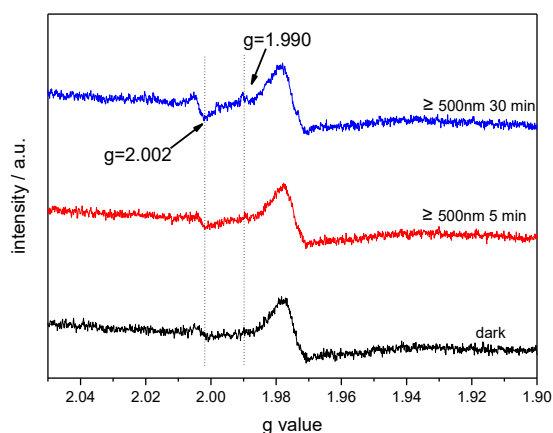
3.4.3 EPR Analysis

Figure 5. EPR spectra of Au-TiO$_2$ obtained in the dark and under visible light illumination ($\geq$ 500 nm) at 90 K.

The photoinduced EPR signals of trapped electrons and holes for bare TiO_2 and Au-TiO_2 were recorded in Ar at 90 K by (applying liquid nitrogen). The EPR parameters of the detected signals and their assignments were presented (supporting information Figure S3 and Table S1), which are in good agreement with the previous literatures. [4, 22, 23, 24]

In the presence of a 500 nm cutoff filter, when comparing the EPR signals of bare Au-TiO_2 obtained in the dark with those observed upon visible light illumination ($\geq$500 nm), small but clear signal of trapped electrons (anatase Ti^{3+} at g=1.990) was observed (see Figure 5), indicating the photo-induced electrons were trapped in TiO_2.

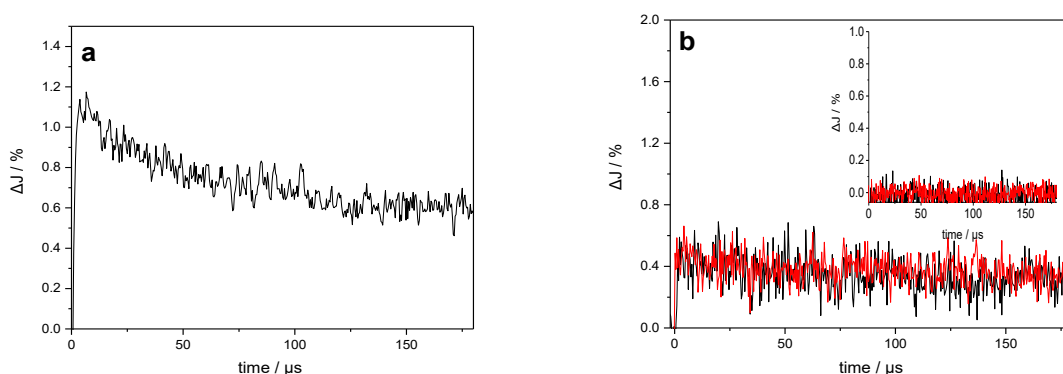3.4.4 Laser Flash Photolysis

Figure 6. a) Transient absorption signals of bare TiO_2 observed at 680 nm upon 420 nm laser excitation; b) Transient absorption signals of bare TiO_2 (inset) and Au-TiO_2 observed at 680 nm (black) and 400 nm (red) upon 532 nm laser excitation in a N_2 atmosphere.

Figure 6 shows the transient absorption signals measured at 400 nm and 680 nm for bare TiO_2 and Au-TiO_2 in the absence of any electron acceptor or donor. From the literature, it is known that Ti^{3+} species absorb in the wavelength range around 680 nm [25a], while the signal of the trapped holes can be monitored at 400-550 nm [25b].

As shown in Figure 6a, the transient signal of the trapped electron in TiO$_2$ was detected indicating that bare TiO$_2$ can be directly excited by 420 nm laser beam. The decay of the transient signals can be related to the internal electron/hole recombination.[18, 25] Upon 532 nm laser excitation, which is the plasmon band of the Au NPs, in addition to the transient absorption signal of the trapped electrons at 680 nm, the signal of the trapped holes in TiO$_2$ (see Figure 6b) was monitored at 400 nm. As expected, no transient signals were observed for bare TiO$_2$ in the blank experiment (see Figure 6b inset). The trapped holes observed at 400 nm exhibit nearly the same transient signal intensity and kinetic like the trapped electrons detected at 680 nm.

3.4.5 DFT Calculation Analysis
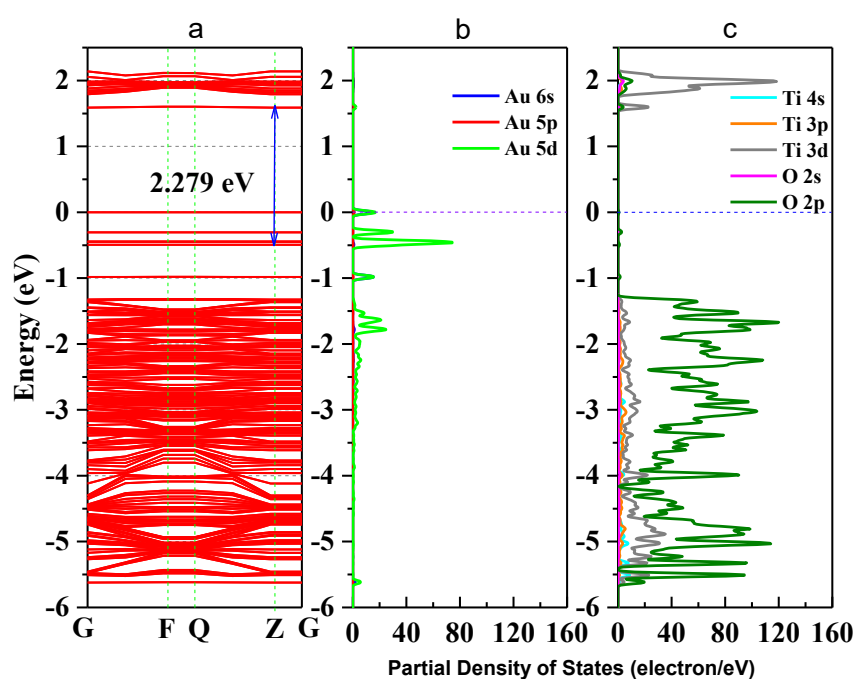
Figure 7. a) band structure of Au-TiO$_2$ slab; b) partial density of states (PDOS) of Au cluster; c) PDOS of TiO$_2$ (101) surface; blue dot line represents Fermi level

To further analyze the enhanced photocatalytic activities of Au-TiO$_2$, the electronic structure of Au-TiO$_2$ system were calculated, showed in Figure 7. As shown in Figure 7a, energy levels of the system are apparently split due to the reduction of symmetry and the

existence of surface dangling bonds. Moreover, new energy levels are appeared, two near the top of valence band and bottom of conduction band each, and four near Fermi level. Meanwhile, Figure 7 presented clear evidence that new isolated impurity energy levels are mainly attributed to d orbitals of Au clusters, and the top of valence band by the hybrid orbitals of Au and TiO_2 surface.

3.5 Discussion

Obviously, Au-TiO_2 can produce H_2 upon visible light illumination (employing a 500 nm cutoff filter). However, bare TiO_2 absorbs no light in the wavelength range above 500 nm and no H_2 can be formed ($\geq$ 500 nm) as evidenced by blank experiments. Besides, the XRD pattern showed no other impurities (e.g. Carbon or PVA) were detected within the detection limit. Hence, it can be excluded that the visible-activity of Au-TiO_2 above 500 nm is caused by a carbon radical stem from polyvinyl alcohol remaining in the catalyst from the synthesis. The observation of any H_2 and signals of trapped electrons and holes can only be related to the Au-SPR effect. As shown in Figure S3, the appearance of new EPR signals can be observed upon illumination ($\geq$ 500 nm) which can be attributed to trapped electrons and trapped holes according to the literature. [4, 22, 23, 24] The new formed EPR signals indicate the excitation of Au-TiO_2 photocatalyst upon visible light illumination above 500 nm. However, as new formed EPR signals are indistinctive (especially the signals at g=2.002-2.005 [4, 22-24]) laser excitation was employed to totally get rid of the confusion caused by the proximity of g values for signals of trapped electrons and trapped holes.

Upon 532 nm laser (~ 2.34 eV) excitation, the transient signals of the trapped electrons and holes in TiO_2 were also observed, which further confirmed the presence of photogenerated electrons and holes. It should be noted here that, the transient signals of the Au-SPR induced electrons can be detected in ps scale [14] and most charges recombine within 1 ns [26, 27]. Therefore, the significant decay process of the transient signals in Figure 6b was not observed within the

detection time scale. In the absence of any electron acceptor or donor, transient signals of the trapped electrons and holes in TiO_2 can be observed on longer time scale (μs), as presented. The long-lived charges can be correlated with the photocatalytic activity of the photocatalysts. [28, 29]

It should be emphasized here that the energy of the incoming photons ($\lambda \geq 500$ nm, $E_{h\nu} \leq$ 2.48eV) is insufficient to excite the electrons from the valence band to the conduction band of TiO_2 and leave the holes in the valence band of TiO_2. However, due to the Au-SPR, many electrons in Au have higher energy than the conduction band of TiO_2, facilitating the electron injection from Au to the conduction band of TiO_2. [13, 30] This provided a reasonable explanation for the observation of the Ti^{3+} in both EPR spectroscopy and laser flash photolysis. As reported,[13, 30] the direct electron injection process is thermodynamically favorable, since the photon energy ($h\nu$) only needs to overcome the gap between the Fermi level (E_f) of Au and the top of TiO_2 conduction band (E_{CB}), that is: $h\nu \geq E_{CB0} - E_f$. Moreover, after the contact of Au and TiO_2, the Fermi level of the Au nanoparticles will be equalized to the work function and the conduction band of TiO_2 will be bent down.[30] Therefore, the trapped electrons leading to the formation of Ti^{3+} are from the "hot electron injection" of the Au nanoparticles, process II (a) in Figure 8.

On the other hand, since no holes can be transferred from the Au nanoparticles to the valence band of TiO_2, the EPR signals of the trapped holes in TiO_2 (signal D) can only originate from the Au-SPR initiated electron-hole pair generation in TiO_2. However, it should be noted here again that the energy of the visible light (≥ 500 nm, i.e., ≤ 2.5 eV) is not sufficient to overcome the band gap energy of TiO_2. In this case, it is assumed that the Au-SPR initiates the Interfacial Charge Transfer (IFCT), as proposed by Creutz.[31] Accordingly, electrons in the valence band of TiO_2 directly transfer to the surface Au clusters, that is not via the excited state,[32] while the holes are trapped in the valence band of TiO_2, process II (b) in Figure 8.

Besides, after electrons injection from Au to the conduction band of TiO_2, monovalent of Au might be generated. Therefore, the DET process also provides the possibility of interfacial charge transfer from valence band of TiO_2 to monovalent of Au.

Moreover, the obtained theoretical calculation results provide further evidences supporting the above proposed mechanisms. Firstly, a good qualitative description of the electronic was obtained (Figure S5) with 3.23 eV band gap for bulk and 3.43 eV for (101) surface. As presented above (Figure 7), with the deposition of Au clusters on the surface of TiO_2, new isolated impurity energy levels appeared mainly due to d orbitals of Au clusters. Therefore, the possibility of electron transfer from Au to the conduction band of TiO_2 is demonstrated by DFT calculation. Besides, the existence of Au impurity energy levels in band gap also provide channels for electrons to be excited with lower energy ($\lambda \geq 500$ nm, $E_{hv} \leq 2.48$eV). Moreover, the maxima absorption wavelength of Au-TiO_2 in Figure 3 (543 nm, 2.288 eV) is in good accordance with the energy difference between an impurity level and the bottom of conduction band in DFT result (2.279 eV). Furthermore, due to the small energy gaps, the electron transfer from the valence band of TiO_2 to the surface loaded Au clusters is thermodynamically feasible, as proposed by IFCT process. Herein, the proposed mechanisms based on the experimental data are favored by the DFT calculation results. In case of the electron transfer processes can occur employing pure anatase as TiO_2 source, the same process should be easier in the case of using the mixture of anatase and rutile TiO_2, for example, in Evonik Aeroxide P25 as TiO_2 source.

Besides, the EPR and the laser flash photolysis spectra (supporting information Figure S3 and Figure 6a) show clear evidence that bare TiO_2 (P25) can be directly excited by visible light illumination ($\lambda \geq 420$ nm) or 420 nm laser beam (process I in Figure 8), which has long been ignored by some studies. Therefore, the investigation of SPR influence on the visible light photocatalytic activity of TiO_2 employing a 400/420 nm cutoff filter does not seem to be correct. Actually, upon visible light illumination ($\lambda \geq 420$ nm), the direct excitation of TiO_2 and the

SPR-induced excitation can both lead to the visible light photocatalytic activity of Au-TiO$_2$, process I+II in Figure 8.

Therefore, upon illumination above 500 nm, due to the Au-SPR, electrons can be directly injected into the conduction band of TiO$_2$, as reported previously. [4a, 10, 13, 14, 26] Simultaneously, the Au-SPR can also initiate electron hole pair generation in TiO$_2$, while the electrons directly transfer from the valence band of TiO$_2$ to the surface Au-related species (IFCT process). The two pathways cooperatively contribute to the SPR-induced visible-driven photocatalytic H$_2$ production ability of Au-TiO$_2$ photocatalyst. This also provides a reasonable explanation for the photocatalytic activity when the plasmonic metal nanoparticles were homogeneously covered with an insulating SiO$_2$ shell.
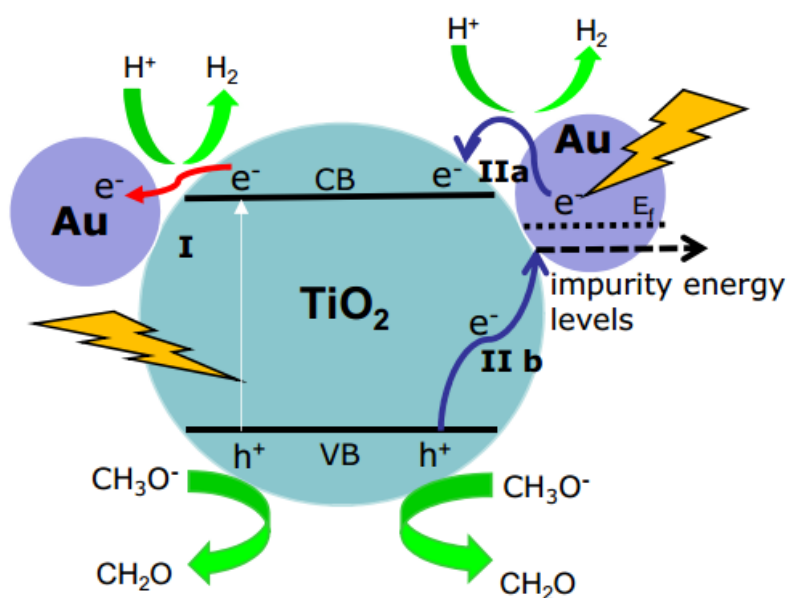

Figure 8. Proposed mechanisms for H$_2$ production using Au-TiO$_2$ in water/methanol mixtures upon visible light illumination ($\geq$ 420 nm: process I + II; $\geq$ 500 nm: process II).

3.6 Conclusions

In conclusion, Au-SPR driven photocatalytic H$_2$ production was observed upon visible light illumination ($\geq$ 500 nm). Direct experimental evidences were presented that Au

nanoparticles can transfer the SPR-induced hot electrons into the conduction band of TiO_2 upon visible light illumination in the wavelength range above 500 nm. Simultaneously, the Au-SPR can also initiate electron-hole pair generation in TiO_2. However, due to the photons energy/E_{SPR} is insufficient to overcome the band gap of TiO_2, the initiated electrons directly transfer to the surface Au-related species through the IFCT process rather than via the excited state. The experimental results are in good agreement with the data obtained from DFT calculation. The DFT calculation analysis clearly shows how the d orbitals of Au clusters create impurity energy levels and decrease the band gap of Au-TiO_2.We are optimistic that our contribution may contribute to the controversial discussion about the origin of the SPR- induced electron formation within Au-TiO_2 thus providing a new horizon for further investigations on exploring more effective visible light harvesting photocatalysts for solar energy conversion.

3.7 Acknowledgement.

3.8 References

[1] J. A. Turner, Science. 1999, 285, 687–689.

[2] A. Kudo, Y. Miseki, Chem. Soc. Rev. 2009, 38, 253-278.

[3] S. K. Cushing, J. Li, F. Meng, T. R. Senty, S. Suri, M. Zhi, M. Li, A. D. Bristow, N. Wu, J. Am. Chem. Soc. 2012, 134, 15033−15041.

[4] a) J. B. Priebe, M. Karnahl, H. Junge, M. Beller, D. Hollmann, A. Brückner, Angew. Chem., Int. Ed. 2013, 52, 11420-11424; b) J. B. Priebe, J. Radnik, A. J. J. Lennox, M. Pohl, M. Karnahl, D. Hollmann, K. Grabow, U. Bentrup, H. Junge, M. Beller, A. Brückner, ACS Catalysis. 2015, 5, 2137-2148.

[5] L. Liu, T. D. Dao, R. Kodiyath, Q. Kang, H. Abe, T. Nagao, J. Ye, Adv. Funct. Mater. 2014, 24, 7754–7762.

[6] M. Murdoch, G. I. N. Waterhouse, M. A. Nadeem, J. B. Metson, M. A. Keane, R. F. Howe, J. Llorca, H. Idriss, Nat. Chem. 2011, 3(6), 489-492.

[7] Y. C. Pu, G. M. Wang, K. D. Chang, Y. C. Ling, Y. K. Lin, B. C. Fitzmorris, C. M. Liu, X. H. Lu, Y. X. Tong, J. Z. Zhang, Y. J. Hsu, Y. Li, Nano Lett. 2013, 13, 3817-3823.

[8] J. W. Hong, D. H. Wi, S-U, Lee, S. W. Han, J. Am. Chem. Soc. 2016, 138, 15766-15773.

[9] A. Stevanovic, M. Büttner, Z. Zhang, J. T. Yates, J. Am. Chem. Soc. 2012, 134(1), 324-332.

[10] C. G. Silva, R. Juárez, T. Marino, R. Molinari, H. García, J. Am. Chem. Soc. 2011, 133, 595– 602.

[11] a) D. B. Ingram, S. Linic, J. Am. Chem. Soc. 2011, 133, 5202−5205; b) S. Linic, P. Christopher, D. B. Ingram, Nature Materials. 2011,10,911-921.

[12] Z. W. Seh, S. Liu, M. Low, S. Y. Zhang, Y. Liu, Z. Liu, A. Mlayah, M-Y. Han, Adv. Mater. 2012, 24, 2310–2314.

[13] K. Qian, B. C. Sweeny, A. C. Johnston-Peck, W. Niu, J. O. Graham, J. S. DuChene, J. Qiu, Y.-C. Wang, M. H. Engelhard, D. Su, E. A. Stach, W. D. Wei, J. Am. Chem. Soc. 2014, 136, 9842−9845.

[14] Z. Bian, T. Tachikawa, P. Zhang. M. Fujitsuka, T. Majima, J. Am. Chem. Soc. 2014,136, 458-465.

[15] K. Awazu, M. Fujimaki, C. Rockstuhl, J. Tominaga, H. Murakami, Y. Ohki, N. Yoshida, T. Watanabe, J. Am. Chem. Soc. 2008, 130, 1676-1680.

[16] Z. Liu, W. Hou, P. Pavaskar, M. Aykol, S. B. Cronin, Nano Lett. 2011, 11 (3), 1111–1116.

[17] S. Zhu, S. Liang, Q. Gu, L. Xie, J. Wang, Z. Ding, P. Liu, Applied Catalysis B: Environmental, 2012, 119–120,146–155.

[18] J. Schneider, K. Nikitin, M. Wark, D. W. Bahnemann, R. Marschall, Phys. Chem. Chem. Phys, 2016, 18, 10719-10726.

[19] K. Z. Milowska, J. K. Stolarczyk, Phys. Chem. Chem. Phys., 2016, 18(18): 12716-12724.

[20] L A. Mancera, D. M. Benoit, Phys. Chem. Chem. Phy., 2016, 18(1), 529-549.

[21] L.A. Mancera, D. M. Benoit, Computational and Theoretical Chemistry, 2015, 1067, 24-32.

[22] D. C. Hurum, A. G. Agrios, K. A. Gray, T. Rajh, M. C. Thurnauer, J. Phys. Chem. B. 2003, 107, 4545-4549.

[23] a) T. Hirakawa, H. Kominami, B. Ohtani, Y. Nosaka, J. Phys. Chem. B. 2001, 105, 6993-6999; b) C. P. Kumar, N. O. Gopal, T. C. Wang, M.-S. Wong, S. C. Ke, J. Phys. Chem. B. 2006, 110, 5223-5229.

[24] V. Jovic, K. E. Smith, H. Idriss, G. I. N. Waterhouse, ChemSusChem. 2015, 8, 2551-2559.

[25] a) D. W. Bahnemann, M. Hilgendorff, R. Memming. J. Phys. Chem. B. 1997, 101, 4265-4275; b) A. O. T. Patrocinio, J. Schneider, M. D. França, L. M. Santos, B. P. Caixeta, A. E. H. Machado, D. W. Bahnemann, RSC Adv. 2015, 5, 70536-70545.

[26] A. Furube, L. Du, K. Hara, R. Katoh, M. Tachiya, J. Am. Chem. Soc. 2007, 129, 14852-14853.

[27] L. Du, A. Furube, K. Yamamoto, K. Hara, R. Katoh, M. Tachiya, J. Phys. Chem. C, 2009, 113(16), 6454−6462.

[28] J. S. DuChene, B. C. Sweeny, A. C. Johnston-Peck, D. Su, E. A. Stach, W. D. Wei, Angew. Chem., Int. Ed. 2014, 53, 7887-7891.

[29] Z. Bian, T. Tachikawa, T. Majima, J. Phys. Chem. Lett., 2012, 3, 1422−1427; b) Z. Bian, T. Tachikawa, W. Kim, W. Choi, T. Majima, J. Phys. Chem. C, 2012, 116, 25444−25453.

[30] X. Zhang, Y. L. Chen, R. Liu, D. P. Tsai, Plasmonic Photocatalysis. Rep. Prog. Phy. 2013, 76, 046401-046441.

[31] a) C. Creutz, B. S. Brunschwig, N. Sutin, J. Phys. Chem. B 2005, 109, 10251-10260; b) C. Creutz, B. S. Brunschwig, N. Sutin, J. Phys. Chem. B, 2006, 110, 25181–25190.

[32] a) H. Irie, K. Kamiya, T. Shibanuma, S. Miura, D. A. Tryk, T. Yokoyama, K. Hashimoto, J. Phys. Chem. C 2009, 113, 10761-10766; b) H. Yu, H. Irie, Y. Shimodaira, Y. Hosogi, Y. Kuroda, M. Miyauchi, K. Hashimoto, J. Phys. Chem. C, 2010, 114, 16481–16487.
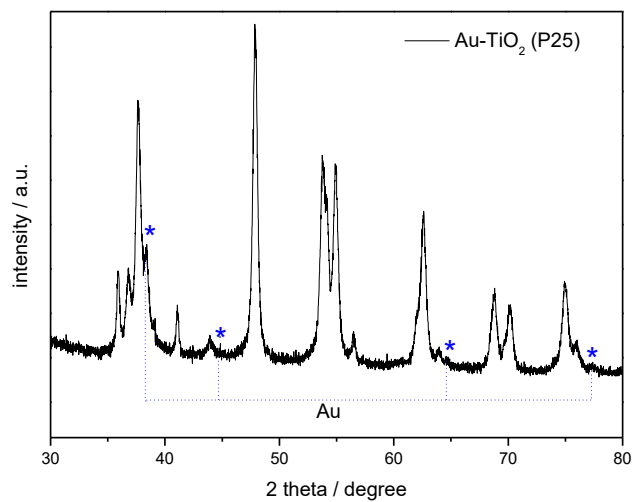
3.9 Supplementary Information
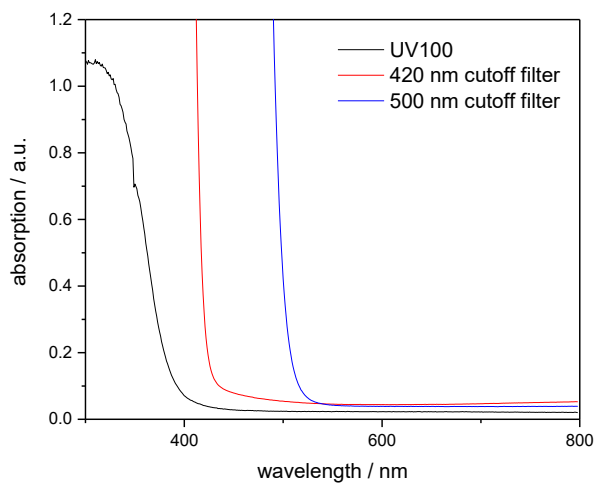

Figure S1. XRD patter of Au-TiO$_2$ (P25)

Figure S2: The UV-Vis spectra of bare TiO$_2$ and of the employed 420 nm (red) and 500 nm cutoff filters (blue).
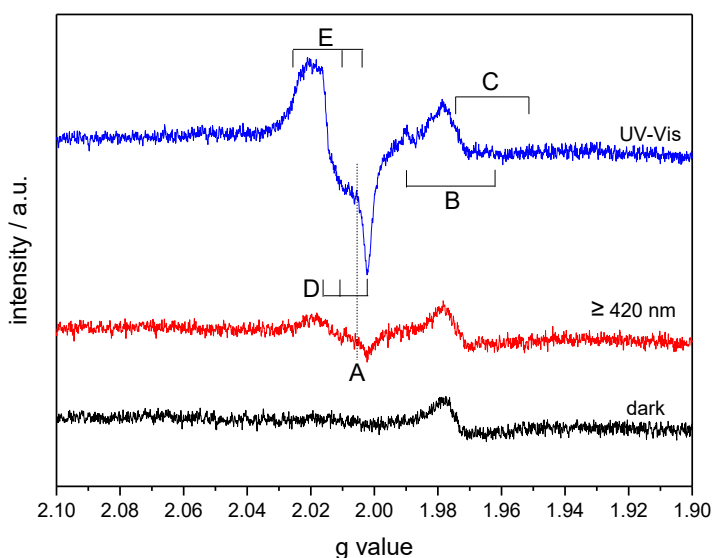
Figure S3. EPR spectra of bare TiO_2 obtained in the dark (black), under visible light illumination (≥ 420 nm) (red) and under UV-Vis (blue) light illumination at 90 K

As shown in Figure S3, upon UV-Vis light illumination electrons trapped at O vacancies (signal A) [4a] and at oxygen molecules (signal E) [22,23] were detected, as well as electrons trapped at Ti^{4+} centers forming the anatase Ti^{3+} (signal C) and rutile Ti^{3+} (signal D) species [4,24]. The signal of trapped holes at O^{2-} forming paramagnetic $O^{\cdot-}$ species (signal D) [23] was also observed. Besides, it should be noted here that signals of trapped electrons and holes were detected for bare TiO_2 upon visible light illumination (≥ 420 nm), indicating that bare TiO_2 can be excited by visible light illumination at around 420 nm. The detected signals and their respective assignments are summarized in Table S1.

Table S1: EPR parameters of detected signals shown in Figure 3 and their assignments based on the literature data.

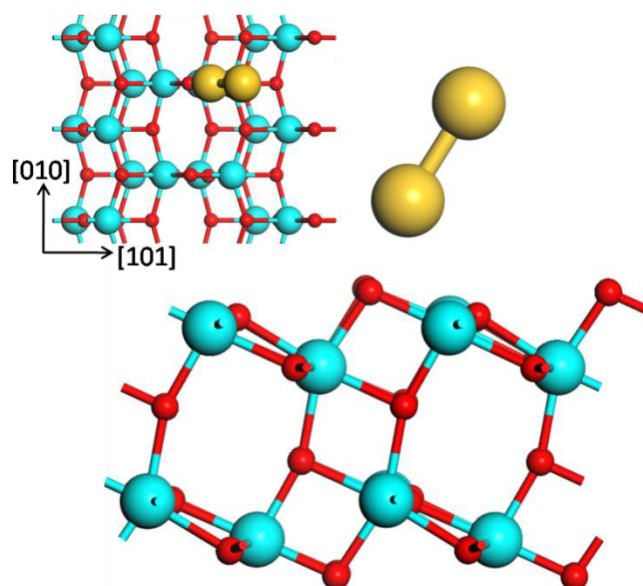| Signal	assignment	g value		
--	--	g_1	g_2	g_3
A	e⁻ trapped at O vacancies	2.005	2.005	2.005 [4]
B	anatase Ti^{3+}	1.990	1.990	1.957 [22]
C	rutile Ti^{3+}	1.975	1.975	1.951 [4]
D	Ti^{4+}-$O^{•-}$-Ti^{4+}-OH^-	2.016	2.012	2.002 [23]
E	Ti^{4+}-$O_2^{•-}$	2.026	2.010	2.003 [4]

Figure S4: Side and top view of Au-TiO₂ model, red, blue and golden balls are O, Ti and Au atom, respectively.
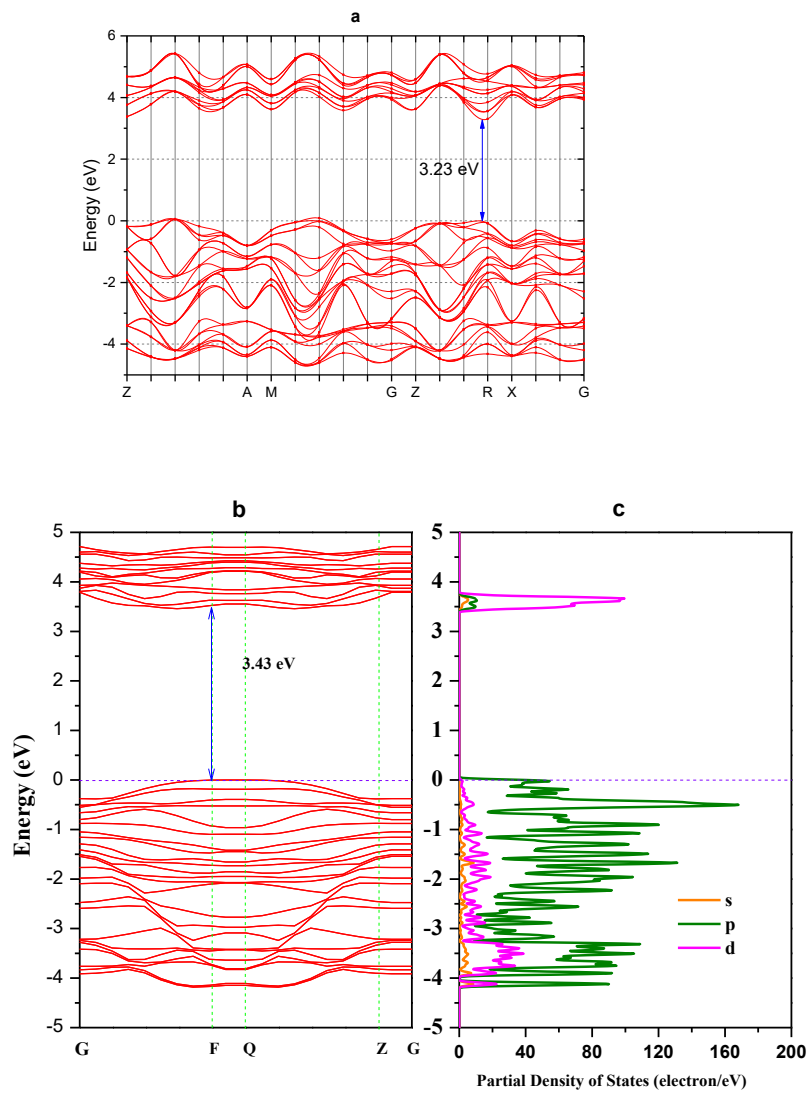
Fig. S5: a) band structure of bulk anatase, b) (101) Surface and c) partial density of states of TiO_2 (101) surface

It has been proven in chapter 1 and chapter 2, Au-TiO$_2$ is a good visible-active photocatalyst and Au-SPR effect can directly lead to H$_2$ generation upon illumination above 500 nm. However, due to the high cost, noble metals are not suitable for large scale industrial applications. Thus, low cost plasmonic metals should be investigated aiming cost-effective photocatalysts. Copper, as one of the most used metals due to its conductivity and low cost, has been reported to exhibit the surface plasmon resonance effect and have been applied for environmental cleaning and H$_2$ energy production. However, the photocatalytic mechanism in the presence of Cu has been poorly studied, especially the effect of Cu$^{II/I}$ chemistry is still controversially discussed in the literature. Therefore, Cu has been employed into the new experiments and the details are presented in chapter 4.

Chapter 4

New Insights into the Plasmonic Enhancement for Photocatalytic H$_2$ Production by Cu-TiO$_2$ upon Visible Light Illumination

J. Nie, A. O. T. Patrocinio, S. Hamid, F. Sieland, J. Sann, S. Xia, D. W. Bahnemann and J. Schneider,

Chapter 4 New Insights into the Plasmonic Enhancement for Photocatalytic H_2 Production by Cu-TiO$_2$ upon Visible Light Illumination

4.1 Abstract:

Cu nanoparticles were deposited on the surface of commercial TiO$_2$ nanoparticles (Cu-TiO$_2$) by different methods aiming at the production of highly efficient visible light photocatalysts. Photocatalytic H_2 evolution rates obtained from methanol/water mixtures revealed no significant influence of the presence of copper oxides in the photoreaction upon visible light illumination. The photocatalytic H_2 production rates were evaluated upon illumination with different spectral ranges (≥ 420 nm or ≥ 500 nm) and the results evinced that the visible light induced charge carrier formation on the Cu-TiO$_2$ photocatalysts consists of two distinct pathways: the direct excitation of TiO$_2$ and the induced excitation by the so-called surface plasmon resonance (SPR) effect of the Cu nanoparticles on the TiO$_2$ surface. Both pathways are present when the full visible range of the spectrum is used (≥ 420 nm), while for irradiation at longer wavelengths (≥ 500 nm), the photocatalytic activity is solely promoted by the Cu-SPR effect. Electron paramagnetic resonance (EPR) and laser flash photolysis measurements were performed to clarify the underlying mechanism of Cu-TiO$_2$ photocatalysts upon visible light illumination.

4.2 Introduction

Photocatalysis has been proven to be one of the most promising methods to harvest solar energy to solve energy and environmental issues.[1-3] The efficiency of the photocatalyst depends basically on four processes: light absorption, charge separation, charge migration, and charge recombination.[4, 5] The photocatalysts reported up to now exhibit limitations on one or more of these four processes.[5] For example, TiO$_2$ is a low-cost, active, environmentally friendly and

stable photocatalyst,[6] being the most extensively studied photocatalyst. However, its wide bandgap limits its photo-absorption to the UV region,[7, 8] and additionally, TiO_2 exhibits high charge recombination rates of the photo-generated electrons and holes.[9]

To overcome these issues, different methods have been applied to extend the absorption edge of TiO_2 to the visible region, as well as to suppress the charge-carrier recombination.[10] Due to the Surface Plasmon Resonance (SPR) effect, surface deposition of noble metal nanoparticles (e.g. Au and Ag) has recently emerged as a promising strategy in enhancing the photocatalytic efficiency of TiO_2-based photocatalysts upon visible light illumination, increasing the prospect of employing sunlight for environmental and energy applications.[11-13] However, due to the high cost, noble metals are not suitable for large scale industrial applications, thus low cost plasmonic metals should be investigated aiming at cost-effective photocatalysts. Copper, as one of the most used metals due to its conductivity and low cost, has been reported to exhibit the surface plasmon resonance effect and have been applied for environmental cleaning and H_2 energy production.[2, 14-17]

Despite the first promising results on Cu-TiO_2 photocatalysts, its SPR-enhanced visible light photocatalytic activity has not been investigated as extensively as that of Au-TiO_2, and the underlying mechanisms of the SPR effect of Cu NPs upon visible light illumination have rarely been reported in detail and are controversially discussed. This is probably due to the instability and/or prone to surface oxidation of the Cu NPs,[18, 19] which can remarkably affect their plasmonic properties.

As a result, several open issues remain unclear. Firstly, the role of intrinsic oxide layers formed on the surface of the Cu nanoparticles is still not clear. Some research groups call the attention that copper nanoparticles are not ideal plasmonic materials due to their superficial oxidation,[14] while other groups claim that copper oxides, mostly CuO and Cu_2O, could act as charge carriers[20a] or even as electron sinks,[20b] to trap the photoexcited electrons and thus

suppress the recombination of the electrons and holes. Due to the narrower band gap of copper oxides, J. Pal *et al.*[15] reported that Cu-Cu$_2$O-ZnO photocatalysts exhibit better visible light photocatalytic activity than Cu-ZnO due to the enlarged light absorption in the visible region. A second issue still under discussion is the role of the SPR effect on the electron/hole pair formation. Some reports indicate no direct influence of the Cu-SPR effect on the e$^-$/h$^+$ formation, while other groups attribute the visible-light excitation of the photocatalysts to the Cu-SPR effect. Y. Lv and coworkers[21] investigated the Cu-SPR effect for the photocatalytic reduction of deca-brominated diphenyl ether (BDE209) employing excitation energies higher than 450 nm which can avoid the direct excitation of TiO$_2$. However, no signal for the debromination was observed, indicating that the Cu-SPR cannot directly initiate the photochemical reaction. Nevertheless, H. Carcia[22] and coworkers presented direct evidence of the transient signals ascribed to Ti^{3+} following the excitation of Cu-TiO$_2$ with 532 nm laser light pulses which is close to the reported plasmon band maximum of Cu.[21] Two mechanisms have been proposed to explain the observed SPR-enhanced visible light activity of Cu-TiO$_2$. For example, M. Kumar[16] proposed that the Cu NPs transfer electrons to the conduction band of TiO$_2$. However, Y. Lv[21] favors the idea that the Cu NPs initiate an electron-hole pair generation in TiO$_2$. Therefore, a deeper investigation is necessary to achieve further advances of this photocatalytic system.

Herein, different methodologies have been employed to prepare Cu-TiO$_2$ photocatalysts with different Cu NPs/TiO$_2$ ratios and also in such a way that the amount of copper oxides formed on the surface of the nanoparticles could be controlled. Thus, their impact on the photocatalytic activity has been analyzed. The Cu-SPR enhanced visible-harvesting abilities upon different excitation energies were investigated by applying appropriate cutoff filters. Electron paramagnetic resonance (EPR) spectroscopy was employed to probe the species formed by the trapping and reaction of the photogenerated electrons and holes. Moreover, laser flash photolysis was performed to study the charge carrier kinetics. The results presented herein

revealed the role and impact of the Cu NPs as well as of copper oxides on the photocatalytic activity.

4.3. Experimental Section

4.3.1 Photocatalyst Preparation

Cu-TiO$_2$ photocatalysts consisting of 2 wt% Cu on TiO$_2$ (Evonik Aeroxide P25, 80% anatase + 20% rutile) were prepared by a typical sol immobilization (labeled as SIM) method, which was conducted by adding an aqueous solution of poly vinyl alcohol (PVA) (1.2 mL, 1wt % sol., Aldrich, >99%) to 3.3 mL Cu(NO$_3$)$_2$ 3H$_2$O (0.1 M, Roth, ≥99%). A freshly prepared NaBH$_4$ solution (2.5 mL, 0.1 M, Aldrich, >96%) was added dropwise to the above solution, with the color turning dark, indicating the formation of the Cu NPs. After 30 min, the TiO$_2$ support (1.0 g) was added and the suspension was further stirred for 12 h at 25 °C. Experiments were performed both in air and under Ar atmosphere. The samples obtained *via* sol immobilization method were denoted as Cu-TiO$_2$ (SIM).

2 wt%/4 wt% Cu-TiO$_2$ photocatalysts were also prepared by the photodeposition (labeled as PD) method, in which TiO$_2$ was added to 60 mL methanol (Aldrich, >99.8%) and the suspension was flushed with argon to remove the remaining oxygen existing from the reactor. Subsequently, the pre-reduction was initiated by illumination employing a 450 W Xe-lamp (Müller) for 30 min. When the color of the suspension turned to blue, indicating the presence of Ti^{3+}, the aqueous solution of Cu(NO$_3$)$_2$.3H$_2$O (3.3 mL, 0.1 M, Roth, ≥99%) was added dropwise to the suspension. The mixed suspension was further stirred for 2 h at room temperature in argon atmosphere. The samples obtained *via* photodeposition method were denoted as Cu-TiO$_2$ (PD).

All samples were centrifuged, washed three times with distilled water and dried for 12 h at 70 °C. The as-prepared samples were used for catalytic and spectroscopic experiments without any other treatment.

The schematic illustration of the different preparation pathways is presented in Figure S4 in Supplementary Information.

4.3.2 Material Characterization

XRD patterns were monitored by a Bruker D8 Advance X-Ray Diffraction system. UV-Vis diffuse-reflectance spectra were recorded employing a UV-Visible spectrophotometer (Varian Cary 100 Bio). TEM images were characterized by Transmission Electron Microscopy (TEM) (FEI Tecnai G2 F20 TMP) equipped with a 200 kV field emission gun (FEG).

X-ray photoelectron spectroscopy (XPS) measurements were conducted in a PHI Versaprobe II Scanning ESCA Microprobe (Physical Electronics) using a monochromatized Al K_α X-ray source (beam diameter 200 µm, X-ray power of 50 W). The analyser pass energy for detail spectra was set to 23.5 eV with a step time of 50 ms and a step size of 0.2 eV. During measurement, the sample was flooded with slow electrons and Argon ions using the built-in ion sputter and electron guns in order to compensate surface charging effects. Data evaluation was performed using CasaXPS software. For the charge correction, the energy of the C1s-line was set to 284.8 eV.

4.3.3 Photocatalytic H_2 Evolution Tests

Photocatalytic hydrogen evolution measurements were conducted in a double-wall quartz glass reactor, connected to a quadrupole mass spectrometer (QMS, Hiden HPR-20). The system is a continuous gas flow system, in which argon was used as the carrier gas as well as to maintain an oxygen-free atmosphere. 1 g/L photocatalyst suspensions were prepared by suspending Cu-TiO_2 in methanol/water mixtures (volume ratio 1:5). All suspensions were

sonicated for 30 min before being transferred into the reactor. The reaction environment was purged with argon for about 15 min to remove any oxygen present in the suspension and in the headspace of the reactor. The argon gas rate was kept constant at 10 cm^3 min^{-1} during the photocatalytic measurement and the inlet gas flow rate for QMS was 1 cm^3 min^{-1}. Before illumination, the system was stabilized in the dark for 1 h to get a stable baseline. Afterwards, the suspension was illuminated employing an Osram XBO 1000 W Xe-Lamp (Müller). Irradiation spectra in the presence of different cutoff filters were collected by a spectral irradiance meter (SpectraRad xpress, B&W TEK) and the total irradiance (in $mW \cdot cm^{-2}$) up to 800 nm was calculated by integration of the irradiation spectra. As the irradiance changed as a function of the cutoff filter the amount of hydrogen gas produced is presented in μmol g^{-1} J^{-1} in such a way that the possible differences could be related only to the photocatalyst efficiency and not to changes in the light intensity. The temperature of the suspension was maintained at 25°C during the entire measurement by utilizing a cooling system (Julabo).

4.3.4 Electron Paramagnetic Resonance (EPR) Spectroscopy

EPR measurements were performed employing a MiniScope MS400 spectrometer (Magnettech GmbH, Germany). The samples were illuminated with a 450 W Xe-Lamp (Müller) equipped with different optical cutoff filters. A commercial EPR cold finger quartz Dewar enabled low temperature (90 K) measurements in liquid nitrogen, with the samples placed in X-Band standard EPR tubes (Wilmad, 2 mm, O.D.). All measurements in the presence of the hole-scavenger indicator TEMPO (2, 2, 6, 6-Tetramethylpiperidine 1-oxyl，free radical, Aldrich, >99.8%) or the electron-scavenger indicator methyl viologen (MV^{2+}) were performed in air at room temperature. The g values were calculated based on the formula $h\nu = g\beta B_0$ (B_0 – external magnetic field, β – Bohr magneton, g_e – Landé g-factor). The frequency was at around 9.42-9.43 GHz.

4.3.5 Laser Flash Photolysis

Laser flash photolysis measurements were performed utilizing an Nd-YAG laser (Brilliant B, Quantel) and the transient reflectance spectra of the trapped charge carriers were monitored by a laser flash photolysis spectrometer (LKS 80, Applied Photophysics). Together with an Optical Parametric Oscillator (OPO) (MagicPRISM, OPOTEK Inc.), the excitation wavelength was tuned to 420 nm (with 6 mm diameter and 6 ns pulse length) by employing the 3rd harmonic (355 nm) of a Brilliant B laser. The 532 nm laser was supplied by the 2rd harmonic (532 nm) of the Brilliant B laser. The analyzing light (supplied by a 150 W xenon arc lamp) was focused onto the sample and the reflected light was guided through the monochromator into the detector (Hamamatsu R928 photomultiplier). Furthermore, all measurements were performed in diffuse reflectance mode under N_2 atmosphere and 200 shots were fast averaged for every transient. The energy densities of the laser beams were kept around 5-10 mJ/cm² per shot. The transient reflectance change ΔJ was calculated as described in the literature.[23b]

4.4 Results

4.4.1 Material Characterization

Figure 1 shows the XRD patterns of bare TiO_2 and $Cu-TiO_2$ nanoparticles prepared by different methods (SIM and PD). In addition to the peaks of anatase TiO_2 (JCPDS # 01-075-2545) and rutile TiO_2 (JCPDS # 01-073-1782), $Cu-TiO_2$ (SIM) synthesized in the presence of air exhibited a further peak for CuO at $2\theta = 35.5°$, indicating the oxidation of the as-synthesized Cu NPs by O_2. If the synthesis was carried out under argon atmosphere, this peak did not appear, as shown in Figure 1. For 2 wt% $Cu-TiO_2$ (PD), peaks attributed to metallic Cu were observed at $2\theta = 43.4°$, 50.5°, 74.1° (JCPDS #01-089-2838). As expected, upon increase of the Cu concentration (4 wt%), an enhancement on the intensities of these peaks is observed, however, no peaks for copper oxides occurred, evincing that through the PD method, the formation of copper oxides can be greatly diminished in contrast to that obtained by the SIM methodology.

Under atmospheric conditions, the superficial oxidation of the Cu NPs is thermodynamically favorable, thus the presence of copper oxides in all prepared photocatalysts is expected. However, for the material prepared by the PD method the amount of formed copper oxide was below the detection limit of the XRD measurements.
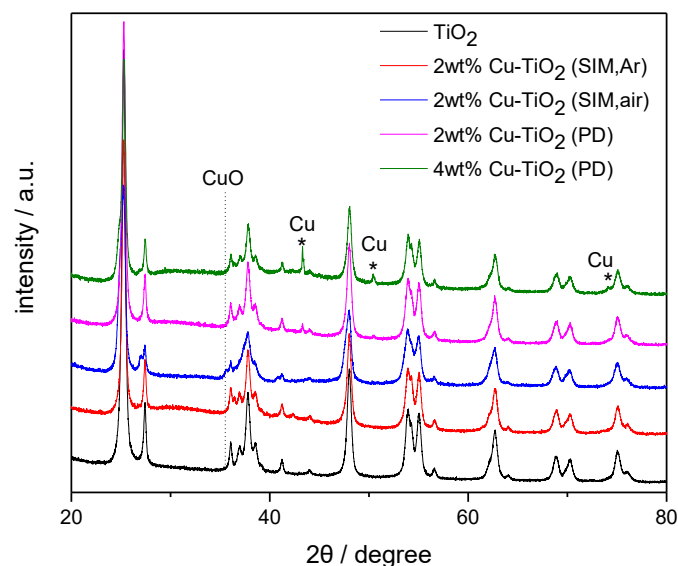

Figure 1. XRD patterns of bare TiO_2 (P25) and of Cu-TiO_2 photocatalysts synthesized *via* different methods.

Further insight into the composition of the as-prepared photocatalysts can be obtained from the UV-Vis absorption spectra. As shown in Figure 2, the Cu NPs obtained in inert atmosphere exhibit a plasmon absorption band with a maximum around 593 nm, which is in accordance with previous reports.[21, 24] When the Cu NPs are exposed to the air, the plasmon absorption band becomes less evident and two new absorption bands at ~455 nm and ~700 nm appeared. These bands can be correlated to the intrinsic absorption features of CuO_x species.[25, 26, 27] For all Cu-TiO_2 composites, the plasmon absorption band at 593 nm cannot be clearly observed and the spectral profile resembles that of the oxidized Cu NPs. Moreover, one can observe that the 2 wt% Cu-TiO_2 composite prepared by the PD method exhibits smaller absorption intensities between 400 and 500 nm as compared with the SIM-prepared samples, which agrees well with

the XRD results and indicates that a reduced amount of CuO_x species were formed. As the concentration of Cu-NPs is increased to 4 wt%, a broad absorption band covering the entire visible range of the spectra is observed that is likely to be an overlap of the Cu-plasmon and the CuO_x absorption bands. It is also clear from Figure 2 that the deposition of Cu-NPs on TiO_2 can greatly enhance the visible-light harvesting ability of the photocatalyst.
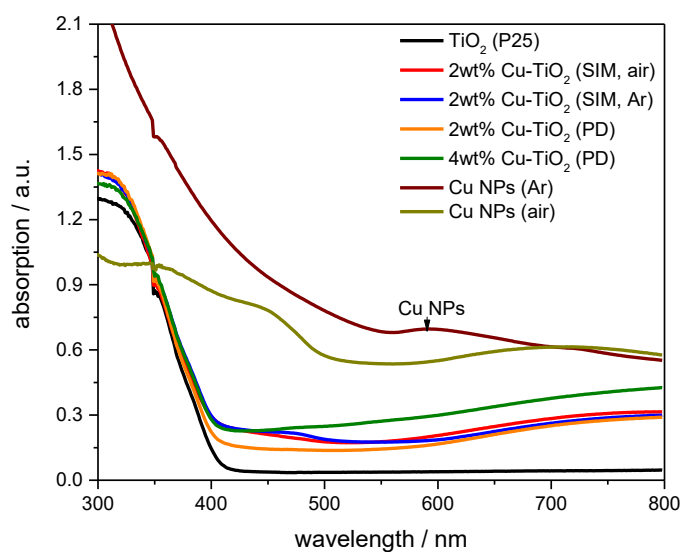

Figure 2. Diffuse-Reflectance UV-Vis spectra of Cu-TiO$_2$ nanocomposites prepared under different conditions along with the spectra for bare TiO$_2$ and for Cu nanoparticles.

The TEM images of the Cu-TiO$_2$ photocatalysts are presented in Figure 3. The brighter spherical structures are the TiO$_2$ (P25) particles, and the darker spots correspond to the Cu NPs, which exhibit particle sizes between 15 nm and 25 nm, being very similar in all samples. The TEM images also revealed that the Cu NPs are well dispersed in the TiO$_2$ matrix. High resolution images (Figure 3e) of the Cu-TiO$_2$ sample prepared by the SIM method under air, allow identifying differences in the crystal lattice on the surface of the Cu NPs in relation to the ones at the core, thus providing further evidence of the surface oxidation.
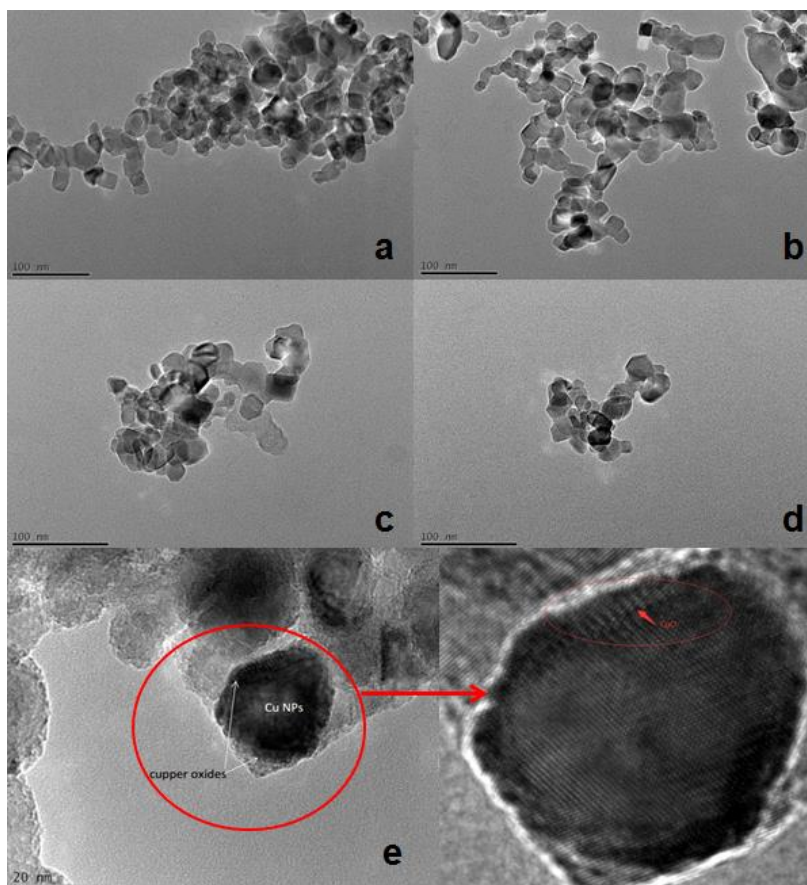
Figure 3. TEM images of a) 2 wt% Cu-TiO$_2$ prepared *via* the SIM method in the presence of air; b) 2 wt% Cu-TiO$_2$ prepared *via* the SIM method in Argon atmosphere; c) 2 wt% Cu-TiO$_2$ prepared *via* the PD method in Argon atmosphere; d) 4 wt% Cu-TiO$_2$ prepared *via* the PD method in Argon atmosphere; e) oxidized Cu NPs on TiO$_2$ deposited *via* the SIM method in the presence of air.

The content of Cu species at the TiO$_2$ surface was analyzed by means of XPS. Accordingly, 1.9% Cu was found in 2 wt% Cu-TiO$_2$ (PD), 2.9% Cu in 4 wt% Cu-TiO$_2$ (PD), 2.2% Cu in 2 wt% Cu-TiO$_2$ (SIM, air), and 1.8% Cu in 2 wt% Cu-TiO$_2$ (SIM, Ar). Furthermore, XPS provides information about the oxidation states of Cu loaded on TiO$_2$. In Fig. S2 detailed spectra of the Cu 2p$_{3/2}$ line for the 4 samples (2 wt% Cu-TiO$_2$ (PD), 4 wt% Cu-TiO$_2$ (PD), 2 wt% Cu-TiO$_2$ (SIM, air), 2 wt% Cu-TiO$_2$ (SIM, Ar)) are shown. The main signal at 932.2 eV can be attributed to either Cu^0 or Cu^I, which are not well distinguishable in the Cu 2p spectrum. The presence of an Auger signal at 917 eV kinetic energy hints towards Cu^I as one component of the main signal, but the signal of Cu^0 at 919 eV is present as well as a weak shoulder in the

stronger Ti 2s signal. In addition to this the Cu $2p_{3/2}$ signal shows a weak satellite structure around 945 eV which is indicative of Cu^{II}. The broadening of the 932.2 eV signal was obtained for all samples, indicating the presence of Cu^{II}. However, it is very difficult to distinguish between Cu(0), Cu(I) and Cu(II) in XPS spectra, especially, to differentiate between Cu(I) and Cu(0). In addition, it should be taken into account that Cu can be easily oxidizied in air, which happens here, as the XPS analysis has not been performed directly after the synthesis. However, as the following photocatalytic H_2 production measrement will show, the presence of Cu ions exhibits almost no effect on the overall efficiency, since they are reduced during the photocatalytic reduction (see Discussion).

4.4.2 Photocatalytic H_2 Production

Figure 4a shows the H_2 evolution rates employing bare TiO_2 and the as-prepared Cu-TiO_2 photocatalysts upon visible light illumination. As different cutoff filters were employed in the experiments, the rates were normalized by the total energy flux density (mW/cm^2) considering the illuminated area of the reactor. No H_2 was detected employing bare TiO_2 as a photocatalyst upon visible light illumination ($\geq$ 420 nm). However, all the prepared Cu-TiO_2 exhibited H_2 production ability upon illumination in the presence of both 420 nm and 500 nm cutoff filters, indicating the enhancement of the visible-harvesting ability due to the Cu NPs and/or the copper oxides.

Comparable H_2 evolution rates were observed for 2 wt% Cu-TiO_2 photocatalysts synthesized *via* different methods and under different conditions, independent on the initial Cu/copper oxides ratios. It should be noted that the color of all the suspensions changed from nearly white to purple (see Figure 4b inset) in the course of the photoreaction, which could be due to reduction of the pre-existing copper oxides. In fact, the H_2 evolution rates measured at the beginning of the illumination (see Figure 4b) exhibit relatively higher variations than the ones observed at longer irradiation times, indicating that part of photogenerated electrons are

consumed by the copper oxides to form Cu^0. Moreover, the H_2 production rates achieved in the presence of a 500 nm cutoff filter are found to be lower than those achieved in the presence of a 420 nm cutoff filter, evincing that the underlying reaction mechanisms in the two cases are not identical.
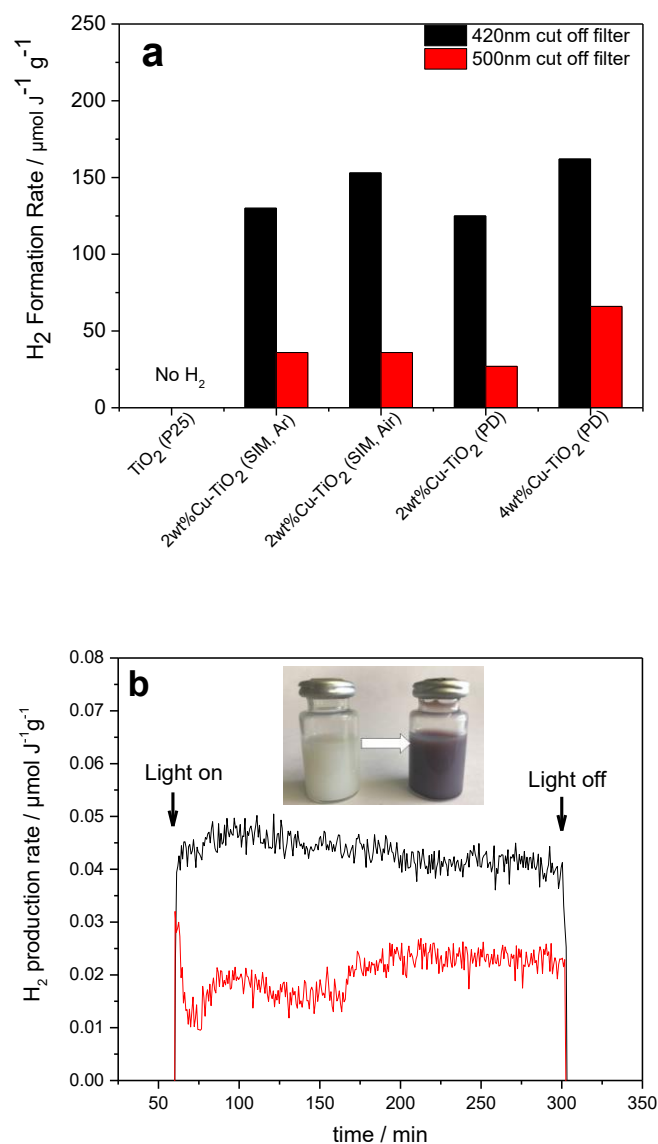
Figure 4. a) Normalized photocatalytic H_2 evolution rates employing bare TiO_2 and the prepared Cu-TiO_2 photocatalysts; b) Normalized photocatalytic H_2 evolution rate of 4 wt% Cu-TiO_2 (PD), obtained from CH_3OH/H_2O mixtures upon visible light illumination in the presence of a 420 nm cutoff filter (black) and a 500 nm cutoff filter (red). Inset: Color change of the Cu-TiO_2 suspension before (left) and after (right) visible light illumination.

The H_2 evolution rate increased in the presence of Cu-TiO$_2$ with higher Cu-loading (4 wt% Cu-TiO$_2$ (PD), especially upon visible light illumination ($\geq$ 500 nm), which is the Plasmon Resonance absorption region of the Cu NPs. This sample was employed for EPR and laser flash photolysis experiments in order to further elucidate mechanistic aspects of the photocatalytic activity of the Cu-TiO$_2$ nanocomposites.

4.4.3 EPR Analyses

EPR spectroscopy was employed to investigate the ability of Cu-TiO$_2$ (PD) composites to produce radical species *via* electron and hole transfers under visible light illumination. Firstly, suspensions containing 4 wt% Cu-TiO$_2$ (PD) were illuminated in the presence of methyl viologen (MV^{2+}). As reported previously, methyl viologen (MV^{2+}) can act as an electron scavenger,[28] since it undergoes a reversible one-electron reduction to form the $MV^{\cdot+}$, which can be visualized by means of EPR spectroscopy:

$$MV^{2+} + e^- \rightarrow MV^{\cdot+} \quad (1)$$
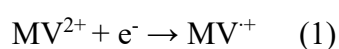
As shown in Figure 5a, MV^{2+} exhibited a small sharp peak in the dark, which is possibly related to contaminants originated from water as evidenced by blank experiments. In the presence of Cu-TiO$_2$ and upon visible light illumination, a strong signal is observed, which can be assigned to the $MV^{\cdot+}$ radical.
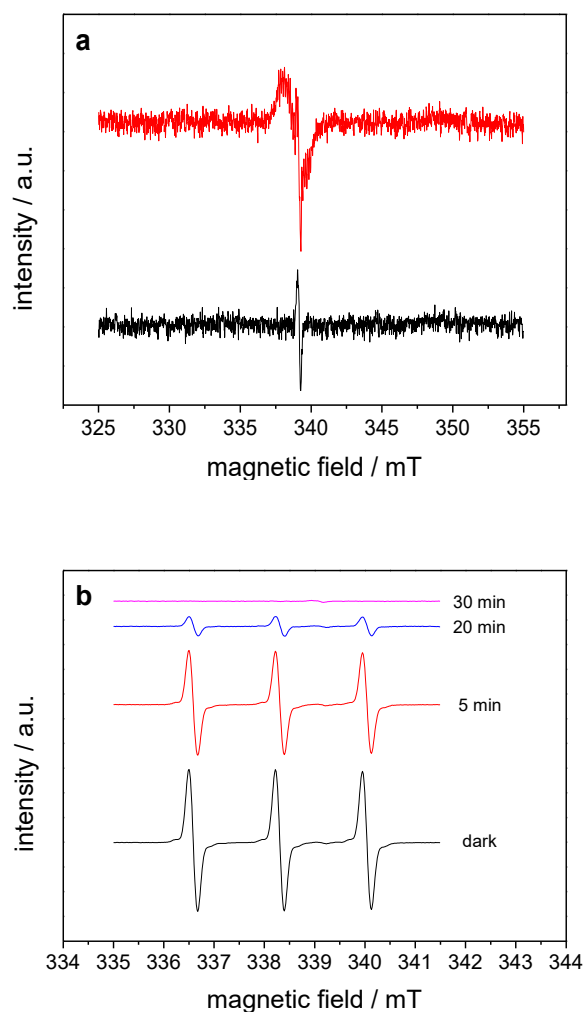
Figure 5. EPR spectra of Cu-TiO$_2$ (PD) measured in the dark (black) and upon visible light ($\geq$ 420 nm) illumination (red) in the presence of a) MV and of b) TEMPO at room temperature.

In addition to the EPR spectra obtained in the presence of an electron scavenger, measurements were carried out also in the presence of a well kwon hole acceptor, that is 2, 2, 6, 6-Tetramethylpiperidine 1-oxyl (TEMPO).[32] In the presence of holes, TEMPO is oxidized to the N-oxo-ammonium salt, according to equation 2. As shown in Figure 5b, in the presence of Cu-TiO$_2$, the EPR signal of TEMPO decreased upon visible light illumination ($\geq$ 420 nm) and disappeared totally within 30 min, indicating that TEMPO can be fully oxidized by the photogenerated holes.

$$+ \, h^+ \longrightarrow \qquad\qquad (2)$$
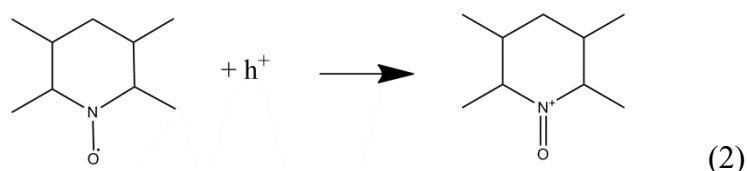
Both experiments shown in Figure 6 show evidence that charge carriers able to promote redox reactions are produced upon light excitation of Cu-TiO$_2$. However, these experiments do not provide information on the origin of the formed charge carriers. The population of the TiO$_2$ conduction band can occur either by direction band-gap or by SPR-induced excitation. Direct evidence of the excitation of bare TiO$_2$ (P25) upon visible light illumination ($\geq$ 420 nm) was provided by the EPR spectra of bare TiO$_2$, Figure 6. In the dark, the remarkable EPR signal of the pre-existing defects identified as rutile Ti^{3+} was observed at around g =1.975, which is in good agreement with previous reports.[30b, 31a] Here, the appearance of new EPR signals (g= 2.00 – 2.03) can be observed under illumination which can be attributed to trapped holes (g= 2.018, 2.014, 2.004) and also to superoxide radicals (g= 2.026, 2.010, 2.003) according to the literature.[30, 31]
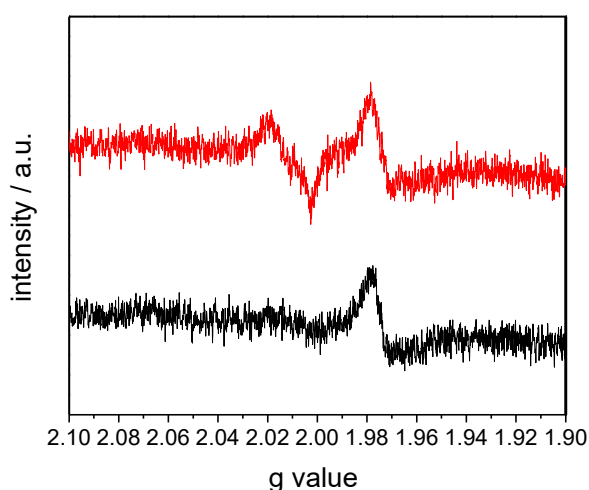

Figure 6: EPR spectra of bare TiO$_2$ measured in the dark (black) and upon visible light ($\geq$ 420 nm) illumination (red) in Ar atmosphere at liquid N$_2$ temperature.

4.4.4 Laser Flash Photolysis

Figures 7a and 7b present, respectively, the transient reflectance signals observed at 680 nm at different excitation wavelengths for bare TiO_2 and for 4 wt% Cu-TiO_2 (PD) in the absence of any electron acceptor or donor. Based on previous reports,[23, 33, 34] transient absorption of electrons trapped on TiO_2 as Ti^{3+} species can be probed at this >650 nm spectral region, while transient signals attributed to trapped holes are more intense at higher energies (400-550 nm). As no electron donor or acceptor is present in the medium, the observed decay of the transient signals can be related to the internal electron/ hole recombination.[23] Looking at the decay profiles (Figure 7a), it can be observed that for the 420 nm excitation, the Cu-TiO_2 photocatalysts exhibit a faster decay of the transient signal during the first 100 μs, which is due to the presence of the Cu NPs acting as electron acceptor.[35] This different behavior observed for Cu-TiO_2 in relation to bare TiO_2 indicates that the presence Cu-NPs on the TiO_2 surface leads to the creation of new trapping sites. Hence, electrons are transferred from the TiO_2 conduction band to the Cu-NPs and backwards, meaning that there is a strong electronic interaction between the oxide and the metallic nanoparticles. Moreover, Figure 7a also presented clear evidence that bare TiO_2 can be directly excited upon 420 nm irradiation.

Figure 7b shows the transient signals of TiO_2 and of 4 wt% Cu-TiO_2 (PD) obtained upon 532 nm laser excitation. As expected, no transient signal can be observed when the bare TiO_2 is excited at 532 nm. On the other hand, the Cu-TiO_2 composites exhibit transient signals at 680 nm evincing the formation of Ti^{3+} species, albeit the intensity of the transient is half of that obtained upon 420 nm excitation. Furthermore, the observation of transient signal attributed to the trapped electrons in TiO_2 upon 532 nm excitation, which is close to the plasmon band of Cu, provide direct experimental evidence that, at the monitored time-scale, excitation of the SPR absorption band of Cu-NPs lead to the population of the TiO_2 conduction band.
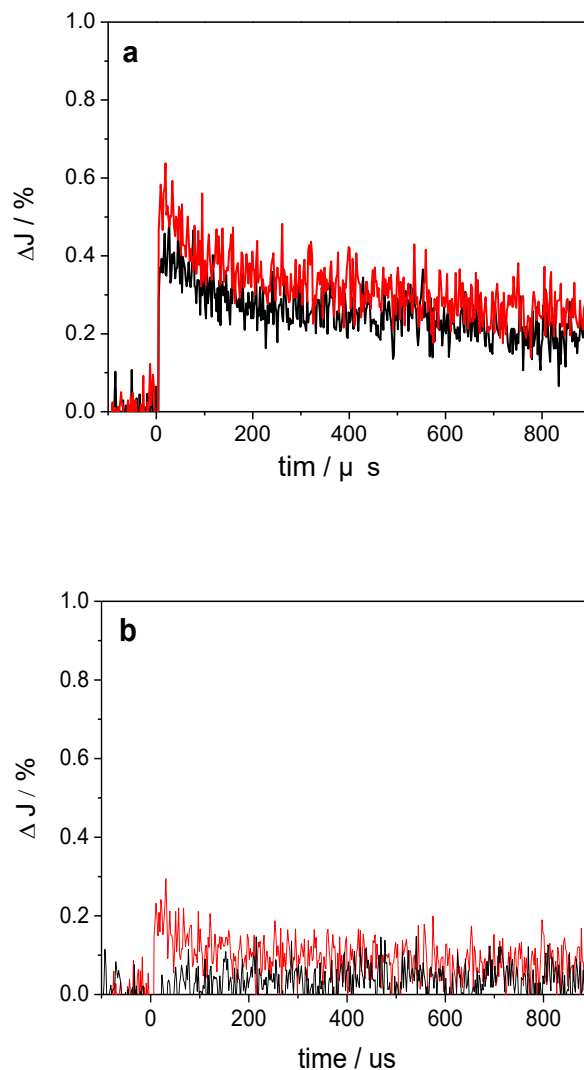
Figure 7. Transient signals of bare (black) TiO$_2$ and of 4 wt% Cu-TiO$_2$-PD (red) observed at 680 nm upon a) 420 nm and b) 532 nm laser excitation in Ar atmosphere.

4.5 Discussion

Cu-TiO$_2$ nanocomposites were successfully synthesized by two different methodologies that are photodeposition (PD) and Sol immobilization (SIM). As evidenced by the XRD patterns (Figure 1) and also by XPS spectra (Figure S2), Cu-NPs can undergo superficial oxidation if the synthesis is carried out in air. This oxidation can be partially avoided under inert atmosphere and in this case the expected plasmonic band of Cu nanoparticles at 593 nm can be clearly

observed. All nanocomposites exhibit visible-light absorption (see Figure 3) and are able to act as photocatalysts for the hydrogen evolution from water/methanol mixtures. The observed rates reveal that the presence of copper oxides does not affect the hydrogen evolution substantially. In fact, based on the observed color change in the course of the reaction, it seems that the initially photogenerated electrons reduce the oxidized copper ions on the surface to metallic copper and then a steady hydrogen evolution rate is observed. The presence of Cu^{2+} and Cu^{+} has been confirmed by means of XPS. Besides the reduction of copper ions, the photogenerated electrons could reduce Ti^{4+} to Ti^{3+}. Ti^{3+} is known for its dark blue color. However, it reacts very fast with oxygen. In contrast, the observed purple coloration remained unchanged over the weeks in the presence of air. Moreover, blank experiments using only TiO_2 does not lead to the permanent color changes as observed for $Cu-TiO_2$. Consequently, the observed color change can be ascribed to the formation of metallic copper. The reduction of copper ions to copper during the photocatalytic reaction is further confirmed by the comparison of XRD patterns of $Cu-TiO_2$ (SIM) before and after visible light illumination (supporting information Figure S1), in which the latter clearly showed the peaks of Cu^0.

The results reported here are in agreement with those published by Neubert et al.[35] who also observed improved charge carrier separation and higher photocatalytic activity in the presence of Cu^{2+}/Cu^{+} species. Hence, no significant negative impact from copper oxides on the photocatalytic H_2 production ability of $Cu-TiO_2$ was observed. In fact, the copper oxides are completely reduced during the course of the irradiation and no longer interfere with the photocatalytic activity. Besides, upon visible light illumination, $Cu-TiO_2$ exhibited comparable H_2 production rate in comparison to $Au-TiO_2$ (supporting information Figure S3) which is known to exhibit good photocatalytic activity with 1 wt% Au NPs[31] on TiO_2 surface. Despite the lower chemical stability of Cu-NPs towards oxidation in comparison with other plasmonic noble metals (e.g. Au), it can be concluded that $Cu-TiO_2$ can be conveniently used as a cost-

saving visible light photocatalyst, since eventual oxidation products are reduced under irradiation.

The photocatalytic reaction could be observed under irradiation with wavelengths above 420 nm, in which TiO_2 can still be excited, despite its bandgap being around 3.2 eV (390 nm). The light absorption in energies smaller than the bandgap energy is typically attributed to the presence of the surface defects such as oxygen vacancies [36]. The photocatalytic activity obtained at wavelengths higher than 500 nm can be attributed to the plasmonic effect of Cu-NPs, where only the excitation through the Cu plasmonic band occurs. The lack of hydrogen production for bare TiO_2 irradiation with wavelengths above 420 nm reveals that the copper nanoparticles also play a role as co-catalysts in the electron transfer reaction to the protons in solution. The observed H_2 evolution rates normalized to the incident light intensities in the presence of a 420 nm cutoff filter are, in fact, higher than those observed when a 500 nm cutoff filter is used, which is indicative for distinct mechanisms being operative when the photocatalysts are excited with different energies. For excitations at lower energies ($\lambda_{ex} \geq 500$ nm) the H_2 evolution rate is enhanced more than 140 % when the Cu loading was increased from 2 to 4 wt% (Figure 4). This behavior differs from the behavior observed upon higher energy excitation ($\lambda_{ex} \geq 420$ nm), in which the H_2 evolution rate increases only by 30 %. This difference clearly shows the important role of the Cu NPs on the light harvesting efficiency at higher wavelengths. Furthermore, the difference in the H_2 evolution rates in the presence of a 420 nm and 500 nm cutoff filters correlates very well with the ns-transient absorption results. Herein, much lower charge carrier concentration (charge carriers which could be utilized for the H_2 production) has been detected upon 532 nm excitation in comparison to 420 nm (see Figure 7).

Recently, it has been taken as a support for the concept that electrons photogenerated upon visible light illumination (≥ 420 nm) cannot originate from the TiO_2 matrix itself [20a, 31, 33, 37, 38] because of its wide band gap (anatase: $E_g = 3.2$ eV, $\lambda_{ox} = 388$ nm; rutile: $E_g = 3.0$ eV, $\lambda_{ox} = 413$

nm). For metal oxide semiconductors modified with metallic nanoparticles, it was proposed that the electrons photogenerated upon excitation at wavelengths higher than 420 nm originate from a plasmonic-induced electron injection.[15, 16, 20a, 31, 33, 37, 38] The EPR and laser flash photolysis measurements performed in the present work with bare TiO_2 (Evonik P25) provide evidence that valence band electrons can indeed be excited in TiO_2 upon ≥ 420 nm illumination, probably due to pre-existing surface defects such as oxygen vacancies[36] or even due to the influence of the rutile content. Moreover, Ohtani *et al.* has reported the visible light activity employing 450 nm filter of rutile rich TiO_2 samples.[39] Obviously, this behavior cannot be generalized and will be dependent on the origin of the metal oxide, its crystal structure, the possible presence of organic contaminants, etc. The direct excitation of TiO_2 could only be excluded upon ≥ 500 nm irradiation. Under these conditions, Cu-NPs can be excited due to the SPR band centered at 593 nm. Subsequently, the higher H_2 evolution rate and higher charge carrier concentration obtained at excitation 420 nm in comparison to 500 nm can be explained by a synergic effect of TiO_2 and Cu excitation.

In terms of the origin of the photogenerated electrons and the underlying mechanism, Kumar et al. proposed that the Cu NPs inject electrons to the conduction band of TiO_2,[16] while other Y. Lu and coworkers claim that the Cu-SPR effect initiate e^-/h^+ generation in TiO_2.[21] The experimental data presented here do not allow to conclusively determine the origin of the electrons, i.e., whether they are originating from electron injection by the Cu-NPs or through a Cu-SPR initiated e^-/h^+ pair generation in TiO_2 resulting from a SPR-enhanced electromagnetic field. However, it should be noted here that the energy of the visible light (≥ 500 nm, i.e., ≤ 2.5 eV) is not sufficient to overcome the band gap energy of TiO_2 ($E_g = 3.2$ eV). In this case, one possible way to explain the visible-light photocatalytic activity caused by the holes can be the Interfacial charge transfer (IFCT), as proposed by Creutz.[40] The Cu-SPR initiates the IFCT

from the valence band to the surface bound Cu-related species (Cu^{2+}, Cu^{+}, Cu^{0}), leading to creation of holes in TiO_2 and electrons on Cu sites.[41]

The above discussed reaction mechanism involving IFCT and emphasizing the catalytic role of Cu is schematically shown in Figure 8.
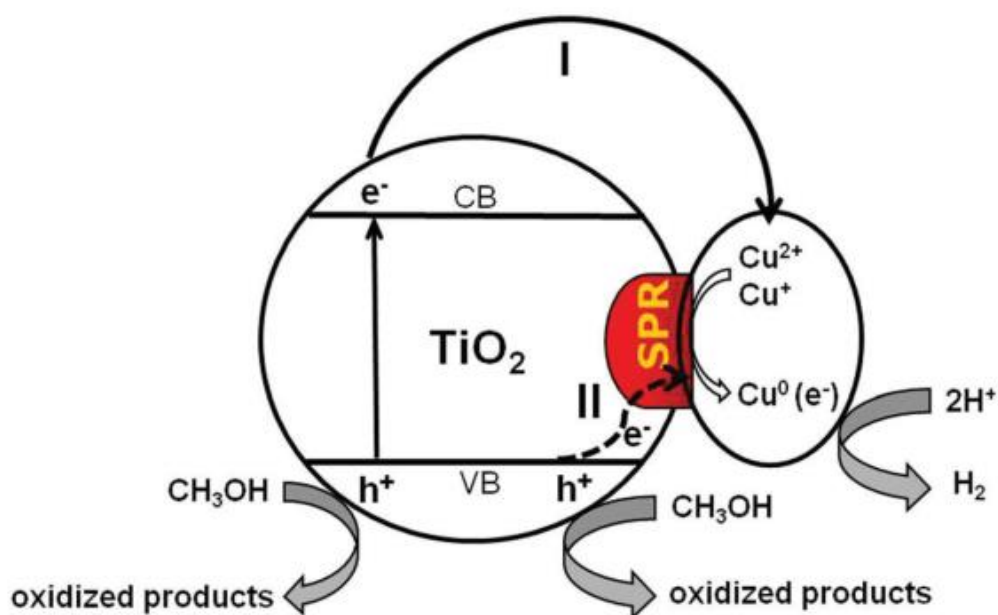

Figure 8. Proposed mechanisms for H_2 production using Cu-TiO_2 in water/methanol mixtures upon illumination at wavelengths above 420 nm (mainly I) and above 500 nm (II).

Independent from the origin of the electrons, it seems to be clear that the electronic coupling between TiO_2 and Cu-NPs promotes a strong electron delocalization which is beneficial for the photocatalytic H_2 production. Additionally, the Cu-NPs act as co-catalysts in the hydrogen evolution reaction, decreasing the activation energy of this reaction. The catalytic role of Cu could be confirmed by the results obtained with laser flash spectroscopy. In the presence of Cu, the transient signal became faster indicating the electron transfer from TiO_2 to Cu NPs. As a result, the formation of molecular hydrogen can only be observed for Cu-TiO_2 composites and not only for Cu-NPs or for bare TiO_2.

4.6 Conclusions

In the present study it has been shown that Cu-TiO$_2$ can be potentially used as a cost-saving visible light photocatalyst for H$_2$ production. Although at the beginning of the photoreaction a negative impact of oxidized Cu species on the photocatalytic H$_2$ production ability is obtained, the presence of copper oxides does not affect the overall hydrogen evolution efficiency substantially. Apparently, the existing Cu^{2+}/Cu$^+$ species were reduced to Cu^0 by the electrons generated from TiO$_2$ upon illumination, which in turn facilitates more electron-hole pair generation under visible light irradiation due to the Cu-SPR effect. Furthermore, direct evidences have been provided that electrons can be generated in bare TiO$_2$ by light illumination at around 420 nm, and at this illumination conditions copper nanoparticles act as co-catalysts in the electron transfer reaction to the protons in solution. Moreover, the electrons generated by direct visible light excitation in TiO$_2$, together with the Cu-SPR induced electrons, contribute to the enhanced photocatalytic H$_2$ production ability of Cu-TiO$_2$ photocatalyst. The detected hydrogen evolution upon excitation above 500 nm can be solely attributed to the Cu-SPR induced charge carrier formation. However, for the understanding of the Cu-SPR role in the photocatalytic reaction further studies need to be carried out.

4.7 Acknowledgement

4.8 References

[1] H. Tong, S. Ouyang, Y. Bi, N. Umezawa, M. Oshikiri and J. Ye, Nano-photocatalytic materials: possibilities and challenges. *Adv. Mater.*, 2012, 24, 229-251.

[2] L. Liu, T. D. Dao, R. Kodiyath, Q. Kang, H. Abe, T. Nagao and J. Ye, Plasmonic Janus-composite photocatalyst comprising Au and C–TiO_2 for enhanced aerobic oxidation over a broad visible-light range. *Adv. Funct. Mater.*, 2014, 24, 7754–7762.

[3] J. Schneider, M. Matsuoka, M. Takeuchi, J. Zhang, Y. Horiuchi, M. Anpo and D. W. Bahnemann, Understanding TiO_2 photocatalysis: mechanisms and materials. *Chem. Rev.*, 2014, 114, 9919−9986.

[4] N. Q. Wu, J. Wang, D. Tafen, H. Wang, J. G. Zheng, J. P. Lewis, X. Liu, S. S. Leonard and A. Manivannan, Shape-enhanced photocatalytic activity of single-crystalline anatase TiO_2 (101) nanobelts. *J. Am. Chem. Soc.*, 2010, 132, 6679−6685.

[5] P. Zhang, T. Wang and J. Gong, Mechanistic understanding of the plasmonic enhancement for solar water splitting. *Adv. Mater.*, 2015, 27, 5328–5342.

[6] M. R. Hoffmann, S.T. Martin, W. Choi and D. W. Bahnemann, Environmental applications of semiconductor photocatalysis. *Chem. Rev.*, 1995, 95, 69-96.

[7] X. Chen and S.S. Mao, Titanium dioxide nanomaterials: synthesis, properties, modifications, and applications. *Chem. Rev.*, 2007, 107, 2891-2959.

[8] R. Asahi, T. Morikawa, T. Ohwaki, K. Aoki and Y. Taga, Visible-light photocatalysis in Nitrogen-doped titanium oxides. *Science*, 2001, 293, 269-271.

[9] (a) A. L. Linsebigler, G. Lu and J. T. Yates, Photocatalysis on TiO_2 surfaces: principles, mechanisms, and selected results .*Chem. Rev.*, 1995, 95, 735-758; (b) A. Fujishima, X. Zhang and D. A. Tryk, TiO_2 Photocatalysis and related surface phenomena. *Surf. Sci. Rep.*, 2008, 63, 515-582.

[10] (a) K. A. Borges, L. M. Santos, R. M. Paniago, N. M. Barbosa Neto, Schneider, J.; D. W. Bahnemann, A. O. T. Patrocinio and A. E. H. Machado, Characterization of a highly efficient N-doped TiO_2 photocatalyst prepared via factorial design. *New J. Chem.*, 2016, 40, 7846-7855; (b) L. M. Santos, W. A. Machado, M. D. Franca, K. A. Borges, R. M. Paniago, A. O. T. Patrocinio and A. E. H. Machado, Structural characterization of Ag-doped TiO_2 with enhanced photocatalytic activity. *RSC Advances*, 2015, 5, 103752-103759; (c) R. Asahi, T. Morikawa, H. Irie and T.

Ohwaki, Nitrogen-doped titanium dioxide as visible-light-sensitive photocatalyst: designs, developments, and prospects. *Chem. Rev.*, 2014, 114 (19), 9824-9852; (d) S. G. Kumar and L. G. Devi, Review on modified TiO$_2$ photocatalysis under UV/visible light: selected results and related mechanisms on interfacial charge carrier transfer dynamics. *J. Phys. Chem. A*, 2011, 115, 13211-13241.

[11] S. Linic, P. Christopher and D. B. Ingram, Plasmonic-metal nanostructures for efficient conversion of solar to chemical energy. *Nat. Mater.*, 2011, 10, 911-921.

[12] Y. Tachibana, L. Vayssieres and J. R. Durrant, Artififial photosynthesis for solar water-splitting. *Nat. Photonics.*, 2012, 6, 511-518.

[13] X. Zhang, Y. L. Chen, R. Liu and D. P. Tsai, Plasmonic photocatalysis. *Rep. Prog. Phy.*, 2013, 76, 046401-046441.

[14] G. H. Chan, J. Zhao, E. M. Hicks, G. C. Schatz and R. P. Van Duyne, Plasmonic properties of copper nanoparticles fabricated by nanosphere lithography. *Nano Lett.*, 2007, 7, 1947-1952.

[15] J. Pal, A. K. Sasmal, M. Ganguly and T. Pal, Surface plasmon effect of Cu and presence of n−p heterojunction in oxide nanocomposites for visible light photocatalysis. *J. Phys. Chem. C*, 2015, 119, 3780−3790.

[16] M. K. Kumar, K. Bhavani, G. Naresh, B. Srinivas and A. Venugopal, Plasmonic resonance nature of Ag-Cu/TiO$_2$ photocatalyst under solar and artificial light: Synthesis, characterization and evaluation of H$_2$O splitting activity. *Appl. Catal. B Environ.*, 2016, 199, 282–291.

[17] J. M. Kum, Y. J. Park, H. J. Kim and S. O. Cho, Plasmon-enhanced photocatalytic hydrogen production over visible-light responsive Cu/TiO$_2$. *Nanotechnology,* 2015, 26, 125402-125406.

[18] J. H. Kim, S. H. Ehrman and T. A. Germer, Influence of particle oxide coating on light scattering by submicron metal particles on silicon wafers. *Appl. Phys. Lett.*, 2004, 84, 1278-1280.

[19] T.D. Pham, B. K. Lee and C.H. Lee, The advanced removal of benzene from aerosols by photocatalytic oxidation and adsorption of Cu–TiO$_2$/PU under visible light irradiation. *Appl. Catal. B Environ.*, 2016, 182, 172–183.

[20] (a) Y. Zou, S.Z. Kang, X. Li, J. Qin and M. Mu, TiO$_2$ nanosheets loaded with Cu: A low-cost efficient photocatalytic system for hydrogen evolution from water. *Int. J. Hydrogen Energy.*, 2014, 39, 15403–15410; (b)

T. D. Pham and B. K. Lee, Cu doped TiO$_2$/GF for photocatalytic disinfection of *Escherichia coli* in bioaerosols under visible light irradiation: Application and mechanism. *Appl. Surf. Sci.*, 2014, 296, 15–23.

[21] Y. Lv, X. Cao, H. Jiang, W. Song, C. Chen and J. Zhao, Rapid photocatalytic debromination on TiO$_2$ with *in-situ* formed copper co-catalyst: enhanced adsorption and visible light activity. *Appl. Catal. B Environ.*, 2016, 194, 150–156.

[22] H. G. Baldoví, Ş. Neaţu, A. Khan, A. M. Asiri, S. A. Kosa and H. Garcia, Understanding the origin of the photocatalytic CO$_2$ reduction by Au- and Cu-loaded TiO$_2$: a microsecond transient absorption spectroscopy study. *J. Phys. Chem. C*, 2015, 119, 6819−6827;

[23] (a) D. W. Bahnemann, M. Hilgendorff and R. Memming, Charge Carrier Dynamics at TiO$_2$ Particles: Reactivity of Free and Trapped Holes. *J. Phys. Chem. B*, 1997, *101*, 4265-4275; (b) J. Schneider, K. Nikitin, M. Wark, D. W. Bahnemann and R. Marschall, Improved charge carrier separation in barium tantalate composites investigated by laser flash photolysis. *Phys. Chem. Chem. Phys.*, 2016, 18, 10719—10726.

[24] S. Mallick, P. Sanpui, S. S. Ghosh, A. Chattopadhyay and A. Paul, Synthesis, characterization and enhanced bactericidal action of a chitosan supported core-shell copper-silver nanoparticle composite. *RSC Adv.*, 2015, 5, 12268-12276.

[25] S. Qi, F. Xin, Y. Liu, X. Yin and W. Ma, Photocatalytic reduction of CO$_2$ in methanol to methyl formate over CuO–TiO$_2$ composite catalysts. *Journal of Colloid and Interface Science*, 2011, 356, 257–261.

[26] G. Colon, M. Maicu, M.C. Hidalgo and J. A. Navıo, Cu-doped TiO$_2$ systems with improved photocatalytic activity. *Appl. Catal. B Environ.*, 2006, 67, 41–51.

[27] P. S. Kumar, M. Selvakumar, S. G. Babu, S. K. Jaganathan, S. Karuthapandian and S. Chattopadhyay, Novel CuO/chitosan nanocomposite thin film: facile hand-picking recoverable, efficient and reusable heterogeneous photocatalyst. *RSC Adv.*, 2015, 5, 57493 -57501.

[28] (a) T. Ogawa, H. Nishikawa, S. Nishimoto and T. Kagiya, Poly (vinyl alcohol) film containing methyl viologen as a highly sensitive dosimeter. *Radiat.Phys.Chem*., 1987, 5, 353-357; (b) S. Nishimoto, M. Ye, Y. Lu, T. Kawamura and T. Kagiya, ESR spectrometric characterization of the methyl viologen dosimeter in poly (vinyl alcohol) film. *T. Radiat. Phys.Chem.*, 1988, 32, 727-730.

[29] C. Nasr and S. Hotchandani, Excited-state behavior of nile blue H-aggregates bound to SiO_2 and SnO_2 colloids. *Chem. Mater.*, 2000, 12, 1529–1535.

[30] (a) T. Hirakawa, H. Kominami, B. Ohtani and Y. Nosaka, Mechanism of photocatalytic production of active oxygens on highly crystalline TiO_2 particles by means of chemiluminescent probing and ESR spectroscopy. *J. Phys. Chem. B.*, 2001, 105, 6993-6999; (b) D. C. Hurum, A. G. Agrios, K. A. Gray, T. Rajh and M. C. Thurnauer, Explaining the Enhanced Photocatalytic Activity of Degussa P25 Mixed-Phase TiO_2 Using EPR. *J. Phys. Chem. B.*, 2003, 107, 4545-4549.(c) C. P. Kumar, N. O. Gopal, T. C. Wang, M. S. Wong and S. C. Ke, EPR investigation of TiO_2 nanoparticles with temperature-dependent properties. *J. Phys. Chem. B.*, 2006, 110, 5223-5229.

[31] (a) J. B. Priebe, M. Karnahl, H. Junge, M. Beller, D. Hollmann and A. Brückner, Water reduction with visible light: synergy between optical transitions and electron transfer in Au-TiO_2 catalysts visualized by in situ EPR spectroscopy. *Angew. Chem., Int. Ed.*, 2013, 52, 11420-11424; (b) J. B. Priebe, J.Radnik, A. J. J. Lennox, M. Pohl, M. Karnahl, D. Hollmann, K. Grabow, U. Bentrup, H. Junge, M. Beller and A. Brückner, Solar hydrogen production by plasmonic Au−TiO_2 catalysts: impact of synthesis protocol and TiO_2 phase on charge transfer efficiency and H_2 evolution rates. *ACS Catalysis*, 2015, 5, 2137-2148.

[32] (a) T. Wu, S.Xu, J. Shen, S. Chen, M. Zhang and T. Shen, EPR investigation of the free radicals generated during the photosensitization of TiO_2 colloid by hypocrellin B. *Free Radic Res.*, 2001, 35, 137-143; (b) P. J. Wright and A. M. English, Scavenging with TEMPO$^{\bullet}$ to identify peptide- and protein-based radicals by mass spectrometry: advantages of spin scavenging over spin trapping. *J. Am. Chem. Soc.*, 2003, 125, 8655–8665.

[33] (a) M. Serra, J. Albero and H. Garcia, Photocatalytic activity of Au/TiO_2 photocatalysts for H_2 evolution: role of the Au nanoparticles as a function of the irradiation wavelength. *ChemPhysChem.* 2015, *16*, 1842-1845; (b) H. Baldoví, G. S. Neaţu, A. Khan, A. M. Asiri, S. A. Kosa and H. Garcia, Understanding the origin of the photocatalytic CO_2 reduction by Au- and Cu-loaded TiO_2: a microsecond transient absorption spectroscopy study. *J. Phys. Chem. C.*, 2015, 119, 6819-6827.

[34] A. O. T. Patrocinio, J. Schneider, M. D. França, L. M. Santos, B. P. Caixeta, A. E. H. Machado and D. W. Bahnemann, Charge carriers dynamics and photocatalytic behavior of TiO_2 nanopowders submitted to hydrothermal or conventional heat treatment. *RSC Adv.*, 2015, 5, 70536-70545.

[35] S. Neubert, D. Mitoraj, S. A. Shevlin, P. Pulisova, M. Heimann, Y. Du, G. K. L. Goh, M. Pacia, K. Kruczała, S. Turner, W. Macyk, Z. Guo, R. K. Hocking and R. Beranek, Highly efficient rutile TiO_2 photocatalysts with single Cu(II) and Fe(III) surface catalytic sites. *J. Mater. Chem. A*, 2016, 4, 3127–3138.

[36] M. K. Nowotny, L. R. Sheppard, T. Bak and J. Nowotny, Defect chemistry of titanium dioxide. Application of defect engineering in processing of TiO_2-based photocatalysts. *J. Phys. Chem. C*, 2008, 112, 5275-5300.

[37] C. Gomes Silva, R. Juárez, T. Marino, R. Molinari and H. García, Influence of excitation wavelength (UV or visible light) on the photocatalytic activity of titania containing gold nanoparticles for the generation of hydrogen or oxygen from water. *J. Am. Chem. Soc.*, 2011, 133, 595– 602.

[38] K. Qian, B. C. Sweeny, A. C. Johnston-Peck, W. Niu, J. O. Graham, J. S. DuChene, J. Qiu, Y. Wang, M. H. Engelhard, D. Su, E. A. Stach and W. D. Wei, Surface plasmon-driven water reduction: gold nanoparticle size matters. *J. Am. Chem. Soc.*, 2014, 136, 9842−9845.

[39] E. Kowalska, O. O. P. Mahaney, R. Abe and B. Ohtani. Visible-light-induced photocatalysis through surface plasmon excitation of gold on titania surfaces. *Phys. Chem. Chem. Phys.*, 2010, 12, 2344–2355

[40] (a) C. Creutz, B. S. Brunschwig and N. Sutin, Interfacial Charge-Transfer absorption: semiclassical treatment. *J. Phys. Chem. B* 2005, 109, 10251-10260; (b) C. Creutz, B. S. Brunschwig and N. Sutin, Interfacial Charge-Transfer absorption: 3. application to semiconductor−molecule assemblies. *J. Phys. Chem. B*, 2006, 110, 25181– 25190.

[41] (a) H. Irie, K. Kamiya, T. Shibanuma, S. Miura, D. A. Tryk, T. Yokoyama and K. Hashimoto, Visible light-sensitive Cu(II)-grafted TiO_2 photocatalysts: activities and X-ray absorption fine structure analyses. *J. Phys. Chem. C*, 2009, 113, 10761-10766; (b) H. Yu, H. Irie, Y. Shimodaira, Y. Hosogi, Y. Kuroda, M. Miyauchi and K. Hashimoto, An efficient visible-light-sensitive Fe(III)-grafted TiO_2 photocatalyst. *J. Phys. Chem. C*, 2010, 114, 16481–16487.
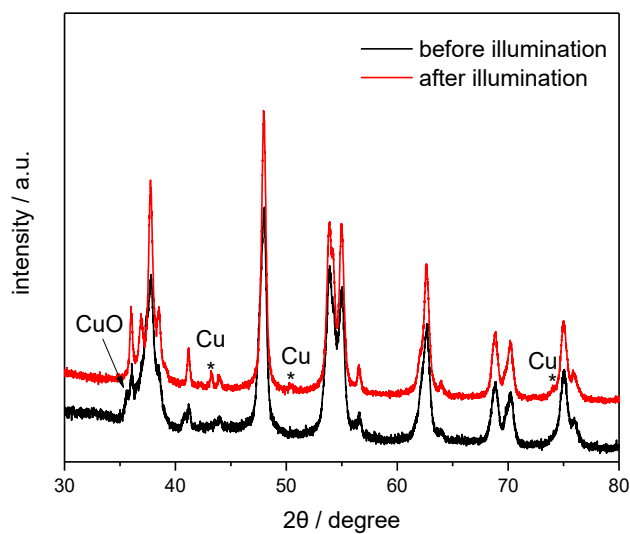
4.9 Supplementary Information

Figure S1. XRD patterns of Cu-TiO$_2$ (SIM) photocatalysts characterized before (black) and after (red) visible light illumination.
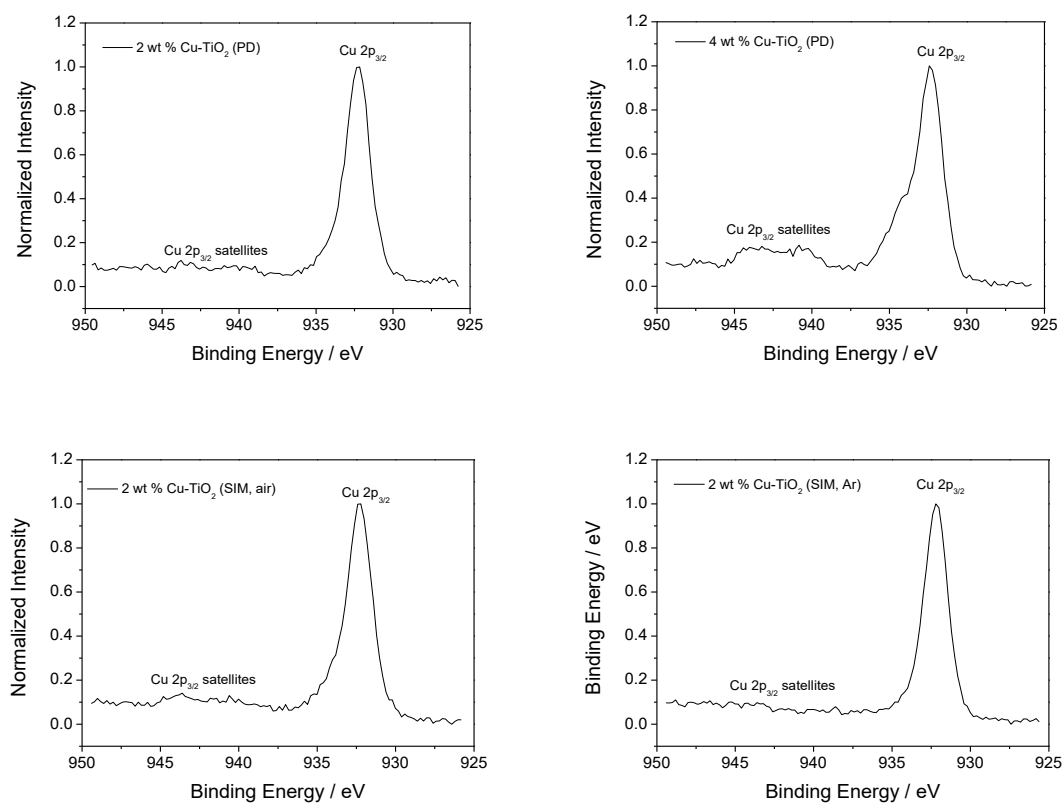
Figure S2. XPS detail spectrum of the Cu 2p$_{3/2}$-line for samples
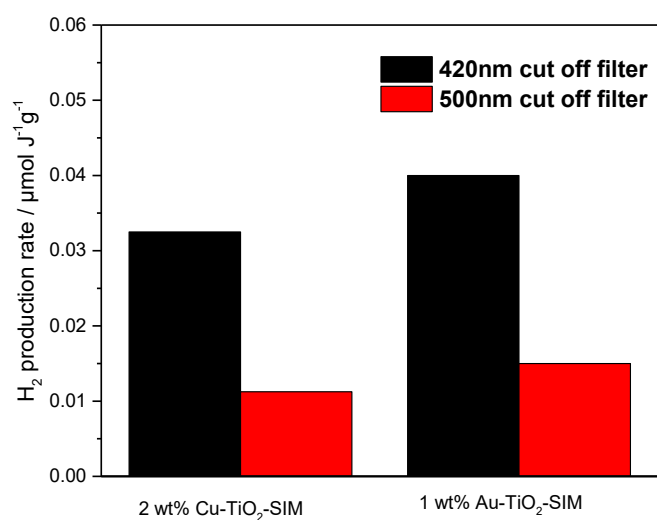
Figure S3. Normalized photocatalytic H_2 evolution rates obtained upon visible light illumination employing 2 wt% $Cu-TiO_2$ and 1wt% $Au-TiO_2$ photocatalysts.

Table S1: Photocatalytic H_2 evolution rates from CH_3OH/H_2O mixtures measured under UV-Vis and visible-light illumination employing different photocatalysts.

Catalyst	H_2 evolution rate / $mmolg^{-1}h^{-1}$		
--	UV-Vis	Vis ($\geq$ 420 nm)	Vis ($\geq$ 500 nm)
Cu NPs	0	0	0
$Cu-SiO_2$	0	0	0

Figure S4. Schematic illustration of the Cu-TiO$_2$ preparation via (a) SIM and (b) PD methods.

Chapter 5 Summarizing Discussion, Conclusion and Outlook

5.1 Summarizing Discussion

As known, M-TiO$_2$ (M=Au and Cu) exhibits visible light photocatalytic H$_2$ production ability and the deposited noble metal na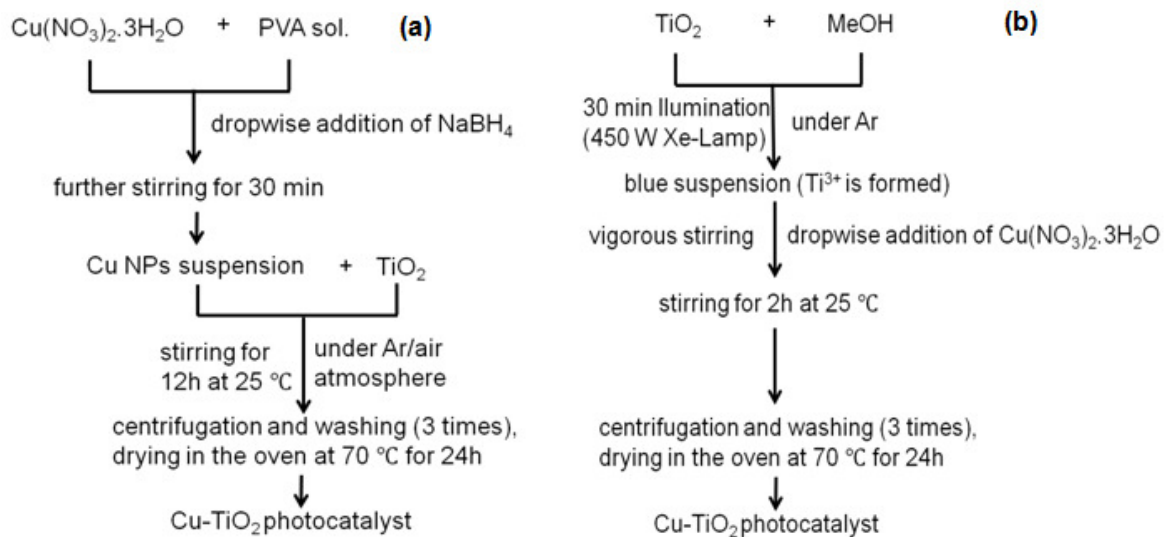noparticle plays a crucial role in the visible light driven photocatalytic reactions. However, the role and impact of these deposited noble metal nanoparticles are still not very clear.

This thesis presents spectroscopic and mechanistic studies of visible light driven photocatalytic H$_2$ production abilities employing TiO$_2$ based materials.

Combining the results of H$_2$ evolution tests together with those obtained during in situ EPR- and Laser Flash Photolysis measurements, as well as the DFT calculation results, the impact of noble metal (e.g. Au and Cu) clusters on the H$_2$-evolution half reaction of TiO$_2$ based photocatalysts upon visible light illumination has been investigated. Besides, by using different indicators and employing different wavelength incident light illumination, the origin of photoinduced electrons and holes has been revealed. The obtained results are summarized below.

5.1.1 The Role of Au Loading for Visible-Light Photocatalytic Activity of Au-TiO$_2$ (UV100)

As known, Au-TiO$_2$ photocatalyst can produce H$_2$ upon visible light illumination ($\geq$ 420 nm). Though some researchers have directly attributed the visible light H$_2$ production ability above 420 nm to the Au-SPR effect. However, the origin of the electrons remains ambiguous. In this research, H$_2$ was observed for Au-TiO$_2$ employing commercial UV100 as TiO$_2$ source in the experiment. Results obtained from EPR and laser flash photolysis also confirmed that bare anatase TiO$_2$ can be excited upon light illumination at around 420 nm, most likely due to pre-existing defects such as oxygen vacancies. Laser flash photolysis even presented direct

evidence that bare TiO_2 can be directly excited by 420 nm laser beam, which has long been neglected in the previous literatures. Besides, in comparison to bare anatase TiO_2, the Au loaded TiO_2 presents an inconspicuous transient absorption for Ti^{3+}, indicating the transfer of the electrons photogenerated in TiO_2 to the Au nanoparticles. In this case, Au nanoparticles simply act as co-catalysts to promote the separation of the photoinduced electrons and holes. It is unconvincing to attribute the visible light photocatalytic activity of Au-TiO_2 to the Au-SPR effect while using a 420 nm cutoff filter. However, due to the fact that Au nanoparticle size strongly affects the SPR intensity and the TiO_2 type also plays a crucial role in the photocatalysis, no Au-SPR induced electrons and/or holes were observed employing anatase as TiO_2 source in the presence of a 500 nm cutoff filter or applying 530 nm laser. Besides, in the presence of a 500 nm cutoff filter, no H_2 was detected within the detection limit. The results obtained from EPR and laser flash photolysis matches well with the results observed in the H_2 production tests. Therefore, the role of Au nanoparticles for visible light photocatalytic H_2 production using Au-TiO_2 (employing UV100 as TiO_2 source) was illustrated in figure 5.1.
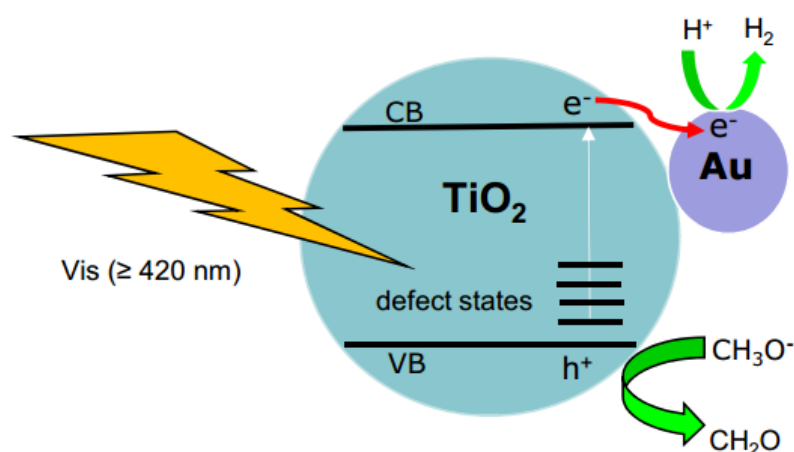

Figure 5.1. The role of Au nanoparticles for H_2 production using Au-TiO_2 (employing UV100 as TiO_2 source) in water/methanol mixtures upon visible light illumination.

The highlights are listed here:

1. Bare anatase TiO_2 can be excited by visible light illumination at around 420 nm.

2. Upon visible-light ($\geq$ 420 nm) illumination, the excited electrons in TiO_2 migrate to the surface-loaded Au nanoparticles.

3. Upon illumination above 500 nm, no SPR-induced H_2 formation was detected for Au-TiO_2, employing pure anatase as TiO_2 source.

However, the obtained results are different from those previous published results employing commercial P25 or self-made TiO_2 annealed at high temperature as TiO_2 source. Therefore, the extensively used commercial P25 was selected as the TiO_2 matrix in the following investigation.

5.1.2 Mechanism of the SPR-Driven Photocatalytic H_2 Production of Au-TiO_2 (P25)

Upon visible light illumination (employing a 500 nm cutoff filter), H_2 was observed using Au-TiO_2 (P25) as the photocatalyst. However, UV-Vis spectroscopy and H_2 production tests clearly showed that bare TiO_2 absorbs no light in the wavelength range above 500 nm and no H_2 can be formed ($\geq$ 500 nm). It was also excluded that the visible-activity of Au-TiO_2 above 500 nm is caused by the impurities remaining in the catalyst from the synthesis. The observation of any H_2 and signals of trapped electrons and holes upon illumination above 500 nm can be solely attributed to the Au-SPR induced charge carrier formation.

It has been confirmed that bare P25 cannot be excited by visible light illumination above 500 nm. EPR and laser flash photolysis both present evidence that Au-TiO_2 can be excited by light illumination above 500 nm or 532 nm laser beam, which exactly covers the plasmon band of Au. In the case, both the signals of trapped electrons and trapped holes were observed. However, the energy of the Au-SPR is insufficient to overcome the bandgap of TiO_2 and no holes can be transferred from the Au nanoparticles to the valence band of TiO_2. Therefore, it is assumed that the signals of the trapped electrons and holes are originated from two distinct processes, rather than the simple electron-hole pair excitation, as illustrated in figure 5.2.
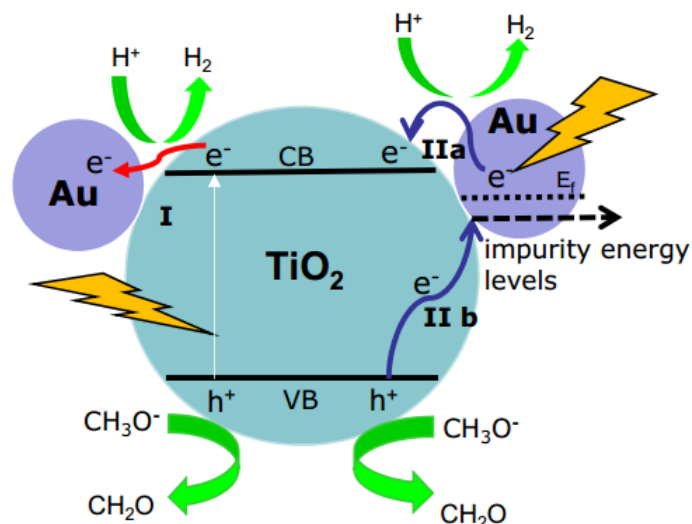
Figure 5.2. Proposed mechanisms for H_2 production using Au-TiO$_2$ in water/methanol mixtures upon visible light illumination (≥ 420 nm: process I + II; ≥ 500 nm: process II).

In this case, it is assumed that Au nanoparticles can inject the SPR-induced hot electrons into the TiO$_2$ conduction band upon visible light illumination (≥ 500 nm). Simultaneously, the Au-SPR can also initiate electron-hole pair generation in TiO$_2$. However, due to the photons energy/E_{SPR} is insufficient to overcome the band gap of TiO$_2$, the SPR-induced electrons directly transfer to the surface Au-related species through the interfacial charge transfer process rather than via the excited state. The DFT calculation results are in good agreement with the experimental data obtained from EPR and laser flash photolysis, which strongly supported the proposed mechanism. Moreover, the DFT calculation analysis clearly shows how the d orbitals of Au clusters create impurity energy levels and decrease the band gap of Au-TiO$_2$.

The highlights are listed here:

1. Au-SPR driven photocatalytic H$_2$ production was observed upon visible light illumination (≥ 500 nm).

2. Upon illumination above 500 nm, Au-SPR-induced hot electrons can transfer into the conduction band of TiO$_2$.

3. Au-SPR can initiate electron-hole pair generation in TiO_2, however, the initiated electrons transfer to the surface Au-related species through the IFCT process rather than via the excited state.

4. The DFT calculation results strongly supported the experimental results and the DFT calculation analysis clearly shows how the d orbitals of Au clusters create impurity energy levels and decrease the band gap of Au-TiO_2.

It has been proven that Au-TiO_2 (P25) exhibits good visible light photocatalytic ability. However, for large scale industrial applications, low cost plasmonic metals, such as copper, should be investigated aiming at cost-effective photocatalysts.

5.1.3 Plasmonic Enhancement for Photocatalytic H_2 Production by Cu-TiO_2 upon Visible Light Illumination

Cu-TiO_2 nanocomposites were successfully synthesized by both PD and SIM methodologies. The role and impact of Cu nanoparticles and copper oxides in the visible light driven photocatalytic H_2 production reaction have been revealed.

It is confirmed that Cu-NPs can be oxidized if the synthesis is carried out in air. This oxidation can be partially avoided under inert atmosphere and in this case the expected plasmonic band of Cu nanoparticles at 593 nm can be clearly observed. Besides, the peak for Cu and copper oxides can be detected in the XRD patterns of the samples prepared in inert atmosphere and in air, respectively. Due to the low chemical stability of Cu-NPs towards oxidation, not only Cu, but also Cu^{2+}/Cu^+ species exist in all the prepared nanocomposites.

All these synthesized nanocomposites can exhibit visible-light driven hydrogen evolution ability from water/methanol mixtures. Although, at the beginning of the photoreaction, negative impact of oxidized Cu species on the photocatalytic H_2 production ability is observed, the presence of copper oxides does not affect the overall hydrogen evolution efficiency

substantially. The color change during the photocatalytic reaction process evinced that the copper ions (Cu^{2+}/Cu^+) are reduced to metallic copper (Cu^0), which is further verified by XRD analysis. Actually, the new formed Cu^0 by the reduction of the existing Cu^{2+}/Cu^+ species will in turn promote the separation of the photoinduced electrons and holes due to the co-catalyst role of Cu and facilitate more electron-hole pair generation under visible light illumination due to the Cu-SPR effect.

Moreover, the apparently distinct H_2 production rates achieved in the presence of a 500 nm cutoff filter and in the presence of a 420 nm cutoff filter evinced that the underlying reaction mechanisms in the two cases are not identical. As mentioned above, electrons can be generated in bare TiO_2 by light illumination at around 420 nm, and in this case, copper nanoparticles act as co-catalysts in the electron transfer reaction. Besides, the detected hydrogen evolution upon excitation above 500 nm can be solely attributed to the Cu-SPR induced charge carrier formation. Therefore, as shown in figure 5.3, the electrons generated by direct visible light excitation in TiO_2 (process I), together with the Cu-SPR induced electrons (process II), cooperatively contribute to the enhanced photocatalytic H_2 production ability of Cu-TiO_2 photocatalyst.
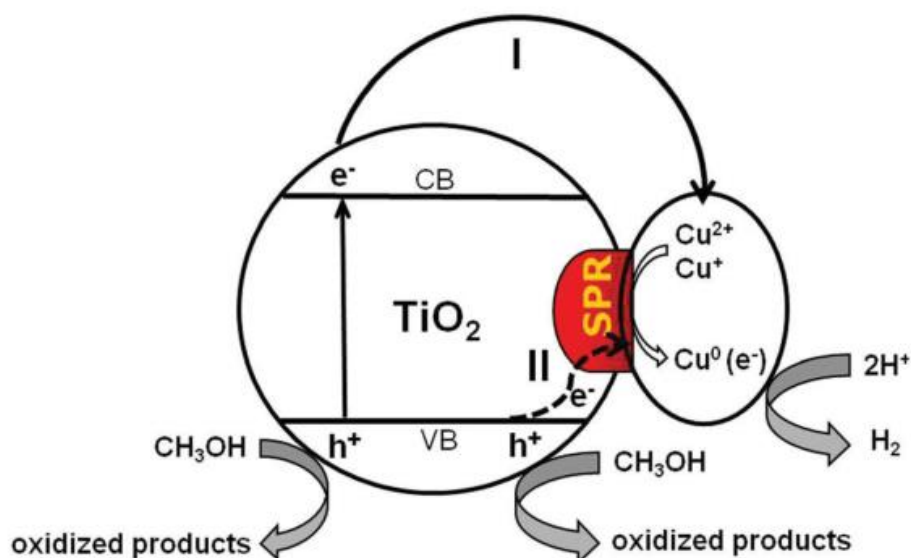
Figure 5.3 Proposed mechanisms for H$_2$ production using Cu–TiO$_2$ in water/methanol mixtures upon illumination at wavelengths above 420 nm (mainly I) and above 500 nm (II)

The highlights are listed here:

1. Cu-TiO$_2$ can be potentially used as a cost-saving visible light photocatalyst for H$_2$ production, even upon illumination above 500 nm.

2. Although at the beginning of the photoreaction a negative impact of oxidized Cu species on the photocatalytic H$_2$ production ability is obtained, the presence of copper oxides does not affect the overall hydrogen evolution efficiency substantially.

3. Due to the low chemical stability of Cu-NPs towards oxidation, not only Cu, but also Cu^{2+}/Cu$^+$ species exist in all the prepared nanocomposites. The existing Cu^{2+}/Cu$^+$ species were reduced to Cu^0 by the electrons generated from TiO$_2$ upon illumination, which in turn facilitates more electron-hole pair generation under visible light irradiation due to the Cu-SPR effect.

4. Electrons generated by direct visible light ($\geq$ 420 nm) excitation in TiO$_2$, together with the Cu-SPR induced electrons, contribute to the enhanced photocatalytic H$_2$ production ability of

Cu-TiO$_2$ photocatalyst. The hydrogen evolution upon excitation above 500 nm can be solely attributed to the Cu-SPR induced charge carrier formation.

5.2 Conclusion

In the present study, visible light photocatalytic activity of Au-TiO$_2$ (UV100) has been observed upon illumination above 420 nm, which is in good agreement with the previous reports. However, direct evidences have been presented that pure anatase TiO$_2$ can be directly excited by illumination above 420 nm or 420 nm laser beam (most likely due to pre-existing defects such as oxygen vacancies), which has long been neglected in the previous literatures. Besides, upon illumination above 500 nm, no Au-SPR initiated H$_2$ production or signals of trapped electrons/holes can be detected within the detection limit employing pure anatase UV100 as TiO$_2$ source, which is also different with the reported studies. Upon visible light illumination ($\geq$ 420 nm), the surface loaded Au nanoparticles only work as cocatalysts in the Au-TiO$_2$ (anatase) system.

In the paper "The Role of Au Loading for Visible-Light Photocatalytic Activity of Au-TiO$_2$ (UV100)", the origin of the visible light ($\geq$ 420 nm) excited charge carriers and the role of the surface-loaded Au nanoparticles have been confirmed.

However, once the UV100 was replaced by the commonly used commercial P25, both the Au-SPR induced H$_2$ and signals of trapped electrons and holes have been observed. But the observed phenomenon can neither be explained by the Direct Electron Transfer (DET) process nor the Resonance Energy Transfer (RET) process. It is assumed that the signals of the trapped electrons and holes are originated from two distinct processes, rather than the simple electron-hole pair excitation. In this case, it is assumed that Au nanoparticles can inject the SPR-induced hot electrons into the TiO$_2$ conduction band upon visible light illumination ($\geq$ 500 nm). Simultaneously, the Au-SPR can also initiate electron-hole pair generation in TiO$_2$. The DFT

calculation results strongly supported the proposed mechanism. Moreover, for the first time, the DFT calculation analysis clearly shows how the d orbitals of Au clusters create impurity energy levels and decrease the band gap of Au-TiO$_2$.

In the paper "Mechanism of the SPR-Driven Photocatalytic H$_2$ Production of Au-TiO$_2$ (P25)", the origin and the transferring processes of the SPR-induced charge carriers have been investigated. Furthermore, based on the experimental data and the DFT calculation results, a new mechanism combining the DET and RET processes have been assumed for the explanation of the SPR-driven photocatalytic H$_2$ production of Au-TiO$_2$.

As known, Au-TiO$_2$ is a good visible-active photocatalyst. For large scale industrial applications, copper, as a relatively low cost plasmonic metal, has been studied and Cu-TiO$_2$ (P25) has been proven to be a cost-effective photocatalysts. The apparently distinct H$_2$ production rates achieved upon illumination with different spectral ranges ($\geq$ 420 nm or $\geq$ 500 nm) evinced that the underlying reaction mechanisms in the two cases are not identical. It is confirmed that the charge carrier formation on Cu-TiO$_2$ photocatalysts consists of two distinct pathways: the direct excitation of TiO$_2$ by visible light and the Cu-SPR induced excitation. Both pathways are present when the full visible range of the spectrum is used ($\geq$ 420 nm), while for illumination at longer wavelengths ($\geq$ 500 nm), the photocatalytic activity is solely promoted by the Cu-SPR effect.

In the paper "Plasmonic Enhancement for Photocatalytic H$_2$ Production by Cu-TiO$_2$ upon Visible Light Illumination", the role and impact of the Cu-related species (Cu^0, Cu^+, Cu^{2+}), as well as the origin of the charge carriers have been clearly illustrated. The reaction processes and mechanisms for H$_2$ production using Cu–TiO$_2$ in water/methanol mixtures upon illumination have been proposed.

5.3 Outlook

Obviously, noble metal loading is an effective method to improve the photocatalytic efficiency of TiO_2-based photocatalysts. And the SPR effect plays a crucial role in the photocatalysis reaction, especially in the visible light driven photocatalytic ability.

However, the visible light driven photocatalytic reaction of $M-TiO_2$ greatly depends on the interaction between noble metal nanoparticles and the TiO_2 matrix. As known, the Au-SPR effect of noble metal nanoparticles deeply relates to their particle sizes. For example, Q. Qian found that the reduction potential of the transferred electron can be easily tuned by varying Au NP size, which provides a simple way of tailoring their photocatalytic activity [1]. Besides, different TiO_2 types exhibit distinct particle sizes, crystallinity, surface morphology, surface defects, *etc.* L. Du and the co-workers [2] found that larger TiO_2 particles resulted in longer charge recombination times because of the longer diffusion length of electrons in TiO_2 particles. Actually, this might have an essential impact on mechanism investigation, as it is possible that due to the fast recombination of electrons and holes, no photocatalytic reaction can be observed in the experiments. Therefore, both the SPR effect and the respective properties of the support materials should be taken into consideration in the following studies on the noble metal deposited TiO_2 photocatalysts. Besides, as to the direct electron injection mechanism, L. Du also found that there were two pathways for the electron injection: one was through direct electron-hole generation for shorter excitation wavelength (<500 nm), and the other was suggested to relate to enhanced electric field by plasmon (>580 nm). Thus, more detailed investigations should be conducted to further reveal the exact mechanism of Au-SPR-enhanced photocatalysis reaction.

In the present work, we also revealed the role and impact of Cu nanoparticles and copper oxides in the visible light driven photocatalytic H_2 production reaction and provided one possible reaction mechanism. However, further investigations are required to present an

overview on the mechanism of Cu-SPR-driven photocatalytic reaction. Moreover, it is known that the photocatalytic efficiency of the most extensively investigated photocatalysts upon UV light illumination is as follows: $Pt\text{-}TiO_2 > Au\text{-}TiO_2 > Cu\text{-}TiO_2$. However, it has been proven that $Cu\text{-}TiO_2$ exhibited comparable H_2 production rate in comparison to $Au\text{-}TiO_2$ upon visible light illumination. As the reaction mechanisms of noble metal deposited TiO_2 materials are different under the two cases (namely, under UV light illumination and under visible light illumination), a better understanding on the photocatalytic reaction mechanism is necessary in further investigations exploring a more effective visible light harvesting photocatalysts.

5.4 References

[1] K. Qian, B. C. Sweeny, A. C. Johnston-Peck, W. Niu, J. O. Graham, J. S. DuChene, J. Qiu, Y.-C. Wang, M. H. Engelhard, D. Su, E. A. Stach, W. D Wei, Surface plasmon-driven water reduction: gold nanoparticle size matters, J. Am. Chem. Soc. 2014, 136, 9842−9845.

[2]L. Du, A. Furube, K. Hara, R. Katoh, M.Tachiya, Ultrafast plasmon induced electron injection mechanism in gold–TiO2 nanoparticle system, Journal of Photochemistry and Photobiology C: Photochemistry Reviews. 2013, 15, 21–30

Publications

1. Jinlin Nie, Jenny Schneider, Fabian Sieland, Long Zhou, Shuwei Xia and Detlef W. Bahnemann, New insights into the surface plasmon resonance (SPR) driven photocatalytic H_2 production of Au-TiO$_2$, RSC Adv., 2018, 8, 25881–25887, DOI: 10.1039/c8ra05450a.

2. Jinlin Nie, Jenny Schneider, Fabian Sieland, Shuwei Xia, and Detlef W. Bahnemann, The role of Au loading for visible-light photocatalytic activity of Au-TiO$_2$ (anatase), Journal of Photochemistry and Photobiology, A: Chemistry, 2018, 366, 111–117, DOI: 10.1016/j.jphotochem.2018.03.016.

3. J. Nie, A. O. T. Patrocinio, S. Hamid, F. Sieland, J. Sann, S. Xia, D. W. Bahnemann and J. Schneider, New insights into the plasmonic enhancement for photocatalytic H_2 production by Cu–TiO$_2$ upon visible light illumination, Phys. Chem. Chem. Phys., 2018, 20, 5264-5273, DOI: 10.1039/c7cp07762a.

(As the first author of the three publications, I conrtibuted more than 70% in each paper.)

Oral presentation

Jinlin Nie, Jenny Schneider, and Detlef Bahnemann, New Insights into the Surface Plasmon Resonance (SPR) Effect in Photocatalysis of Au/TiO$_2$, 4th German-Russian Workshop "Solar Fuel Generation ", 28-30 November 2016, Hannover, Germany.

Poster presentation

1. Jinlin Nie, Jenny Schneider, and Detlef Bahnemann, New Insights into the Surface Plasmon Resonance (SPR) Effect in Photocatalysis of Au/TiO$_2$, 1th First International Conference on New Photocatalytic Materials for Environment, Energy and Sustainability (NPM-1), 7-10 June 2016, Göttingen, Germany.

2. Jinlin Nie, Jenny Schneider, and Detlef Bahnemann, Investigation of the Surface Plasmon Resonance (SPR) Effect on Au/TiO$_2$, 6th International Conference on Semiconductor Chemistry (SP-6), 11-14 September, Oldenburg, Germany.

Curriculum Vitae

Personal Information：

Surname, name   Nie Jinlin

Gender: Male   Nationality: China

Date and Place of Birth: 1988/08/01, Weifang-China

Marital Status: Married

Education：

2015.9 - present   PhD in Chemistry

                   Institute of Technical Chemistry, Leibniz university of Hannover,

2013.9 - 2018.6   PhD in Marine Chemical Engineering and Technology

                   College of Chemistry and Chemical Engineering, Ocean University of China

2011.9 - 2013.6   Master in Materials Science

                   College of Material Science and Engineering, Ocean University of China

2007.9 - 2011.6   Bachelor of Materials Chemistry

                   College of Material Science and Engineering , Qingdao University of
                   Science and Technology